Alma Mater Studiorum – University of Bologna

SCHOOL OF SCIENCE
Department of Industrial Chemistry "Toso Montanari"

Second cycle degree in

Low Carbon Technologies and Sustainable Chemistry

Degree Programme Class LM-71 – Industrial Chemistry

Synthesis *via* microemulsion of photo-catalysts for glycerol conversion

Experimental degree thesis

CANDIDATE
Caterina Zoffoli

SUPERVISOR
Chiar.mo Prof. Francesco Basile

CO-SUPERVISORS
Stefania Albonetti
Pio Gramazio
Andrea Fasolini

Academic Year 2020-2021

ABSTRACT

The current environmental crisis and increasing demand for fuels represent a problem in energy production. Indeed, all over the world, many policies are being implemented to aim at the decarbonisation of the energetic sector by introducing sustainable and renewable sources of energy. In this perspective, H_2 plays a fundamental role since it may be used in transports and power generation. Photocatalytic reactions represent one of the alternatives to produce sustainable H_2, as solar energy is converted into chemical energy. To perform these reactions, a semiconductor is needed and titanium dioxide is a suitable material to be employed, also considering its great morphological, chemical and optical properties, especially when its particles are in the nano-dimensions.

A way to synthesise titania nanoparticles consists in the exploitation of microemulsions (ME), which are dynamic systems that can act as nanoreactors. The ME synthetic route allows a certain flexibility of the reaction parameters, which permits a fine tuning of the final properties of the titania nanoparticles. In this work, the standard (STD) ME synthesis, developed in previous studies, is revised by introducing some modifications in the hydrolysis and heating time, in the type of acid used and with the addition of a ME containing a base. In the latter case, the neutralization is achieved with ammonium hydroxide (NH_4OH) or sodium hydroxide (NaOH) and it permits a better control on the final characteristics of the titania nanoparticles. By implementing these modifications, it was possible to synthesise TiO_2 samples with better properties than the STD titania sample, namely a lower bulk density and a higher surface area. In addition to that, titania particles were obtained in nanoscale dimension and the utilization of NH_4OH with a base/acid ratio (molar) higher than 0.7 allowed to synthesise just the anatase polymorph of titania. If a longer stirring time was used or if HCl was employed rather than HNO_3, also the rutile crystalline phase of titania formed as the only polymorph. On the other hand, the presence of NaOH resulted in the synthesis of an anatase and rutile mixture.

Then, the TiO_2 samples with the best characteristics were tested in the glycerol photo reforming reaction, since this substrate is obtained in huge amounts as a by-product from biodiesel production. The photoactivity of the bare TiO_2 supports is expressed as H_2 productivity (μmol $H_2/g_{catalyst}/h$). The sample synthesised with NH_4OH and a base/acid ratio of 0.7 showed the highest value for H_2 productivity, even greater than the STD and commercial P-25 samples. Moreover, in this case, glyceraldehyde and glycolaldehyde were produced as liquid products, meaning that the decomposition of glycerol started. Conversely, using the STD sample no liquid products have been observed, thus mainly the water splitting reaction occurred.

RIASSUNTO

L'attuale crisi ambientale e l'aumento della domanda di combustibili rappresentano un grosso problema nell'industria di produzione energetica. L'idrogeno svolge un ruolo fondamentale nella decarbonizzazione del settore energetico. Inoltre, le reazioni foto-cataliche rappresentano un'alternativa promettente per produrre H_2 rispetto ai metodi tradizionali, poiché viene utilizzata energia solare, poi convertita in energia chimica. Un semiconduttore è necessario per condurre reazioni fotocatalitiche, e il biossido di titanio (TiO_2) è un materiale adatto a questo scopo date le sue ottime proprietà morfologiche, chimiche e ottiche, in particolare quando viene utilizzato in dimensioni nanometriche. Tra i metodi per ottenere nanoparticelle di TiO_2, la sintesi per microemulsione (ME) è una valida alternativa. Le microemulsioni sono sistemi dinamici utilizzati per la sintesi di nanoparticelle inorganiche poiché le micelle fungono da nano reattori. La sintesi tramite ME permette una certa flessibilità nei parametri di reazione e, di conseguenza, la variazione di alcuni parametri finali della polvere di TiO_2. In questo lavoro, la sintesi standard (STD) per microemulsione, sviluppata precedentemente in altri studi, viene rielaborata modificando i tempi di idrolisi e riflusso, il tipo di acido utilizzato e introducendo una ME contenente una base (idrossido di ammonio o idrossido di sodio). In quest'ultimo caso, l'obiettivo è neutralizzare l'acido per poter controllare e modificare la proprietà finali delle nanoparticelle di TiO_2. Quindi, è stato possibile sintetizzare campioni di TiO_2 con caratteristiche migliori rispetto alla polvere STD, tra cui una maggiore area superficiale e una minore densità apparente. Inoltre, le particelle di TiO_2 sono state ottenute con dimensioni nanometriche e l'utilizzo di NH_4OH con un rapporto base/acido di 0,7 ha permesso di sintetizzare solo la fase cristallina anatase. Al contrario, se vengono impiegati tempi di idrolisi più lunghi o se HCl viene usato al posto di HNO_3, anche la fase cristalline del rutilo si forma. Mentre l'utilizzo di NaOH come base per la neutralizzazione favorisce la formazione di entrami i polimorfi. I campioni di TiO_2 con le migliori proprietà sono stati testati nella reazione di foto reforming del glicerolo, poiché questo substrato viene sintetizzato in grandi quantità come co-prodotto nella produzione del biodiesel. L'attività foto catalitica del TiO_2 è espressa come produttività di H_2 (µmol $H_2/g_{cat}/h$). Il campione sintetizzato con NH_4OH e un rapporto base/acido 0,7 ha mostrato il valore più alto di produttività, anche superiore rispetto al campione STD e alla TiO_2 commerciale (P-25). Inoltre, gliceraldeide e glicolaldeide sono state rilevate tra i prodotti liquidi, indice dell'inizio della reazione di decomposizione del glicerolo. Al contrario, il campione STD non presenta conversione in prodotti liquidi, quindi, in questo caso, avviene solo la reazione di water splitting.

TABLE OF CONTENTS

1. INTRODUCTION

1.1. Microemulsion

The term microemulsion was introduced for the first time by Schulman et al. in 1959[1]. They were able to synthetize a macroemulsion and then titrate it with a co-surfactant. The result was the formation of a transparent system with a low viscosity, isotropic and thermodynamically stable[1]. Moreover, spherical micro droplets with a diameter between 600 and 8000 nm were obtained. At that time, the word "micro" was chosen to express the small dimensions achieved, but it did not have any correlation with the actual length scale[2]. A microemulsion is defined by IUPAC as a system with a diameter of the dispersed phase in the range of 1-100 nm[1]. The single phase is homogeneous only at a macroscopic level, while microscopically the system is heterogeneous.

In general, an emulsion is a dispersion formed by two immiscible phases (e.g., aqueous phase and organic phase). In these systems, immiscible phases will tend to stay separated forming interactions only with molecules of the same phase. The mixability can be partially reached by stirring but the system is not stable enough, hence the droplets will coalesce forming again the two separated phases[2]. If a different type of interactions is formed between the polar and non-polar phase, it is possible to stabilize the system obtaining a single phase[3]. When an active molecule, such as a surfactant, is used, it allows the mixing of the two phases[3], so that the surface tension of the two immiscible components is reduced. In this way, also the attraction between molecules of the same component is reduced, and the two phases can interact with each other. A surfactant is an amphiphilic molecule, meaning that it contains a hydrophobic and hydrophilic part. This characteristic allows the formation of interactions with both phases, reducing the superficial tension and the free energy. As the concentration of the surfactant increases, the molecules will aggregate into self-assembled monolayers and eventually form micelles when the critical micelles concentration (CMC point) is reached (**Figure 1.1-A**).

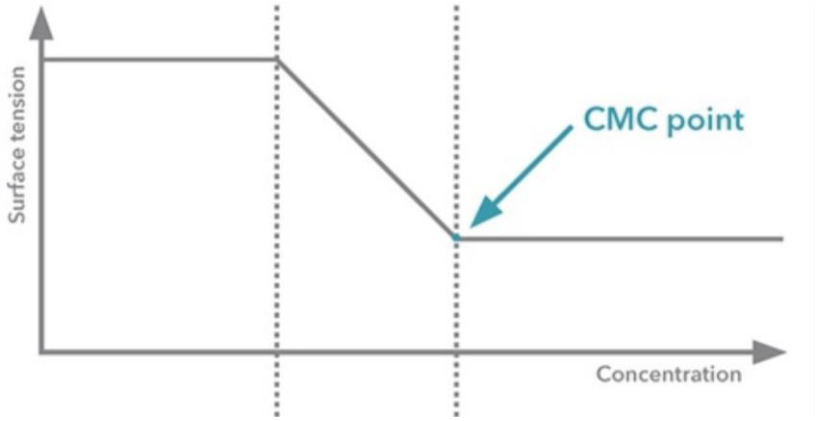

***Figure 1.1-A**. Trend of the surface tension with respect to the concentration of surfactant (logarithmic scale). Adapted from[4].*

Figure 1.1-B represents an example of a micelle formed within an emulsion, in particular it is a reverse micelle. The surfactant interacts differently with the two solvents, also depending on which of the two phases is predominant. In this case, the aqueous phase is confined as the dispersed phase and it is surrounded by the polar part of the surfactant molecules. Conversely, the organic solvent is the continuous phase, thus it will interact preferably with the non-polar part of the surfactant. Therefore, the presence of the surfactant is fundamental for the formation of a stable system composed by two immiscible phases, that otherwise would not have mixed. Furthermore, a surfactant helps creating an adjustable micro-environment of the reaction, thus a better control of particles growth is reached and this can lead to a higher selectivity for a certain crystalline phase[5].

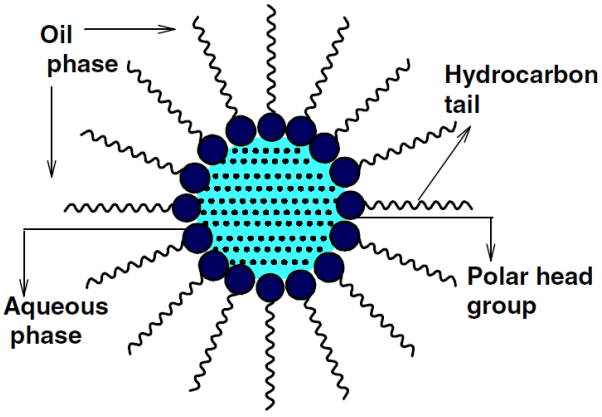

***Figure 1.1-B**. Schematic representation of a micelle[1].*

In addition to that, a co-surfactant may be used to enhance the micelles formation. A co-surfactant is a second surface active molecule, as the surfactant, that favours the establishment of the nano-sized dispersed phase into the continuous phase.

1.1.1. Composition and properties

A microemulsion is a colloidal system with a high degree of dispersion and narrow dimensions of the micelles. The diameter of the dispersed phase in a microemulsion goes from 1 to 100 nm[1]. As the dimensions of the micelles decrease, the polydispersity lowers as well, resulting in better properties and wider applications[6]. The size of micelles can be controlled by tuning the water-to-surfactant concentration ratio (R_w). The surfactant plays a fundamental role in the formation of W/O or O/W emulsions as this depends on its hydrophobic/hydrophilic character. This ratio is called hydrophilic-lipophilic balance (HBL). Consequently, surfactants with high HBL values can be used to obtain O/W emulsions, while the ones with a low HBL are useful to form W/O emulsion[7]. Moreover, the shape of the surfactant influences the type of micelle that will form. If the surfactant as a small polar head with a branched hydrocarbons chain, spherical reverse micelles (W/O) are obtained because the tail have a bigger steric hindrance and so they tend to dispose on the outer surface[8].

The main parameters to control in the formation of microemulsions are temperature and composition since, unlike emulsions, microemulsions are thermodynamically stable systems that will form spontaneously with low effort under the proper conditions[9]. Indeed, emulsions are rather unstable from a thermodynamic point of view and a great amount energy is required by the system to form and maintain their structure[2]. Consequently, when the composition is appropriate, microemulsions are obtained as a transparent systems with a low viscosity[2].

Microemulsions are dynamic systems where collisions among droplets occur frequently, and this is given by the continuous Brownian motions. If these collisions are strong enough, the external part of micelles, composed by the surfactant layer, will break permitting an inter-micellar exchange[9]. So, surfactant molecules can exchange freely with others from the micelle assembly to the bulk area, composing a dynamic system. This important property of microemulsions can be exploited to perform confined reactions in nanoreactors.

Concerning the composition, in general a microemulsion is formed by a polar phase, a non-polar phase, a surfactant and, sometimes, a co-surfactant[1]. Moreover, since a microemulsion

contains 3 (or 4) different elements, its composition can be described by a ternary phase diagram (**Figure 1.1.1-A**), as each side represents one of the components. If a co-surfactant is used, it can be comprehended within the surfactant edge. Depending on the ratio of the various components, the shape of the dispersed phase can change, for example forming a bicontinuous microemulsion or cylindrical micelles[2,10].

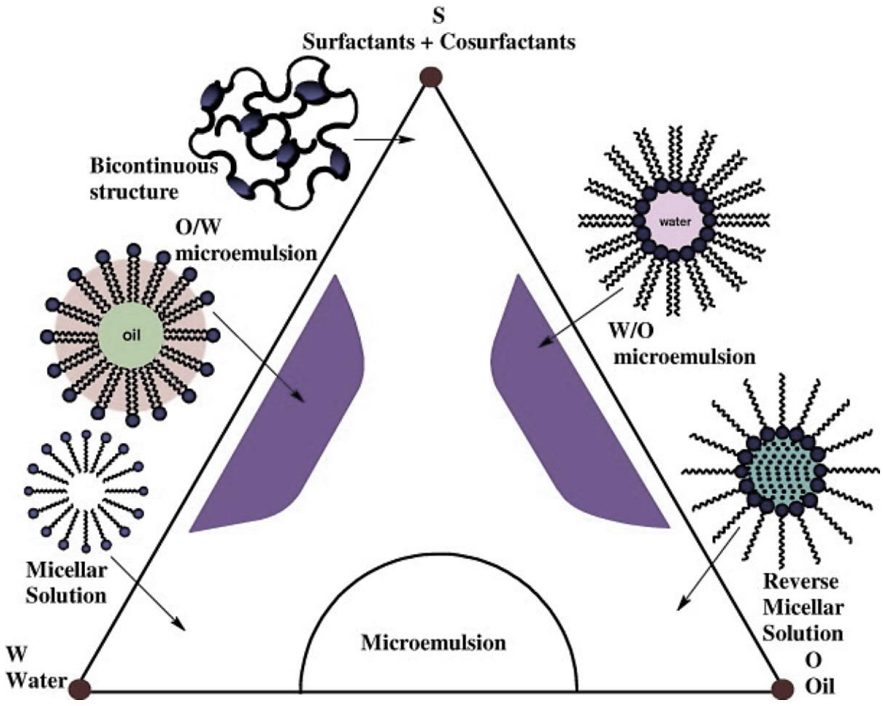

***Figure 1.1.1-A**. Ternary phase diagram for a microemulsion[1].*

In a microemulsion, one of the two phases is present as the prevailing one, so it is called the continuous phase, while the other one is the dispersed phase. Starting from this concept, two types of system can be obtained. Oil-in-water emulsions (O/W) are produced when water is the dispersed phase; while water-in-oil (W/O) emulsions are formed when water is the continuous phase (**Figure 1.1.1-B**). In the latter case, the micelles are called reverse micelles and they are particularly interesting from an industrial point of view (see *Paragraph 1.1.2*).

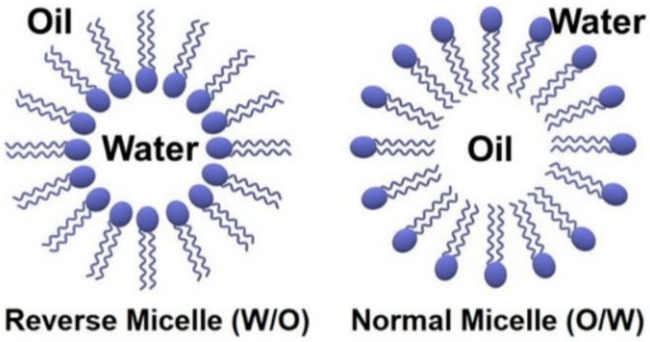

***Figure 1.1.1-B**. Schematic representation of the two different types of micelles[6].*

1.1.2. Industrial applications of microemulsions

Since their discovery, microemulsions have been widely studied for many possible applications. The first employments of microemulsions were in the formulation of liquid waxes and in the field of oil enhanced recovery[11]. Nowadays, one of the most important usage of microemulsions is for the synthesis of nanoparticles. In this case, microemulsions are used as the reaction medium due to the large and dynamic interfacial area; moreover, their micelles can be exploited as nanoreactors to synthesis both inorganic and organic nanoparticles. In particular, the synthesis of catalysts through ME is highly interesting because of the possibility to finely tune the finale properties, especially the dimensions of the particles. For this purpose, W/O emulsions are usually used since they result in better properties and performances of the nanoparticles obtained with respect to other methods[9]. Another advantage of this approach is the limitation of reagents incompatibility since, being able to interact with both phases, microemulsions allow the use of reagents with different polarities. On the other hand, a huge drawback in the use of W/O microemulsion is the great amount of solvents and reagents used, which are not sustainable from an environmental point of view. Moreover, the high production costs of the ME approach is one of the factors limiting its industrial application in the synthesis of catalysts if compared to the more common production methods[12]. Even though the synthesis of ME is not at the industrial step yet, many researches showed the wide range of applications for this type of catalysts, like in fuel cells[13,14], in partial oxidation of methanol[15,16] or methane[17] and in the water-gas shift reaction[18].

Another important application may be in the pharmaceutical industry, where microemulsions may be used for drug delivery of lipophilic drugs[11]. Moreover, microemulsions can be exploited in the pesticides and antibacterial industry since they are considered to have an antimicrobial activity as bacteria are not able to survive in an organic medium[2].

1.1.3. Utilization for the synthesis of nanomaterials

Microemulsions are promising systems to synthesise nanomaterials. First of all, micelles are suitable to be used as nanoreactors because of the extremely large and dynamic interfacial area that favours reactions at the nanoscale. Moreover, due to the frequent collision, also reagents in different phases (i.e., a precursor soluble in the aqueous phase) can react forming a product that is soluble in just one of the two phases, overcoming the limit of solvent immiscibility[19]. By using this approach, it is possible to synthesise both organic and inorganic particles confined inside the micelles of the microemulsion. Furthermore, it is possible to tune the dimensions of the products, allowing to obtain nanoscale materials. This can be done both by tuning the R_w or by changing the components and varying their concentration. In the former case, a lower value of R_w corresponds to a lower concentration of water, meaning that the micelles are more packed and thus smaller[6].

Usually, W/O microemulsions are preferable to synthetise nanoparticles as the metal precursor can be solubilized in the water pools (internal part of micelles)[6]. A possible route to obtain nanoparticles is to use a metal precursor and a reductant. As shown in the scheme below (**Figure 1.1.3-A**), if both the metal precursor and the reductant are inserted in the form of microemulsions, the micelles may collide, coalesce and eventually form dimers where reagents can be exchanged or react, depending on which microemulsion they will encounter[6].

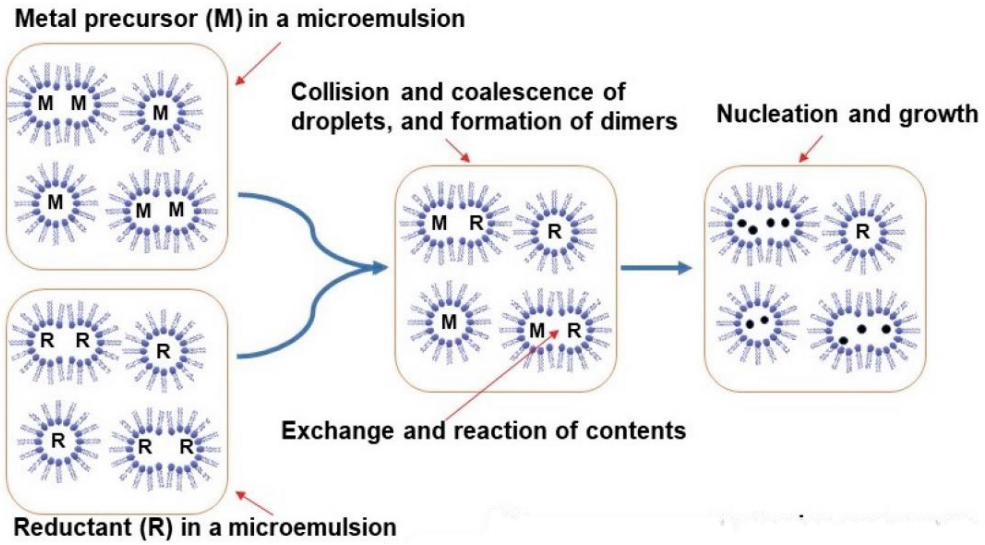

***Figure 1.1.3-A**. Synthesis of colloidal systems through W/O microemulsions. (a) Direct addition of the reductant. (b) Addition of the reductant in a microemulsion[6].*

Clearly, the formation of nanoparticles is a complex and multistep process that requires collisions between micelles containing different reagents, their nucleation and growth due to the exchange of material[19]. Consequently, the probability of nucleation, the total amount of precursor used to synthesise the nanoparticles and the relevance of particles coalescence are all factors affecting the dimensions of the particles obtained[19].

Another parameter that influences the outcome and especially the size of nanoparticles is the amount of surfactant used. Indeed, as its concentration increases, smaller particles are obtained since the R_w decreases and the number of micelles rises[5]. Thus, the nucleation rate can be controlled properly and the uncontrolled growth of particles is avoided. As a result, the surfactant concentration can lead the formation of particles into smaller dimensions and also into a more homogeneous size distribution[6].

The great advantage of microemulsion exploitation for the synthesis of nanoparticles relies in the possibility to control and modify their properties, especially the dimensions. Also, spherical particles are usually obtained when the microemulsion technique is used, but it is not the only determining factor. Indeed, the presence of different anions could interfere in the nanoparticle shape depending on the type of adsorption created by the ions during the crystals growth[8,20].

1.2. Titanium dioxide

1.2.1. State of the art

Titanium dioxide, also called titania, is the natural occurring oxide of titanium[21] and it is part of the transition metal oxides[22]. The interest in titania started to rise in 1972 when Fujishima and Honda managed to obtain water splitting through photocatalysis on a TiO_2 electrode[22]. After that moment, many research groups studied titania as a catalyst in different fields, such as organic photosynthetic reactions and lately also in heterogeneous catalysis.

Titania exists in different crystalline structures, called polymorphs. The most relevant ones are rutile, anatase and brookite. They are all formed by TiO_6 octahedra linked by sharing the octahedral edges, and the difference is in the spatial arrangements of these structures, which is showed in **Figure 1.2.1-A**[23].

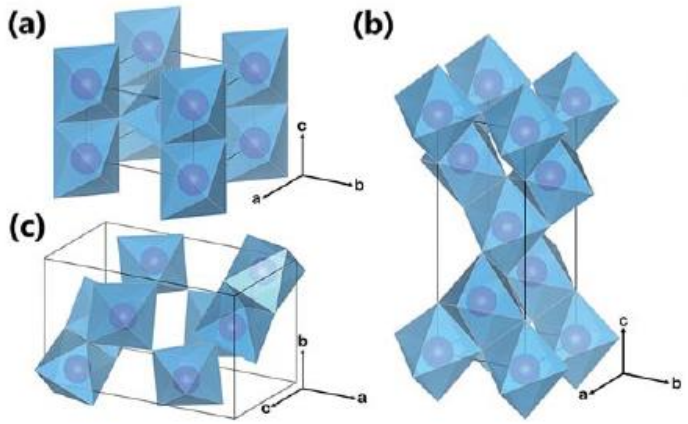

***Figure 1.2.1-A**. Crystal structures of TiO_2 polymorphs: (a) rutile, (b) anatase, (c) brookite[23].*

The main physical, chemical and electronic characteristics of titania polymorphs are grouped in **Table 1.2.1-A**.

- Rutile has a tetragonal structure slightly distorted and it is the thermodynamically stable form of bulk titania[23]. Rutile polymorph has a band gap of 3.03 eV and it can be used as a photocatalyst even though its activity is overall poorer with respect to anatase[22].
- Anatase also has a tetragonal structure with a distortion larger than rutile. This polymorph is usually preferred in photocatalysis since it shows higher activity in charge carrier dynamics and in photo-degradation of organic compounds[22]. Moreover, it displays better surface chemistry properties. Anatase polymorph has a band gap of 3.2 eV.

- Brookite has an orthorhombic structure and its band gap is 2.96 eV. Brookite and anatase are metastable in the bulk form, but when switching to nano-dimensions they can be stable due to their smaller surface energy[23].

Crystalline phase	Rutile	Anatase	Brookite
Band gap energy (eV)	3.2	3.03	2.96
Unit cell	Tetragonal	Tetragonal	Orthorhombic
N°. TiO_2/unit cell	2	4	8

***Table 1.2.1-A**. Main properties of TiO_2 polymorphs.*

Titania has some important and useful properties that can be exploited in many industrial applications, especially in photocatalysis. Indeed, titania is a semiconductor with a high catalytic efficiency and great electronic, physic and chemical properties[21,22]. Furthermore, titanium dioxide is a quite cheap material and it has not toxic effects for humans or the environment[22].

1.2.2. Synthesis of titania nanoparticles via microemulsion

The synthesis of nanoparticles allows to exploit different properties respect to bulk materials. Especially in catalysis, this has a huge relevance since surface characteristics are widely studied and modified to obtain better and better catalysts tailored to target reactions. Lately, titania nanoparticles have been studied for this purpose and it is well known that TiO_2 is more active in the form of nanoparticles rather than bulk powder, showing innovative optical, chemical and electronic properties[21,22,24], especially when it is synthetized with dimensions below 20 nm[25]. Indeed, when moving to the nanoscale, materials show quite different properties compared to the macroscale. Many factors depend on the size range over which they are measured, so the surface area to volume ratio. Thus, when particles go down to the nano-dimensions, the surface area increases while the volume lowers. The effects of a higher surface area are multiples. First, a bigger percentage of atoms are present on the surface rather than in the bulk of the material. This corresponds to a greater surface energy of the particles which in turn is related to an improved reaction rate[25].

There are many synthetic routes to obtain titania nanoparticles, also enabling to control the morphological and chemical characteristics of the final powders. In general, these factors are:

- Titanium precursor,
- Type and concentration of the components,
- Reaction temperature, pression and time,
- Calcination temperature and time.

Different titanium precursors can be used, both organic and inorganic. Some examples are titanium tetrachloride, $TiCl_4$; titanium oxychloride, $TiOCl_2$ and titanium isopropoxide, $Ti[OCH(CH_3)_2]_4$, but the most used is titanium tert-butoxide, $Ti[OC(CH_3)_3]_4$.
Moreover, the type of surfactant has an impact because it influences the R_w factor and thus the dimensions of the titania particles, as previously mentioned (*Paragraph 1.1.1*).

Considering other possible components, the synthesis of titania through microemulsion is usually performed in an acid environment and the type of acid has a relevant impact on the type of polymorph that will be obtained. If nitric acid is used, the anatase phase will form, while with hydrochloric acid, rutile is the main crystalline phases present in the titania powder. Indeed, the type of anions in the solution influences the formation of the different polymorphs of titanium dioxide. The growth of TiO_2 crystals is based on the orientation of the TiO_6^- octahedra and it is graphically represented in **Figure 1.2.2-A**. If these structures will share four edges, the development of the crystal will be along the (211) Miller index with a zigzag packing, and the outcome will be the synthesis of anatase[26,27]. Conversely, if the octahedra will share just two edges they will form the (011) plane in a linear packing, characteristic of the rutile polymorph[26,27]. In the former case, a cis coordination occurs, favouring the synthesis of the metastable product; while in the latter case, there is a trans coordination with the formation of the thermodynamic product, which is rather unstable under kinetic conditions. Indeed, it is reported that for a hydrolysis step of 4 days, the rutile phase will be synthetized even by using HNO_3, since it is the thermodynamic product and thus the octahedra have more time to rearrange their structure[27].

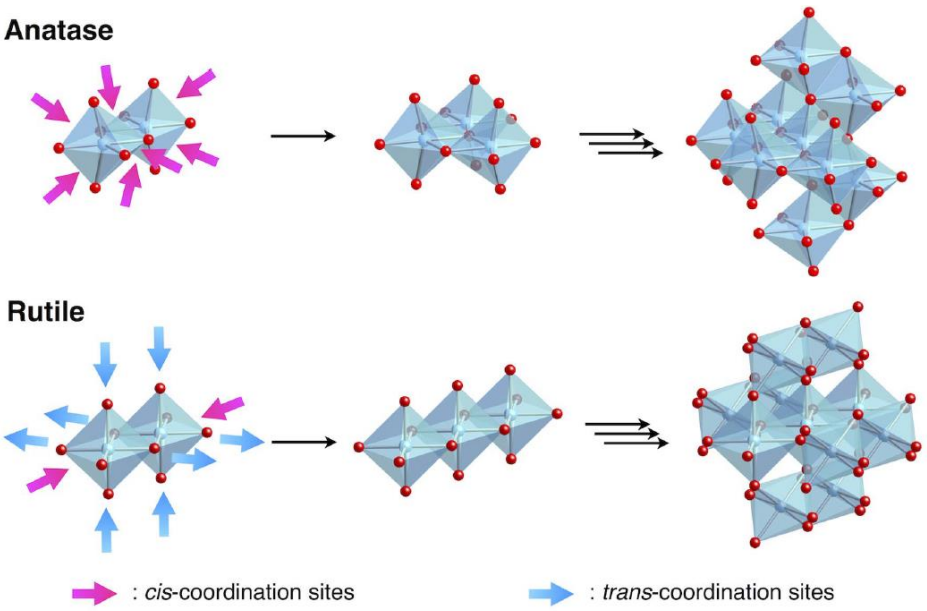

Figure 1.2.2-A. *Graphic representation of the growth for titania crystals, favouring one polymorph over the other one*[26].

Also, Yan et al. proposed a similar explanation for the formation of rutile and anatase when Cl^- and SO_4^- anions were used in different percentages and led to the synthesis of titanium dioxide with different grades of the two polymorphs[28].

In this project, titanium dioxide is synthetized with a water-in-oil microemulsion (W/O ME) using titanium tert-butoxide (TBT) as the titanium precursor. This is an organic compound that is soluble in the organic phase composed by cyclohexane. The aqueous phase, confined within the micelles, is acidic. Moreover, a surfactant and a co-surfactant are used to form the microemulsion. The hydrolysis with water of the TBT component is allowed by the presence of a flexible layer composed of the surfactant and co-surfactant and by the frequent collisions between the micelles. So, the reactivity in the synthesis of titania *via* microemulsion is boosted by the presence of a biphasic system. The mechanism of the overall reaction is presented in **Figure 1.2.2-B** and it is described as follows[27,29]. First, the TBT undergoes the attack of water, which is a nucleophile, and the coordination number of titanium increases by one forming a transition state. Then, the alkoxide can extract a hydrogen from the water molecule, becoming a better leaving group and the starting coordination number of titanium is restored. The hydrolysis proceeds until all the tert-butoxide groups are replaced by hydroxyl groups. The co-product, tert-butanol, is soluble in the organic phase and so it can exit the micelles easily through the flexible surfactant/co-surfactant layer. As soon as the hydrolysed TBT is formed,

two pathways are possible: the further hydrolysis or the condensation, eventually forming Ti-O-Ti dimers or chains in both cases. It is possible to control which of the two steps will be favoured and thus the rate of the reaction. In an acid environment, the condensation is faster than the hydrolysis since it is more affected than the condensation reaction[27]. So, by using an acid in the aqueous phase the overall system is controlled by the condensation. Moreover, the concentration of the acid influences the stability of the system. It is reported that, if 0.5 M HNO_3 is used, a white precipitate forms, while when the concentration is increased up to 5 M the solution is stable for a longer time[27]. This can be explained by a better control of the reaction rate since the hydrolysis is slowed down.

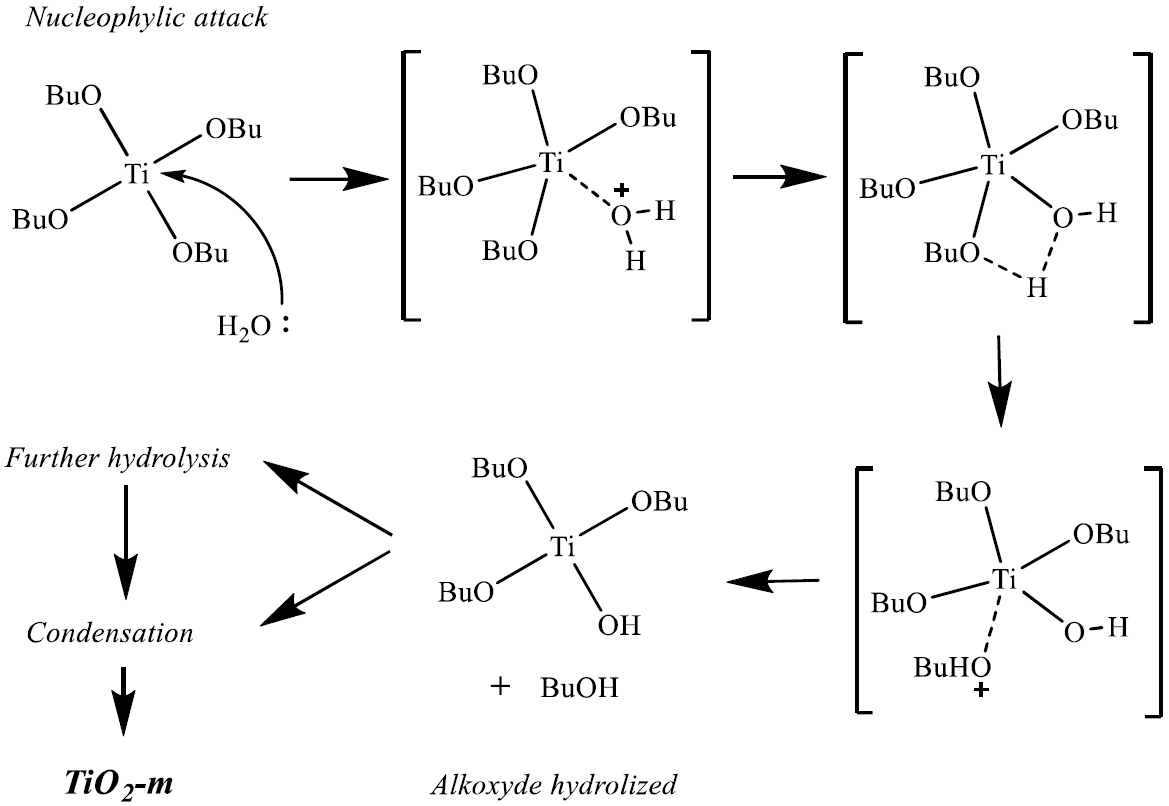

***Figure 1.2.2-B**. Scheme of the mechanism for the hydrolysis with water of the TBT. Adapted from literature[29].*

After this step, the TiO_2 particles are present as a white precipitate inside the micelles and they need to be released. The micelles are not stable above 40°C, so it is quite easy to break them just by heating the solution. An alternative is to centrifugate the system, so that the centrifuge force will allow the disruption of the micelles. Some further steps are required to completely separate the TiO_2 powder from the system and obtain it in a pure form, as washing the

precipitate with the proper solvent to remove salts and impurities created during the synthesis. A general scheme for the microemulsion synthesis of TiO_2 is presented in Figure **1.2.2.-C**, and the reagents are the ones used within the project.

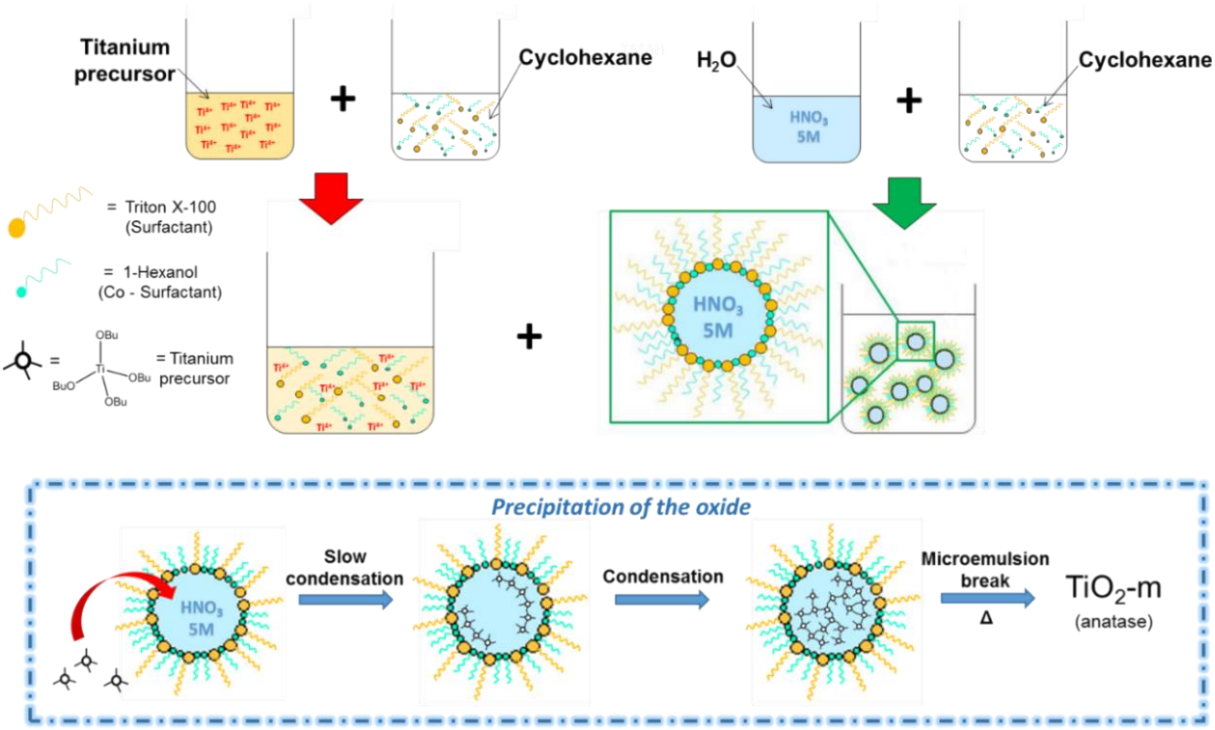

***Figure 1.2.2-C**. General scheme for the STD synthesis of titania via microemulsion*[30,31].

Eventually a heat treatment is required to transform the amorphous material into a crystalline one. In addition to that, it helps to remove all the impurities coming from the synthesis, like co-products or residual reagents, which occurs above 400°C[22]. Calcination is usually performed on the synthesized titania for these reasons. The heat treatment affects the morphology, porosity and crystallinity of the powder. As the calcination time and heating rate increase, the surface area lowers. This is a consequence of the pores collapse since the material is being transformed from amorphous to crystalline[22]. In literature, it is reported that the highest surface area is obtained when the calcination temperature is 400°C; while further increase of temperature leads to a drop of surface area values[32]. Also, the dimensions of titania particles are a function of the calcination temperature since they tend to agglomerate as the heating temperature increases[32,33]. Moreover, the titania undergoes a phase transformation from anatase to rutile, which is reported to start around 600-700°C and it is completed above 900°C[33,34]. Considering all these information, in this project the microemulsion-synthesised titania is dried at 100°C and then

calcined at 400°C to retain its morphological properties as much as possible, while obtaining a crystalline structure as well.

The microemulsion method is widely used for titania preparation, but other viable synthetic routes exist. The sol-gel synthesis consists in the hydrolysis of a titanium precursor in water, or other solvents, followed by the condensation when the gel forms and the solvent evaporates[35]. It allows to obtain a highly pure and homogeneous powder, while working at low temperatures[36,37].

Another alternative is the hydrothermal synthesis where the titanium precursor is placed in aqueous solution with an acid or a base. The system is heated at high temperature and pressure[36], usually in an autoclave. In both cases, as for the microemulsion approach, it is possible to modify many reaction parameters, as the temperature, pH, reaction time and amount of titanium precursor; by doing that, the morphology of the final powder can be finely tuned[35,36]. For the hydrothermal synthesis, poly-dispersed powders will form because of the higher synthesis temperature[38].

1.3. Biomass

As a consequence of the increasing demand for fuels and the emerging environmental issues, a greater interest in renewable sources of energy is increasingly spreading. Plant biomass is a promising alternative being highly available and convertible into biofuels[39]. Biomass comprehends all the organic material deriving from animals and plants, but usually only the latter is considered for energy production. Indeed, the photosynthesis allows plants to store the energy coming from the sunlight in form of chemical bonds. The composition of biomass is diverse depending on the type of plant and on the area where it is grown; moreover, it expresses whether a plant is suitable or not to be transformed into a biofuel[40].

Compared to fossil fuels, biomass is generated in a shorter time span, thanks to the photosynthetic process. Additionally, one of the biggest advantages of biomass utilization is the possibility to exploit a renewable source of energy which has the potential to limit greenhouse gas (GHG) emissions with respect to fossil-based fuels. Plus, biofuels are considered carbon-neutral since they derive from plants that absorb CO_2 during their growth and this compensate the CO_2 emitted when the biomass is used as fuel. Anyway, a major drawback of biomass utilization is the competition with food consumption because many crops suitable for energy production are the ones used in the food industry, leading to potential effect on food security in developing countries. For this reason, nowadays the challenge is to work with dedicate biomass crops, non-edible parts of plants and exploit areas not suitable for the growth of food crops. In this case, second-generation fuels are obtained; conversely, first-generation fuels come from crops originally dedicated to the food industry[41].

1.3.1. Glycerol as a substrate

Among all the methods to exploit biomass, biodiesel is a promising alternative to fossil fuels. The biodiesel production started in 2003 and drastically increased since then[42]. This also led to a massive production of glycerol as a low purity by-product stream. Indeed, biodiesel is synthesized through the reaction of transesterification of vegetable oils with methanol, obtaining glycerol accordingly to the stoichiometry of the reaction presented in **Figure 1.3-A**. Different types of feedstocks for vegetable oils are suitable to be used for biodiesel production. Among the first generation ones there are palm oil, rapeseed oil, soybean oil, sunflower oil, olive oil and peanut oil[37,43]. The second generation feedstocks mainly comprehend oils from not edible crops and industrial or residential wastes[37], like waste cooking oils[44]. Also, many

studies are focused on the exploitation of microalgae for biodiesel production because they are able to produce a great amount of oil, but up to date this approach is not economically viable yet [45,46].

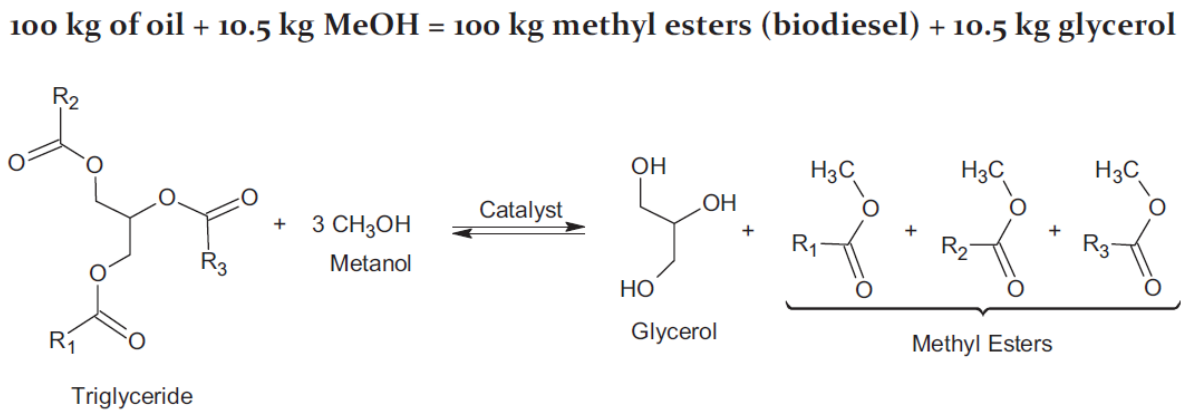

***Figure 1.3.1-A**. Transesterification of triglycerides, obtained from vegetable oils, with methanol for biodiesel production[42].*

The biodiesel production created a surplus of glycerol on the market forcing most of the glycerol production factories to close. Indeed, synthetic glycerol covers less than 1% of the total amount produced each year[42]. Being non-toxic, biodegradable, highly water-soluble and environmentally safe, glycerol has a large variety of uses, like in animal feeding[47], in the food and beverage industry[48], drugs, pharmaceuticals and personal care items[43,48]. However, all these employments cannot cover the whole market for the glycerol produced every year, thus the majority of it may be suitable for the production of other value-added chemicals[47]. Indeed, glycerol is a highly functionalised molecule containing three hydroxyl groups and this allows numerous possible reactions for derivatization. Therefore, new applications are currently being studied since it is believed that looking for alternative methods for glycerol utilization will boost the biodiesel production creating a market where the bio-fuel is economically comparable with the fossil-based counterpart[49].

1.4. Hydrogen

The current environmental crisis is extremely impelling since climate change is showing its effects all over the world. The latest Intergovernmental Panel on Climate Change report (IPCC 2020) clearly states that the human activity had a strong influence on the climate change and that actions must be taken to limit the GHG emissions, especially CO_2, and to reverse the trend for the temperature increase[50]. However, global warming is not the only consequence, as climate change has many other negative effects on the Earth and its ecosystems, like an intensified water cycle, the expansion of dry areas and ocean acidification[50]. To face these problems, EU Commission delineated a road map for a clean energy transition to reach the carbon neutrality by 2050 through the European Green Deal[51]. Among the targets, the development of an energy sector, based on renewable sources, is prioritized and hydrogen is playing a fundamental role in the decarbonisation of the EU energetic system[51,52]. Currently, in Europe, 95% of the hydrogen is produced starting from fossil-based resources[53], so a heavy development is needed to switch to renewable resources and more sustainable production methods, which right now are not cost-competitive with the fossil-counterpart. In addition to that, 800 Mt/y of CO_2 are emitted into the atmosphere through the production of hydrogen from non-renewable sources alone[54].

In general, even if hydrogen is still produced from fossil sources, its global demand has strongly increased in the recent years (**Figure 1.4-A**), but its main applications are in oil refining and ammonia production, for fertilizers. Just a small percentage is used for other purposes. Thus, the research is focusing on the expansion of hydrogen employments as in transports, building industry and power generation[51], together with a more sustainable production.

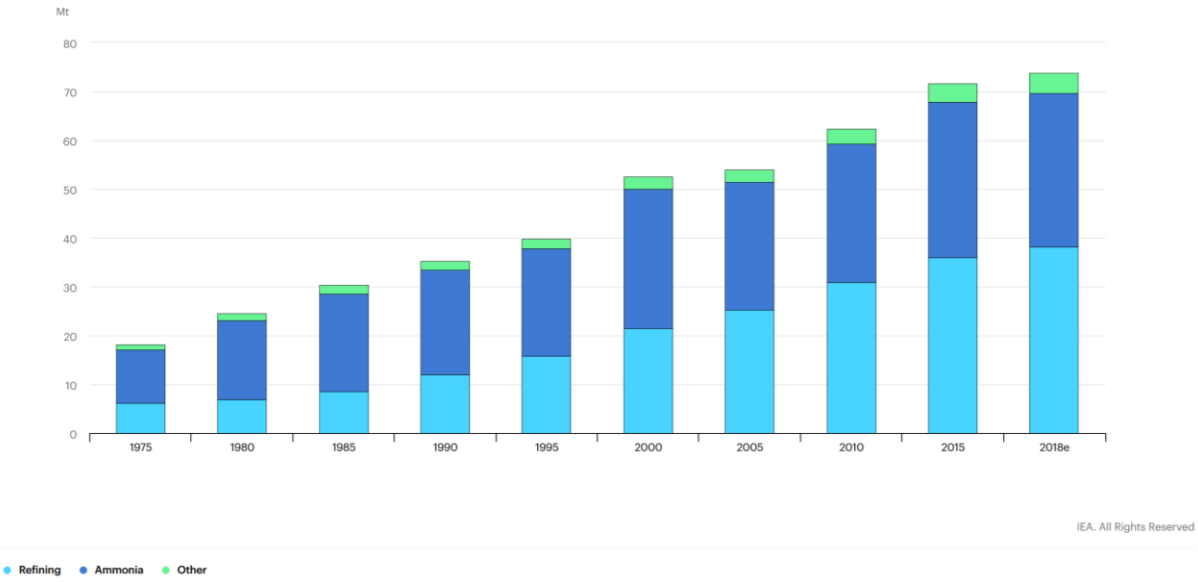

Figure 1.4-A. *Global demand for pure hydrogen, from 1975 to 2018, with the relative usage sector*[54].

1.4.1. H_2 properties and production

Hydrogen (H_2) is a colourless and odourless inflammable gas which can be exploited as a fuel because of its high energy content, even greater than some of the more common fossil fuels[55]. Moreover, hydrogen is storable, transportable and it does not emit CO_2 during its combustion. Anyway, hydrogen is not available in nature and thus, it must be produced through some chemical processes. Hydrogen can be produced with a great variety of methods depending on the raw materials, fossil-based or renewable resources, and on the type of process, e.g., chemical, thermochemical or biochemical (**Figure 1.4.1-A**).

Mehmeti et al. performed an LCA analysis on different hydrogen production processes, starting from the most common ones to emerging technologies, and they showed how the processes using fossil fuels resulted in a greater global warming potential (GWP) than the ones exploiting renewables[56]. However, these renewable technologies are still powered by fossil-fuels, so the study also proved that the GWP would be definitely lower if renewable sources of energy are used to feed the process. The main problem is the cost of these new technologies, which are not cost-competitive with the already commercial and well-established hydrogen production methods. Considering the commercial processes based on fossil sources, the possibility to combine them with carbon capture, utilization and storage (CCUS) was investigated. Some

researchers confirmed the reduced emissions of CO_2 when CCUS is performed; moreover, the energy efficiency can be improved by the integration of CCUS in the chemical plant[57–59].

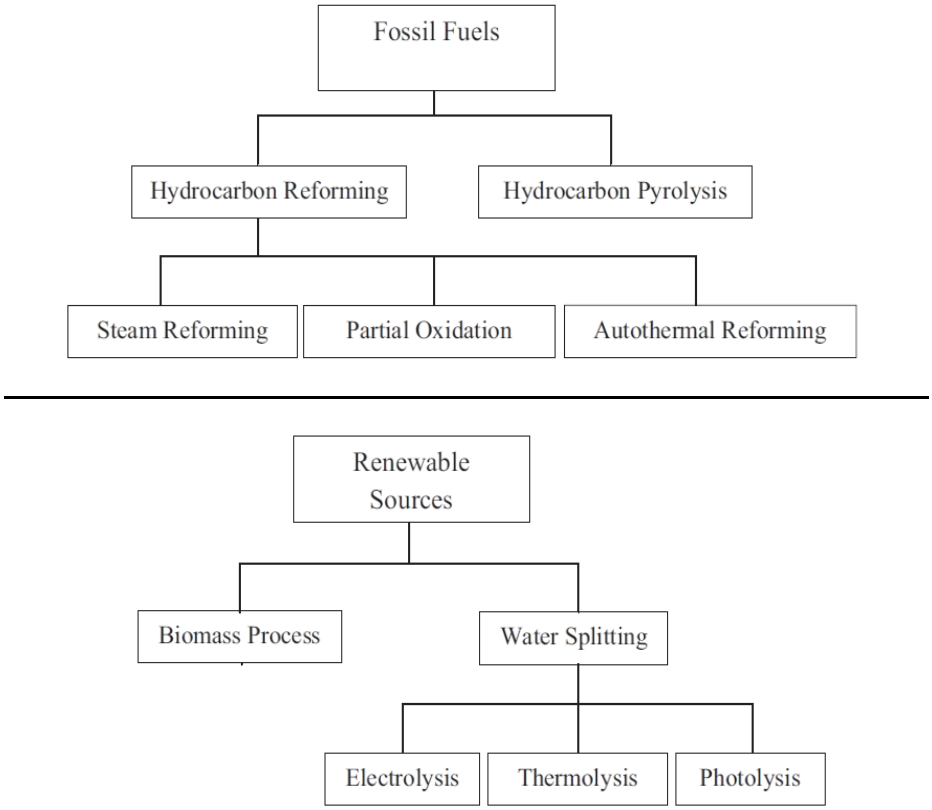

***Figure 1.4.1-A**. Different hydrogen production methods starting from fossil or renewable resources. Adapted from[60].*

Currently, most of the hydrogen is produced through the steam methane reforming (76%), followed by coal gasification (around 23%) and less than 2% is obtained with electrolysis[54]. A short review of these production methods follows.

- Steam Reforming (SR)[60]

SR is a catalytic conversion of hydrocarbons in the presence of steam to produce syngas. Then, a water gas shift (WGS) reactor helps to decrease the CO/H_2 ratio. Eventually, the hydrogen is purified through the pressure swing adsorption (PSA). The process works at high temperature and high pressure; moreover, nickel-based catalysts are used.

Methane is predominantly exploited as raw material for steam reforming (SMR), but also natural gas and light hydrocarbon can be used after a pre-treatment.

$$CH_4 + H_2O \rightleftarrows CO + 3H_2 \quad \text{(SMR)}$$

$$CO + H_2O \rightleftarrows CO_2 + H_2 \quad \text{(WGS)}$$

- Coal Gasification (CG)[60,61]

CG is a partial oxidation where coal is treated with steam and oxygen to obtain syngas. Because of the presence of water in the form of steam, the WGS reaction takes place. Eventually pure hydrogen is obtained thank to PSA.

$$2\,C + O_2 + H_2O \rightleftarrows CO_2 + CO + H_2 \quad \text{(CG)}$$

$$CO + H_2O \rightleftarrows CO_2 + H_2 \quad \text{(WGS)}$$

Coal was historically used as substrate, but also other types of raw materials are suitable, as methane, light and heavy hydrocarbon, and heavy oil residues.

- Electrolysis[60]

Electrolysis is the most promising method to produce hydrogen, even though it is still based on fossil fuels. The advantage of electrolytic processes is that they can rely on sustainable technologies to produce electricity, e.g., solar and wind; in this case they will be cost-competitive with the already-commercial processes based on fossil resources. Electrolytic processes are based on the water-splitting reaction mediated by electricity since it is an endothermic process.

$$2\,H_2O + \text{electrical energy} \rightleftarrows O_2 + 2H_2$$

The most advanced and commercial technologies to exploit electrolysis are alkaline, proton exchange membrane (PEM) and solid oxides electrolysis cells.

1.4.2. Photo-reforming

Photocatalysis is based on the exploitation of the energy coming from the sun, thus it is a sustainable approach to produce renewable energy. The conversion of solar energy into chemical energy can be performed by CO_2 reduction into hydrocarbons or by H_2 production[62]. The possibility to produce hydrogen with new methods respect to the commercial ones is extremely urgent (see *Paragraph 1.4.1*) and photo-reforming presents a valuable alternative. In

addition to that, Rodriguez et al. demonstrated that solar-driven hydrogen production is potentially cost-competitive with the conventional fossil-based processes[63].

H_2 can be produced using water, a renewable and highly available resource, in the water splitting (WS) reaction or exploiting organic substrates as hole scavengers. Considering the thermodynamic, the latter case is less demanding since organic molecules act as sacrificial agents and they have lower oxidation potentials which allow them to consume h^+ faster and thus limit the electron/hole recombination[62] and improve hydrogen evolution (**Reactions 1-3**). Moreover, organic substrates work both as hole scavengers and as proton source, so the overall reactions occurring are the oxidation of an organic molecule (**Reaction 4**) along with proton reduction to H_2.

$$2H^+ + 2e^- \rightarrow H_2 \qquad \text{Reduction half reaction (1)}$$

$$2H_2O + 4h^+ \rightarrow O_2 + 4H^+ \qquad \text{Oxidation half reaction (2)}$$

$$2H_2O + 2O_2 \rightarrow 2H_2 \qquad \text{Overall water splitting (3)}$$

$$C_xH_yO_z + (2x\text{-}z)H_2O \rightarrow (2x\text{-}z+y/2) + xCO_2 \qquad \text{Photo reforming (4)}$$

The reaction of photo-reforming is possible if a semiconductor material is used and if this has a band gap energy at least with the same energy value of the light irradiated. In this case, the light is absorbed by the semiconductor, the electrons are excited and promoted from the valence band (VB) to the conduction band (CB) creating a hole (h^+). To allow the photoreaction, the bottom of the CB of the semiconductor must be more negative than the H^+/H_2 redox half reaction[62,64,65]. In the case of water splitting, the top of the VB must be more positive than the O_2/H_2O half reaction, which is quite difficult because WS is a highly endothermic reaction, so few semiconductors are suitable for this process[62,66]. Conversely, when organic substrates are used, the lower oxidation potential permits an easier reaction from the thermodynamic point of view. So, after the light irradiation, the electron and hole pairs (e^-/h^+) are formed and they move to the surface of the catalyst where they can proceed with the oxidation of organic substrates and the proton reduction, as showed in **Figure 1.4.2-A**.

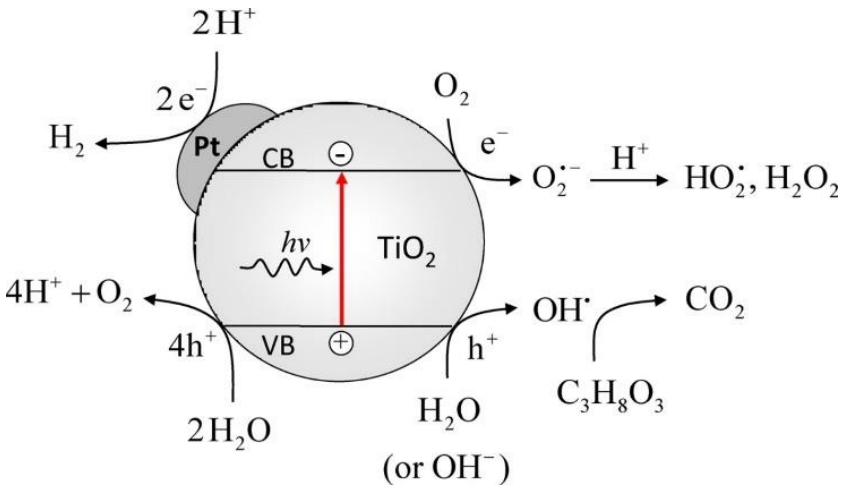

***Figure 1.4.2-A**. Photo-reforming over TiO_2 catalyst with proton reduction and oxidation of organic substrates[67].*

The use of a co-catalyst, obtained by the addition of a metal on the support, can strongly improve the photo-activity[64]. If the loading is too high, the catalytic sites of the semiconductor support will be covered, thus limiting the light absorption. Therefore, a proper amount of metal, usually Pt, Pd, Au or Ag, is required to enhance the activity of the co-catalyst[64]. The metal contributes to charge separation and electrons transportation because the photoinduced e^- are rapidly moved and trapped by the metal species, after the promotion to the CB, further limiting the e^-/h^+ recombination rate[65]. Moreover, the metal species can increase the H_2 production as they are able to reduce protons, as showed in **Figure 1.4.2-A**.

1.5. Glycerol photo-reforming with TiO_2

Glycerol is a suitable substrate for the photo-reforming (PR) reaction as it is produced in huge amounts as a by-product in biodiesel production (see *Paragraph 1.3*). Moreover, glycerol contains three hydroxyl groups which are considered to increase the efficiency of H_2 production in photo-reforming having a dual function. Indeed, they help the absorption on the catalyst working as anchors and they also act as hole (h^+) scavengers[62,67].

Despite the continuous development of new catalysts for PR, titanium dioxide still remains the most used due to its great properties. In particular, it has the proper band gap energy value to be exploited as a semiconductor, even for the water splitting reaction[68]. In particular, the anatase phase is more active than the rutile one because of the faster e^-/h^+ recombination of the rutile polymorph[68]. The main issue associated with TiO_2 in PR is the limited absorption of the sunlight, since its wide band gap allows the absorption mainly in the UV region which is just 5% of the solar spectrum[64].

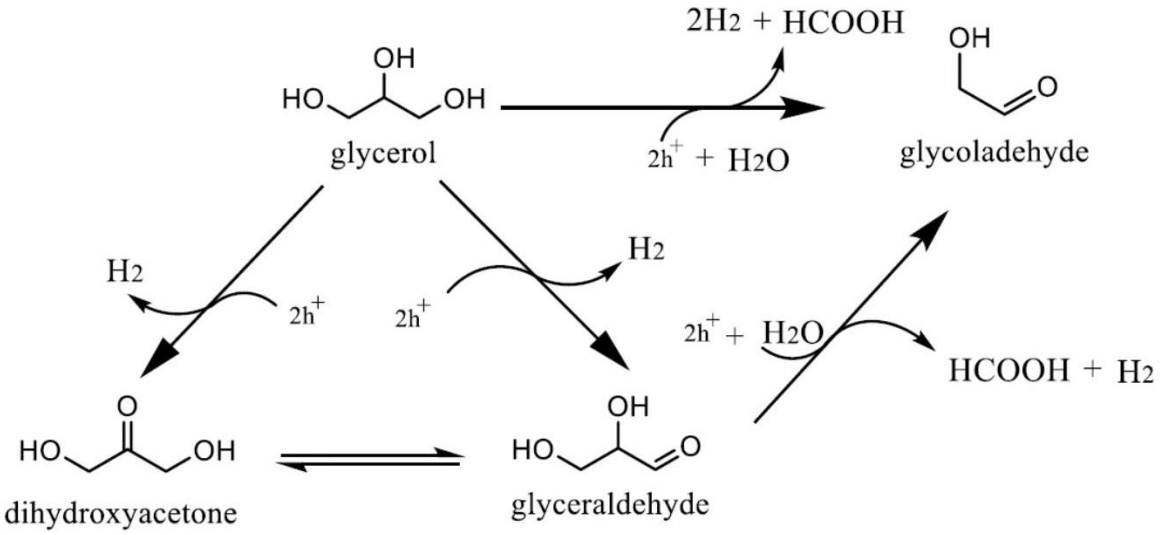

***Figure 1.5-A**. Reaction mechanism for glycerol catalytic photo-reforming[31].*

By irradiation under solar light and with a TiO_2-based catalyst, glycerol undergoes decomposition according to the reaction scheme in **Figure 1.5-A**[31]. Glyceraldehyde is formed as one of the primary products after the cleavage of a C-H bond that results in the formation of a carbonyl group. This is possible because the h^+ sites are trapped by the oxygen surface sites of the TiO_2 lattice and they are able to abstract a hydrogen atom, simultaneously producing H_2

at the cathodic site[69]. Then, the oxidation proceeds to glycolaldehyde and formic acid. Glycolaldehyde can also be obtained directly from glycerol through a direct C-C bond cleavage and producing two molecules of H_2. Another possible primary product is dihydroxyacetone, also formed straight from glycerol through the cleavage of the C-H bond of the secondary hydroxyl group, resulting in a carbonyl group.

2. AIM OF THE PROJECT

This work is aimed at developing a catalyst based on TiO_2 by modifying the syntheses already present in literature. In particular, the goal is to investigate different aspects of the synthesis *via* microemulsion and by doing that, improving the properties of the titania support. Indeed, the characteristics of a catalyst have a fundamental role in its activity, especially the surface area and the bulk density. A high surface area gives access to more sites on the catalyst surface and thus it is correlated to a greater activity. On the other hand, a low bulk density allows the powder to be dispersed more homogeneously, also increasing the light absorption.

Within this project, it is studied how to better control these properties of the titania powder during the ME synthesis by tuning and modifying some key parameters, as the acid used, the hydrolysis and heating time and the possibility to use a base (neutralization approach). The outcome is to synthetize a titania powder with better morphological and chemical properties than the already existing ones, as the commercial titania P-25. Moreover, the possibility to obtain selectively a titania polymorph over the other is investigated by modifying the main parameters of the synthesis, especially the type of acid used and the stirring time (hydrolysis step).

Eventually, the titania supports with the most promising characteristics are tested in the reaction of glycerol photo-reforming to produce H_2 and other valuable liquid products. The photo-catalytic reaction is possible since TiO_2 is a semi-conductor material and can absorb light promoting the oxidation of organic substrates and the reduction of protons to H_2.

3. MATERIALS AND METHODS

3.1. Standard TiO_2 synthesis via microemulsion

The titania is synthetized with the microemulsion approach, in particular, a water-in-oil emulsion is used following the procedure proposed by Maslova et al.[31] (STD synthesis). The continuous phase is composed of Cyclohexane (Sigma Aldrich, ≥95%), while the surfactant is Triton X-100 (Alfa Aesar) and the co-surfactant is Hexanol (Alfa Aesar, 98%). Moreover, Titanium (IV) Tert-Butoxide, TBT, (Sigma Aldrich, 97%) is exploited as the titanium precursor and Nitric Acid (Sigma Aldrich, ≥65%) is used to perform the hydrolysis of the TBT. The water-to-surfactant ratio (Rw) is 21.

Three solutions are prepared separately and the organic precursors are added in the following order: TX-100, hexanol and cyclohexane.

- A: solution containing the organic precursors and the precursor of titanium (TBT),
- B: aqueous solution of nitric acid (5M),
- C: solution of the organic precursors.

Solution B is poured little by little into solution C and stirred until the solution is clear again. Then, solution A is added in the same way to solution BC and the stirring is maintained for 1h. This time will allow the hydrolysis (HYD) of the titanium precursor at the interface of the micelles. After that, the microemulsion is transferred in a round-bottom flask equipped with a thermometer, a stirring system and a refrigerator and then, it is heated up to 72-74°C for 5 hours with reflux. A white precipitate forms in the meantime. At the end the solution is centrifuged at 4500 rpm for 10 minutes and the white solid is washed and dispersed in ethanol. This procedure is performed 5 times. Eventually, the solid is dried in the oven at 100°C overnight and then calcined at 400°C for 3 hours with a ramp of 2°C/minute.

A further synthesis is performed in the same way of the STD one, just changing the hydrolysis (20 minutes) and heating time (1 hour). This synthesis is called R1.

3.2. TiO_2 synthesis via microemulsion through neutralization

In this case, the synthesis is modified with respect to the standard one as a microemulsion containing a base is added to the system. This synthesis is tested with two different bases, Ammonium Hydroxide (Sigma Aldrich, 28.0-30.0%) and Sodium Hydroxide (Sigma Aldrich,

98%, in pellet), and four base/acid ratios (molar) are chosen for each base: 1, 0.9, 0.7, 0.5. The Rw is the same for both microemulsions containing the acid and the base, so that the overall value is 21, as for the STD synthesis.

In this case, a fourth solution containing the base is prepared:

- A: solution containing the organic precursors and the precursor of titanium (TBT),
- B: aqueous solutions of nitric acid (5M),
- C: solution containing the organic precursors,
- D: solution containing the organic precursors and the base (NH_4OH or NaOH).

Solution B is added to C and then BC is poured little by little into solution A and stirred for 20 minutes. This is the hydrolysis step. After that, the solution is transferred inside a round-bottom flask and solution D is added dropwise (1 drop/sec). When ammonium hydroxide is used, this step is usually done with an ice/water bath due to the exothermic reaction that develops for the presence of a strong acid. The following steps are the same described in the STD synthesis, but the heating time with reflux is just 1 hour.

3.2.1. Modifications on the neutralization synthesis of TiO_2

The synthesis with the neutralization approach is tested also with some modifications on the procedure to investigate the effects on the kinetic of the reaction. To do that, the best sample of titania obtained in the previous synthesis is used (S6).

- Synthesis S6-B

The only difference in the procedure is the reversal of order for the addition of the two microemulsions. So, the solution hydrolysed is added dropwise to the microemulsion with the base. The base used is ammonium hydroxide and the base/acid ratio is 0.7. The Rw value is 21. The following steps are the same described in the previous synthesis (*Paragraph 3.2.*).

- Synthesis S6-C

In this case, the hydrolysed solution is added dropwise to the microemulsion containing the base. The base used is ammonium hydroxide and the base/acid ratio is 0.7. At each addition, the acid in the hydrolysed solution is neutralized with a solution of ammonium hydroxide (not a microemulsion), so that the microemulsion with the base is not altered. Hence, for 1 ml of the hydrolysed solution, 1.2 ml of ammonium hydroxide is used to neutralize the acid. The final Rw is 27. The heating temperature in this case is lower (50°C) because above this point the

solution starts to boil vigorously. Eventually, the solution is treated as in the previous synthesis (*Paragraph 3.2*).

3.3. Synthesis of TiO_2 rutile phase via microemulsion

In this case, the procedure is the same described for the STD synthesis (*Paragraph 3.1.*) but after the hydrolysis no further heating treatments are required. Moreover, the titania is prepared with 4 days of stirring (hydrolysis step) following the procedure already reported by Maslova et al.[70] After that, the solution is directly centrifuged and washed with ethanol for 5 times, without the heating step under reflux. Eventually, the sample is dried in the oven at 100°C and then calcined at 400°C for 3 hours.

3.4. Synthesis of TiO_2 rutile phase via microemulsion using HCl

In this synthesis, HCl is used instead of HNO_3. In order to not change too much the STD synthesis procedure, two microemulsions are prepared, one containing the precursor of titanium in microemulsion and the other with the hydrochloric acid (Sigma Aldrich, ≥37%). Then, they are mixed and left under stirring for 24 hours at room temperature. After that, the solution is heated with reflux at 74°C for 5 hours and eventually, dried in the oven at 100°C and calcined at 400°C for 3 h.

3.4.1. Synthesis of TiO_2 rutile phase via microemulsion through neutralization

Ammonium hydroxide is used as the base and it is tested with the best base/acid ratio (0.7) found previously in the syntheses with HNO_3 (*Paragraph 3.2.*), while in this case HCl is used. Moreover, the syntheses are performed with different hydrolysis times, 24h and 16h, maintaining constant the other parameters. So, after the hydrolysis, the microemulsion with the base is added and the solution is kept under reflux at 74°C for 5h.

A further modification consists in reducing both the hydrolysis and heating time to 1 hour. This synthesis is tested both with ammonium hydroxide and sodium hydroxide in base/acid ratio 0.7. Moreover, part of the solution is directly centrifuged after the addition of the base to the hydrolysed solution, while the rest of it is heated at 74°C as usual. The work-up steps are the same previously described for the STD synthesis.

3.5. Characterization techniques

3.5.1. N_2 physisorption (S_{BET})

This technique allows to obtain information about the surface area of the sample and it is performed with the instrument Sorpty 1750 (CE Instruments).

The value of surface area is measured through the N_2 physisorption analysis and BET model. The value obtained after the analysis is divided by the mass weighted to obtain the specific surface area (S_{BET}) in m^2/g. All the samples undergo this analysis after the calcination step, if not specified otherwise.

3.5.2. Diffuse Reflectance Spectroscopy (DRS)

The DRS analysis is performed through a Perkin Elmer Lambda 19 instrument. A quartz cuvette is used to load the solid samples and the analysis works in the wavelength range of visible and ultraviolet light. The Diffuse Reflectance Spectroscopy analyses the reflectance of a solid. For the purpose of this work, the wavelength range of the analysis goes from 800 nm to 200 nm with an interval of 1 nm.

From the reflectance spectra it is possible to calculate the band gap of the sample. The method used is the Tauc plot. First of all, the Kubelka-Munk (**equation 5**) is used to convert the reflectance obtained from the analysis.

$$\mathrm{KM} = \frac{(1-R)^2}{2R} \qquad (\mathbf{5})$$

Then, the Tauc equation is used to calculate the band gap energy value (**equation 6**).

$$\alpha h\upsilon = A(h\upsilon - Eg)^n \qquad (\mathbf{6})$$

where α is the absorption coefficient, h is Planck's constant ($h=6.62607004*10^{-34}$ Js), υ is the frequency of light (s^{-1}), A is the absorption constant and n is a corresponding coefficient that is 0.5 when associated with a direct allowed band gap transition. Since α is proportional to KM function, it is possible to graph a curve and extrapolate the linear part when $(KMh\upsilon)^{1/n} = 0$. This will give the value of the energy band gap (Eg in eV)[71].

3.5.3. X-Ray Diffraction (XRD)

The XRD analysis is carried out with the instrument Philips PW1050/81 equipped with a graphite monochromator and controlled by a unit PW1710 (Cu Kα, λ = 0.15418 nm). The angle range goes from 20° to 80° with a scanning speed of 40°/h. The XRD spectra are analysed with the programme X'Pert High Score Plus.

The XRD spectra give information about the phase composition and crystalline structure of the sample. Moreover, it is possible to calculate the average dimensions of crystallites (d) through the Scherrer formula (**equation 7**). For the purpose of this work, the dimensions of crystallites are considered as the dimensions of particles.

$$d = \frac{k*\lambda}{b*cos\theta} \quad (7)$$

Where k is the particle shape factor and it is fixed at 0.9 considering that a particle is spherical, λ is the X-ray wavelength, b is the Full Width at Half Maximum (FWHM) and θ is the angle.

3.5.4. Gas-Chromatography (GC)

The gaseous products are analysed right after the reaction with an off-line Agilent Technologies equipped with CP Molesieve 5A UM 25m x 0.53mm x 50μm and a TCD detector.
To calculate the total amount of H_2 produced by the reaction, the dead volume of the reactor is taken into account, by knowing the total volume of it. Moreover, H_2 is considered to be present only in gas phase.

3.5.5. High Performance Liquid Chromatography (HPLC)

The liquid phase is analysed after the photocatalytic reaction with an Agilent HPLC over Rezex ROA Organic Acid column (0.0025M H_2SO_4 eluent, oven temperature 30°C and 0.6 mL/min flux) with DAD (λ=202, 223, 250, 284nm) and RID detectors. The calibration of possible components in the liquid phase is required to determine and quantify the reaction products and it is done with commercial standards. Calibration curves of dihydroxyacetone (DHA) and glycerol are obtained from two separate solutions as their peaks may overlap.

The conversion (X%) of the substrate, e.g., glycerol, the yield (Y%) and the selectivity for each product (S%) are calculated according to the following **equations 8-10**.

$$X\ \% = \frac{concentration\ (glycerol)_i - concentration\ (glycerol)_e}{concentration\ (glycerol)_e} * 100 \quad \textbf{(8)}$$

$$Y\% = \frac{\Sigma\ mol\ (product) * SF}{mol\ (reagent)} * 100 \quad \textbf{(9)}$$

$$S\% = \frac{mol\ (product) * SF}{\Sigma\ mol\ (product) * SF} * 100 \quad \textbf{(10)}$$

Where SF is the stochiometric factor and it is equal to 1 for glyceraldehyde and dihydroxyacetone, 2/3 for glycolaldehyde and 1/4 for H_2[70].

3.5.6. Scanning Electron Microscopy (SEM)

The SEM/EDS analyses are performed using the instrument E-SEM Zeiss EVO 50 Series (Carl Zeiss spa) equipped with a microanalysis system INCA Energy 350 EDS (Oxford Instruments Analytical). The voltage used is 20 kV and the collecting time for the spectra is 60 seconds.

3.5.7. Raman Spectroscopy

Raman spectra are recorded at room temperature with a 514 nm Ar^+ laser excitation by Renshaw RM1000 spectrometer equipped with Leica DMLM microscope and CCD camera. Power output was 6.25 mW and grating 1200 lines/mm. The analyses were recorded with the following operative conditions: 50x magnification, low gain, 10% power, time = 15 s, 3 accumulations, frequency range from 0 cm^{-1} to 800 cm^{-1}.

Anatase shows six modes in the vibrational spectrum that are Raman active, which are at 143 cm^{-1} (E_g), 197 cm^{-1} (E_g), 397 cm^{-1} (B_{1g}), 516 cm^{-1} (B_{1g}, A_{1g}), 638 cm^{-1} (E_g). Rutile has four modes that are Raman active and they are at 143 cm^{-1} (B_{1g}), 445 cm^{-1} (E_g), 610 cm^{-1} (A_{1g}); moreover, it displays a broad peak at 240 cm^{-1}, which is a second-order Raman scattering[72].

3.6. Photocatalytic tests

The activity of the TiO_2 catalyst is tested in the photo-reforming of glycerol. The overall set-up is presented in **Figure 3.6-A** and it is described as follows. The reaction is performed inside a sealed top-irradiated glass photo-reactor with a circulating ethylene glycol bath to control the temperature, an inlet and outlet for gaseous products, a stirring system at the bottom and a quartz disk on top.

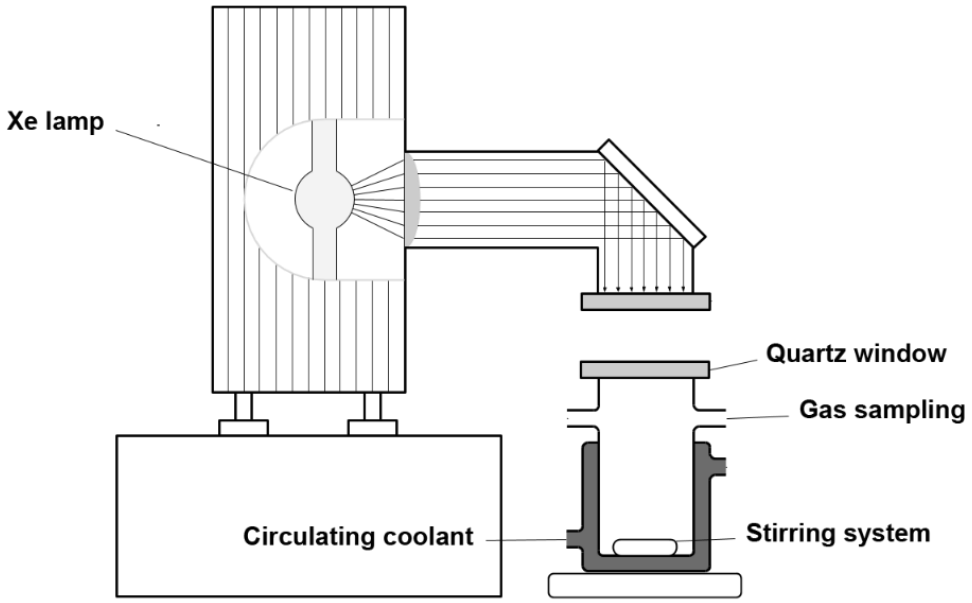

***Figure 3.6-A**. Set-up of the photo-reactor and the solar simulator used during the photocatalytic tests*[70].

Above the reactor, the solar simulator LS0306 by LOT Quantum Design is placed and it is equipped with a 300 W Xe-lamp that generates light in the range 250-2500 nm. The light is delivered as 40 mm diameter collimated beam. As reference for the solar radiation the AM1.5G spectrum is used, following the directions ASTM G-173-03. The solar spectrum AM1.5G represents an average between the solar radiation when the sun is at its zenith and when it is at the horizon. As it is presented in **Figure 3.6-B**, the emission spectrum of the solar simulator is not the same as the solar spectrum itself, especially in the range 450-470 nm and in the infrared zone, but it is sufficiently similar to be used for the scope of this work.

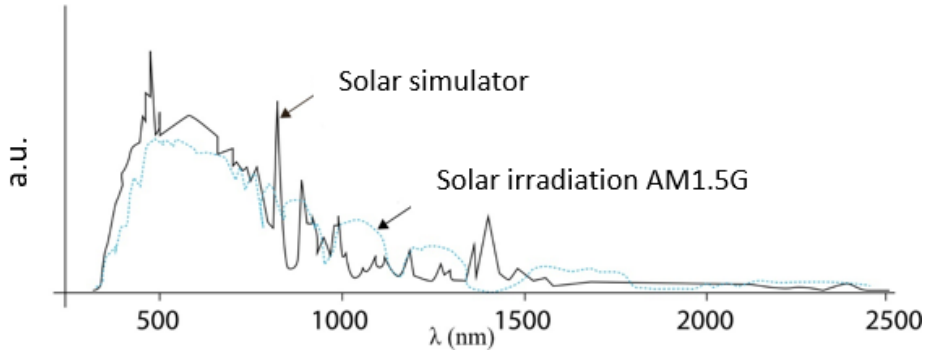

***Figure 3.6-B**. Comparison between the spectrum of the solar simulator used in this project and the solar spectrum AM1.5G.*

To perform the photocatalytic tests of glycerol reforming the following procedure is used.

- A solution of glycerol 1M is prepared and 21.5 mL of it are added to the reactor,
- The ethylene glycol bath is connected to the reactor and set-up at 30°C,
- The catalyst is weighted in order to obtain a concentration of 0.5 $g_{catalyst}$/L and added to the solution inside the reactor,
- The reactor is closed with a quartz disk and kept under nitrogen flux to work with inert conditions for 20 minutes to reach the thermodynamic equilibrium,
- The reactor is sealed and pressurized up to 0.5 bar to verify that it is gas-tight, eventually the reaction starts when the solar simulator is switched on.

The solution inside the reactor is continuously mixed thank to a magnetic stirrer to maintain a homogeneous slurry. The reaction proceeds for 6 hours and after that the gaseous and liquid products are analysed with the GC and HPLC respectively.

A summary of the operative reaction conditions is provided in **Table 3.6-A**. In particular, the concentration of the titania powder is 0.5 g/L since it is already reported in literature for the same type of reactions with glycerol[31,70].

Catalyst concentration	0.5 g_{cat}/L
Glycerol concentration	1 M
Reaction time	6 h
Pressure	Atmospheric pressure
Temperature	30°C
Reaction environment	Inert (N_2)

***Table 3.6-A**. Operative conditions for the photo-catalytic reforming of glycerol using TiO_2-m.*

3.6.1. Transmittance tests

Two probes (Radiometer HD2102.2 DELTA OHM) are used to measure the intensity of light at different concentrations of the TiO_2 catalyst in the solution (solvent and substrate). The two probes enable to have values of the light transmitted both in the UV and visible range of the spectrum. Therefore, the first one works between 1000 nm and 400 nm and the second one between 400 nm and 300 nm.

3.6.2. Calculation of Quantum Efficiency

The Radiometer HD2102.2 DELTA OHM with the two probes, one in the UV range and the other in the visible range of the spectrum, are used to perform this analysis. In particular, the transmitted and scattered light is measured. Moreover, a filter for the lamp of the solar simulator is used to work at one wavelength. Two filters are available, the former at λ=365 nm and the latter λ=400 nm. In both cases, the transmitted light is measured as the light that passes directly through the system, so from the source of the lamp to the bottom of the reactor. While, the scattering of the light beam is detected from the side of the system perpendicularly, as it is the light deflected. The reactor is covered with a black cloth.

4. RESULTS AND DISCUSSION

Different titania samples were synthesized with the microemulsion technique modifying the synthetic procedure with the aim of understanding the change in the material characteristics and the influence on the final properties of the catalysts.

During the synthesis of titania *via* microemulsion, there are some parameters that can be tuned to modify the final physical-chemical characteristics of the powder and they are:

- Neutralization of the acidic ME with a base and the type of base used,
- Acid chosen to hydrolyse the TBT,
- Hydrolysis time (HYD), so for how long the ME will be stirred at room temperature,
- Heating time at 74°C with reflux,
- Order of addition of the components.

A summary of the modifications performed on the STD synthesis of titania with a W/O microemulsion is presented in **Table 4-A**.

	Synthesis	ME components	Operative conditions
Synthesis 3.1	STD, R1	TX, cyclohexane, hexanol, TBT, HNO_3	Stirring for 1h or 20 minutes (HYD) and heating for 5 h or 1h
Synthesis 3.2	Neutralization with different base/acid ratios	TX, cyclohexane, hexanol, TBT, HNO_3, Base (NH_4OH or NaOH)	Stirring for 20 minutes (HYD) and heating for 1h
Synthesis 3.3	Rutile polymorph	TX, cyclohexane, hexanol, TBT, HNO_3	Stirring for 4 days (HYD). No heating treatment
Synthesis 3.4	Rutile polymorph	TX, cyclohexane, hexanol, TBT, HCl	Stirring for 24h (HYD) and heating for 5h
Synthesis 3.5	Rutile polymorph via neutralization	TX, cyclohexane, hexanol, TBT, HCl, Base (NH_4OH or NaOH)	Stirring for 24h, 16h or 1h (HYD) and heating for 5h or 1h

***Table 4-A**. Summary of all the syntheses performed and their operative conditions.*

4.1. Synthesis of titania with the neutralization approach

The STD synthesis (*Synthesis 3.1) via* microemulsion exploits HNO_3 as it helps to regulate the relative velocities of hydrolysis and condensation. The reactivity is enhanced because there is a biphasic system (see *Paragraph 1.1.1*). The TBT precursor is highly soluble in the organic phase, while water is confined inside the micelles. TBT and water will react in the hydrolysis step and the hydrolysed molecules will condensate forming Ti-O-Ti dimers[30]. The aim of the acid is to slow down the hydrolysis, so that the overall process is controlled by the condensation. If the acid was not inserted in the system, the hydrolysis would be so fast that a control over the particles properties would not be possible. By introducing a base, it is possible to neutralize the acid and thus its addition helps to tune the final characteristics of the titania, especially the particles dimensions. Since the final goal is to use the ME-synthetized titania as a photo-catalyst, some fundamental properties are analysed to find the most suitable samples. In **Table 4.1-A**, the main parameters studied are presented for all the samples obtained through the STD synthesis (*Paragraph 3.1*), its modification R1 and for the ones synthesised with the neutralization approach (*Paragraph 3.2*).

The hydrolysis and heating time used in the neutralization syntheses with a base were previously optimized and the optimal ones turned out to be 20 minutes and 1 hour, respectively[73]. The optimization was done modifying the STD synthesis by decreasing the time and obtaining the R1 sample. This titania powder is composed just of anatase, with no rutile, which is associated to longer stirring and reflux time as it is the thermodynamically favoured product. Furthermore, the dimensions of crystallites in the R1 sample are smaller than the ones in the STD. This is probably due to the fact that there are less hydrolysed sites and less effective collisions between particles due to the shorter reaction time and this prevents their coalescence maintaining the narrow dimensions.

In the neutralization approach, the base is added at first in stoichiometric amount (molar) with respect to the acid, but then different base/acid ratios are tested in order to find a possible trend and the best ratio to obtain the optimal characteristics in the powder.

Sample	Bulk Density (g/ml)	S_{BET} (m^2/g)	Band Gap (eV)	TiO_2 crystalline phase	d_{XRD} Anatase (nm)	d_{XRD} Rutile (nm)
STD	1.2	135	3.08	A=95%; R=5%	10	9
R1	0.88	115	2.96	Anatase	7	/
S1	0.99	158	2.91	Anatase	10	/
S2	0.75	87	2.95	A=91%; R=9%	9	18
S3	/	85	2.92	A; R (*)	/	/
S4	0.76	144	2.96	A=66%; R=34%	7	26
S5	0.73	29	2.89	A=85%; R=15%	5	12
S6	0.58	197	3.04	Anatase	8	/
S9	0.69	149	3.09	Anatase	10	/
S10	0.66	39	3.00	A=92%; R=8%	15	60

Table 4.1-A. *Summary of the main characterization data obtained from the titania samples synthetized through the neutralization approach with HNO_3. The S_{BET} is measured on the samples after calcination. The d_{XRD} values express the dimensions of crystallites. (*) In this case, it was not possible to calculate the percentage for each polymorph and the dimensions of crystallites.*

In the following paragraphs, the different properties of the synthesized titania samples and the influence of the reaction parameters will be discussed. If not specified, all the following analyses are performed on the titania powders after calcination at 400°C for 3h.

- XRD analysis

The XRD analysis allows to gather information about the crystalline phases contained in the samples, as titania presents three different polymorphs (anatase, rutile and brookite). Anatase and rutile are the most common forms and generally; moreover, anatase is more active in photocatalytic degradation than rutile[74]. Anyway, in the last years, many studies focused on the combination of anatase and rutile since it was proved to enhance the photoactivity of titania with respect to the pure form[75,76]. Also, the commercial titania P-25 is formed by a mixture of anatase (80%) and rutile (20%), as well as the STD sample[27,31,70]. In this context, it is interesting to synthetise titania powders containing pure anatase, or rutile, and compare their photoactivity with the commercial TiO_2 P-25 or the STD sample. So, the XRD analysis is needed to understand which polymorphs is obtained and in which percentages, and thus whether a synthesis can be selective for the development of a pure form of titania or not.

Moreover, from the XRD spectra it is possible to calculate the dimensions of crystallites in the sample through the Scherrer equation (*Paragraph 3.5.3*) and, within the scope of this project, they are considered equal to the dimensions of the titania particles.

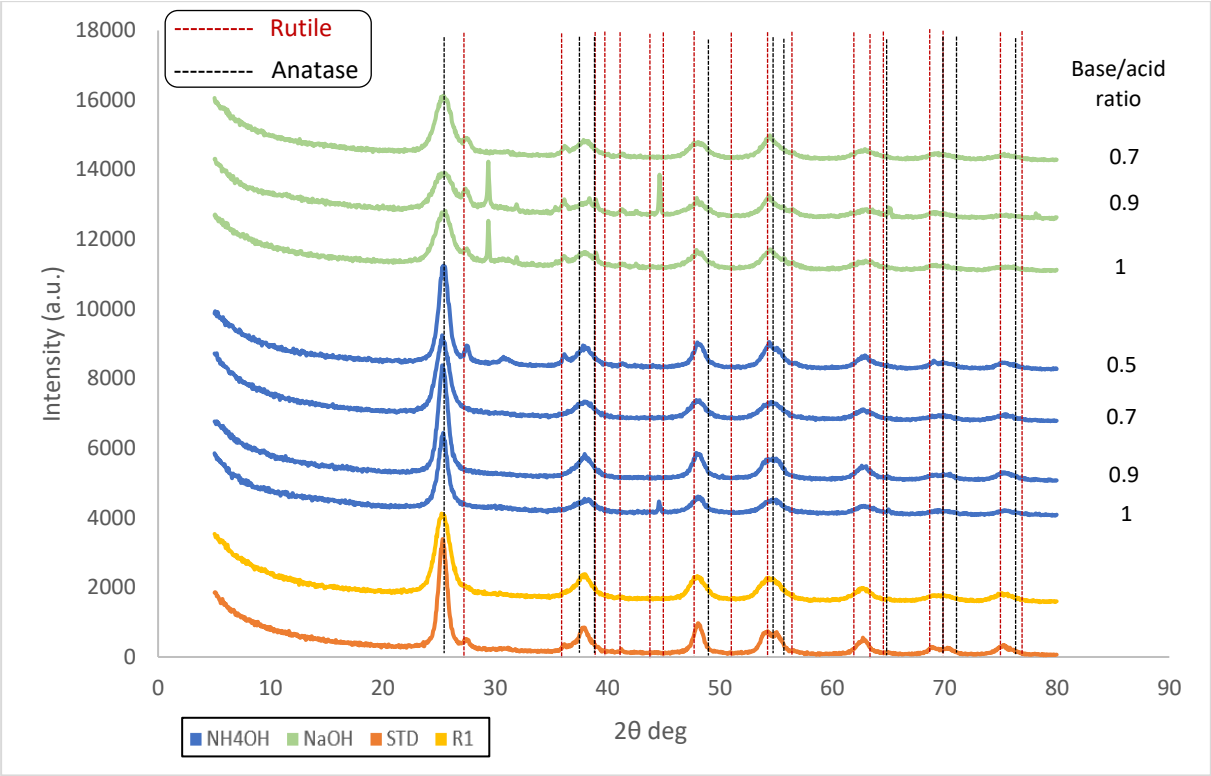

Graph 4.1-A. *Comparison of XRD spectra for the samples obtained through the neutralization syntheses, the STD sample (orange) and its modification (yellow). The spectra in blue are obtained from the NH_4OH samples, while in green are from the NaOH ones. The rutile and anatase reference patterns are also inserted in the spectrum.*

Graph 4.1-A shows a comparison of all the samples obtained through neutralization, the R1 and the STD ones. In order to clearly identify the crystalline phases of titania, the reference patterns, characteristic of anatase ad rutile, are displayed on the graph. Brookite was not detected, so its reference pattern is not inserted. Anatase is present in all the samples analysed; moreover, in the ones obtained with NH_4OH and a base/acid ratio equal to 1, 0.9 and 0.7, it is the only polymorph. Conversely, in the remaining sample with NH_4OH (0.5), in the ones synthetised with NaOH and in the STD sample, also rutile is present, even though it covers a minor percentage. In these cases, it is also possible to measure the amount of each crystalline phase, resulting that anatase is the main polymorph in every sample of titania. Analysing the R1 sample, it is possible to notice that only anatase is present. This can be explained by a shorter reaction time (both for the hydrolysis and for the heating step) that prevents the formation of rutile since this is the thermodynamic stable form of titania[27]. Instead, when the neutralization with the base is added as a variable in the synthesis, especially NaOH, the shorter reaction time seem to play a marginal role because also a small percentage of the rutile is formed in some of the samples.

The data for the dimensions of the crystallites are presented in **Graph 4.1-B**. Firstly, it is worth noticing that it was possible to synthetize titania particles with nano dimensions through the microemulsion method. Overall, the crystallites dimensions for the anatase phase are comparable, even though the samples prepared with NaOH show slightly narrower values. In this case, the quantity of rutile is higher with respect to the other samples and this can limit the growth of the anatase crystallites, also considering the wider dimensions of the rutile crystallites. Indeed, when analysing the rutile phase, the dimensions of crystallites are way bigger than the ones of anatase and these values are also more scattered. The higher is the content of rutile in the sample, the broader the dimensions of its crystallites will be.

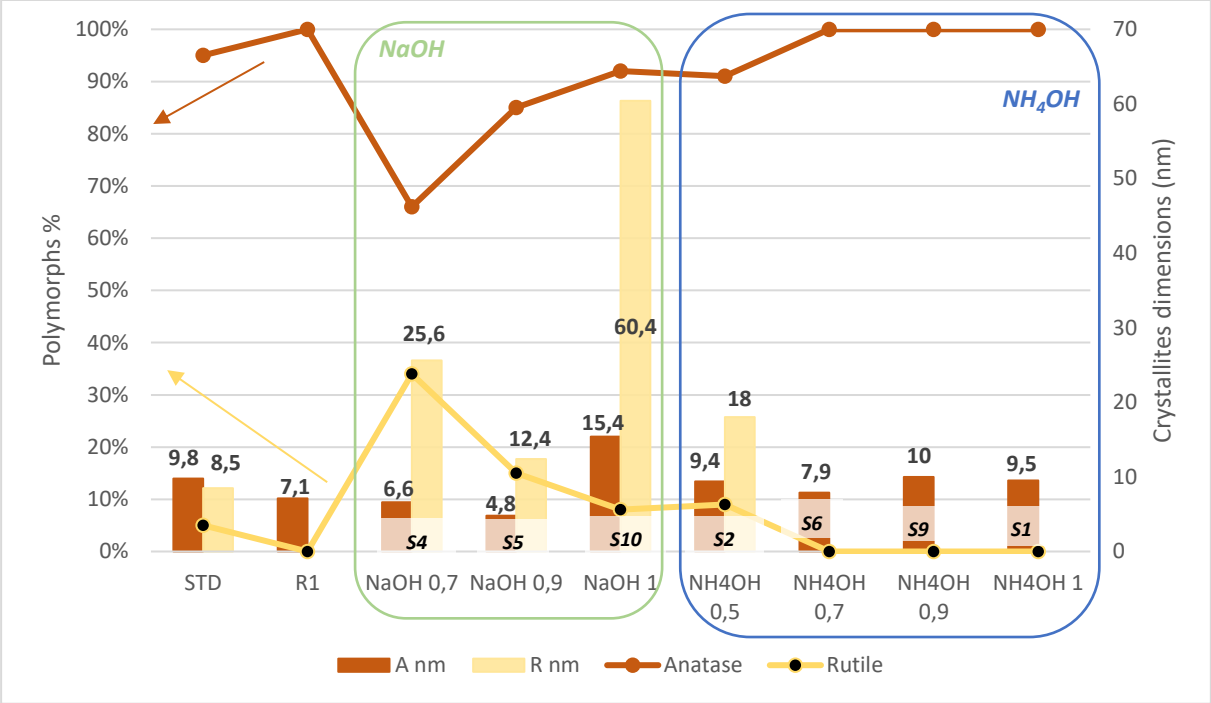

***Graph 4.1-B**. Comparison for the dimensions of crystallites in the STD sample, its modification R1 and the samples from the neutralization syntheses. Also, the percentage of crystalline phase is added for each sample. These data are obtained from the XRD spectra in Graph 4.1-A. The straight line is for the polymorph percentage, while the bars are for the dimensions of crystallites. A=anatase, R=rutile.*

For the sample prepared with NaOH and the lowest base/acid ratio (0.5), it was not possible to perform the XRD analysis due to the low yield of the synthesis. Consequently, a Raman analysis is carried out and it confirms the presence of both anatase and rutile in the titania powder. Thus, also with this base/acid ratio (0.5), the presence of NaOH in the synthetic process allows to

obtain both crystalline phases, as it is shown in **Graph 4.1-B** for the other samples synthesised with NaOH.

- Bulk Density

The bulk density may be a factor that influences the progression of the reaction in the photo-reforming because a better dispersion of the powder in the aqueous media will result in a stronger absorption of the light per gram of catalyst. Thus, it is important to measure this parameter to ensure a homogeneous distribution of the powder in the reaction slurry. The measurement is done by putting the solid inside a graduated test tube. The volume is read and then the test tube is weighted. By the ratio of the mass and the volume, the bulk density is obtained.

Graph 4.1-C shows the comparison of bulk densities for all the samples prepared with the standard synthesis (STD), its modification (R1, *Synthesis 3.1*) and the neutralization ones. These last samples are grouped considering the base/acid ratio, so that a comparison between the two bases used is possible.

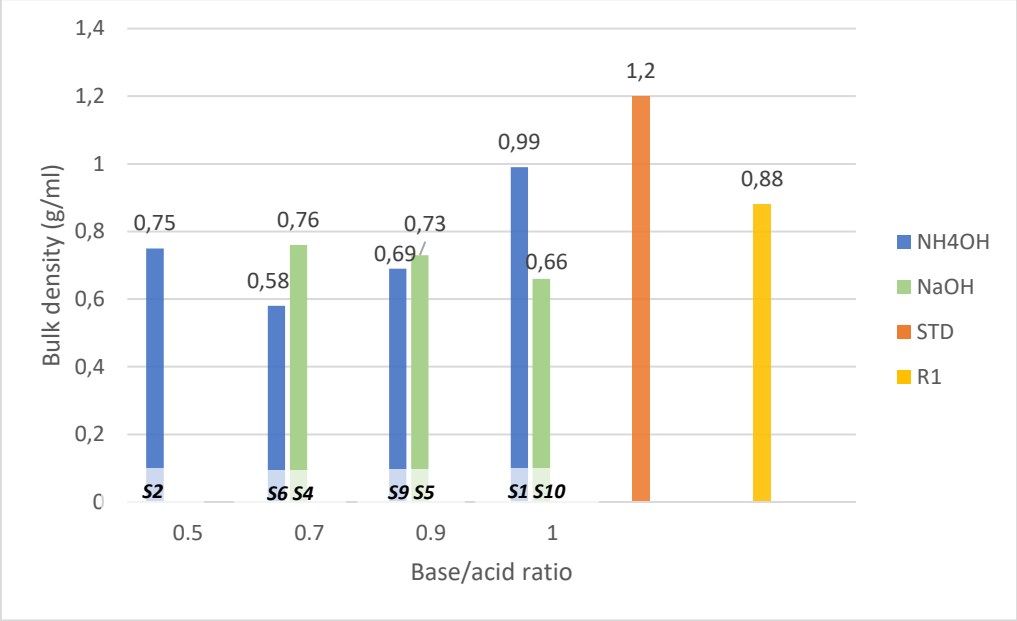

***Graph 4.1-C**. Comparison of bulk density for the samples obtained through the neutralization syntheses, the STD one (orange bar) and its modification R1 (yellow bar). The bars in blue represent the syntheses with NH_4OH, while the ones in green are for the syntheses with NaOH. The name of the samples is also reported at the bottom of each bar.*

For the sample S3 (NaOH with base/acid ratio 0.5) it was not possible to calculate the bulk density because, due to the low yield of the synthesis, the amount of solid was not enough to be read in the graduated test tube. All the samples obtained with the neutralization syntheses and the sample R1 have a bulk density lower than 1 g/mL. The STD sample, synthetized without neutralization, has the highest bulk density (1.2 g/ml) among the set of samples analysed. This can be attributed to the longer stirring time in the STD synthesis respect to the others. Longer hydrolysis times could lead to the coalescing of titania nuclei forming more packed and dense aggregates. The sample S6 (NH_4OH with base/acid ratio 0.7) has the lowest bulk density among the titania powders. In general, for the sample prepared with NH_4OH as a base, it is not possible to define a trend that correlates the bulk density with the base/acid ratio. On the other hand, the samples prepared with NaOH as the base for the neutralization, show comparable values for the bulk density.

For comparison, it is reported than none of the previous samples presents a bulk density comparable to the value of the commercial titania P-25 (0.1 g/ml). The bulk density of the P-25 titania is particularly interesting, since it allows to obtain a homogeneous slurry of the powder in the reaction media, enhancing the mass transfer phenomena and the light absorption during the photo-catalytic reaction. Moreover, the synthesis of a titania sample with a bulk density so low will permit to compare different studies. This is usually not possible because of the dense titania powder synthetized during the research projects.

- Specific Surface Area (S_{BET})

The specific surface area is a key parameter for a catalyst because it allows to obtain a wider contact between the catalyst and the reagents. Indeed, a high surface area is related to an increased number of active sites available on the catalyst, thus a greater ability for compounds to be adsorbed on the surface[25,77]. **Graph 4.1-D** displays the values for the specific surface area of the STD sample, its modification R1 and the neutralization samples.

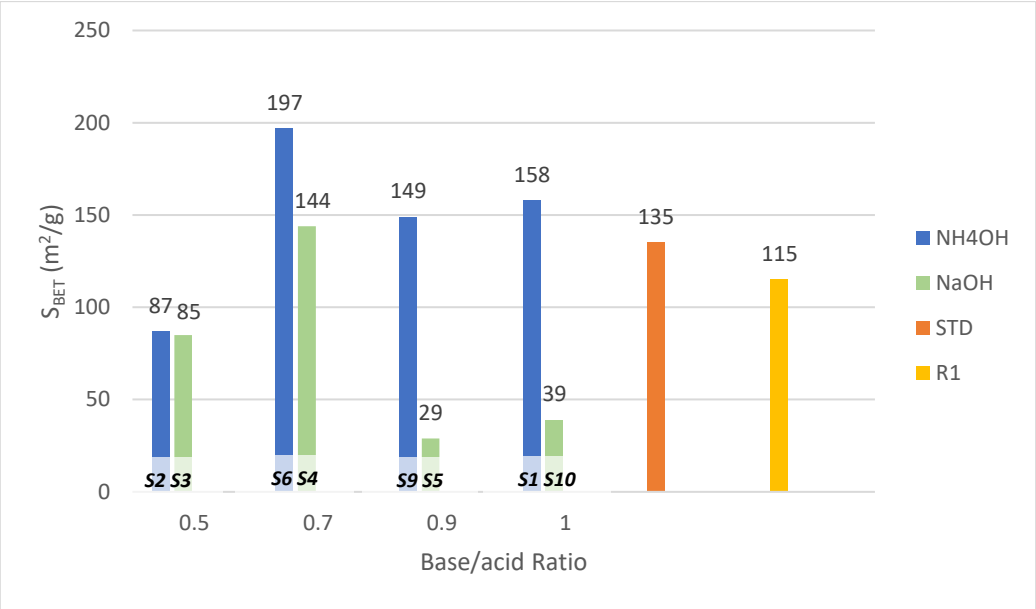

***Graph 4.1-D**. Comparison of specific surface area (S_{BET}) for the samples obtained via the neutralization syntheses, the STD one (orange bar) and its modification (yellow bar). The bars in blue represent the syntheses with NH_4OH, while the ones in green the syntheses with NaOH. The name of the samples is also reported at the bottom of each bar.*

The STD sample has a specific surface area slightly lower than the one obtained in the study followed for the STD synthesis[31], which shows a value of 160 m^2/g. Probably some parameter was not controlled properly during the synthesis. It has also to be considered that, in this project, the STD sample synthesis was scaled up since it was possible to standardize it. Thus, the scaling of the synthesis could have affected some parameters of the catalyst, such as the surface area. Anyway, this value is consistent with other studies performing the same synthesis[27,70]. Concerning the neutralization syntheses, for both bases the samples with the lowest base/acid ratio (0.5) do not give high values of specific surface area, at least not comparable with the STD sample. On the other hand, the samples with the intermediate base/acid ratio (0.7) show promising results, as the specific surface area is even higher than the STD sample one. The same goes increasing the NH_4OH/acid ratio up to 1. Otherwise, the same sample synthetised with NaOH (base/acid ratio 1) gave the worst result in terms of specific surface area, along with the sample obtained with the base/acid ratio 0.9. In general, the samples where NH_4OH is used exhibit higher values of specific surface area with respect to the ones with NaOH, especially as the base/acid increases. This can be explained by the presence of $NaNO_3$ salts that were not efficiently removed during the work-up steps of the synthesis as it is confirmed by the XRD analysis. Overall, it seems like the utilization of a base might increase the surface area with respect to the STD sample, probably due to a higher nucleating rate, which is responsible for

the formation of titania nanoparticles in an ordered structure[30]. Anyway, the base/acid ratio must be taken into consideration since there is a maximum value of surface area for both bases tested, and above that, the values will decrease. Moreover, from both **Graph 4.1-C** and **4.1-D**, a correlation between the surface area and the bulk density can be drawn, since when the former decreases, the latter rises.

- DRS spectra and Band Gap calculation

The light absorption properties of the samples were analysed by UV-VIS analysis. This is a fundamental property in photocatalytic reactions and can deeply influence the catalytic activity. The spectra presented in **Graph 4.1-E** are obtained by the UV-VIS analysis of all the samples of titania synthetized through the neutralization synthesis. All the spectra show a drop in reflectance around 400 nm; thus, the absorption range goes from 400 nm to 200 nm, in the UV region. Sample S1 and S6, both synthetized with NH_4OH, have a slightly different trend. This is correlated with the colour of the powder. Indeed, all the sample are white except for the samples S1 and S6, that are light yellow. This could be the reason why the reflectance decreases earlier and they tend to absorb already in the visible part of the spectrum. The different colour could be an indicator of the presence of nitrogen in the crystalline structure of titania, as it is reported in literature[78–80]. When the base/acid ratio is 0.5 the resulting powder is white, so probably the amount of base, contributing to the N-doping, is not enough to be inserted in the crystalline structure.

The **Graph 4.1-F** displays the values for the band gap calculated for each neutralization sample with the Kubelka-Munk method (see *Paragraph 3.5.2*). They are compared to the band gap of the STD sample and the sample R1. Overall, the band gaps are comparable among them and similar to the STD sample. Moreover, they are also consistent with the data found in literature[70,71] and with the value of band gap for the commercial titania P-25, that turns out to be 3.15 eV.

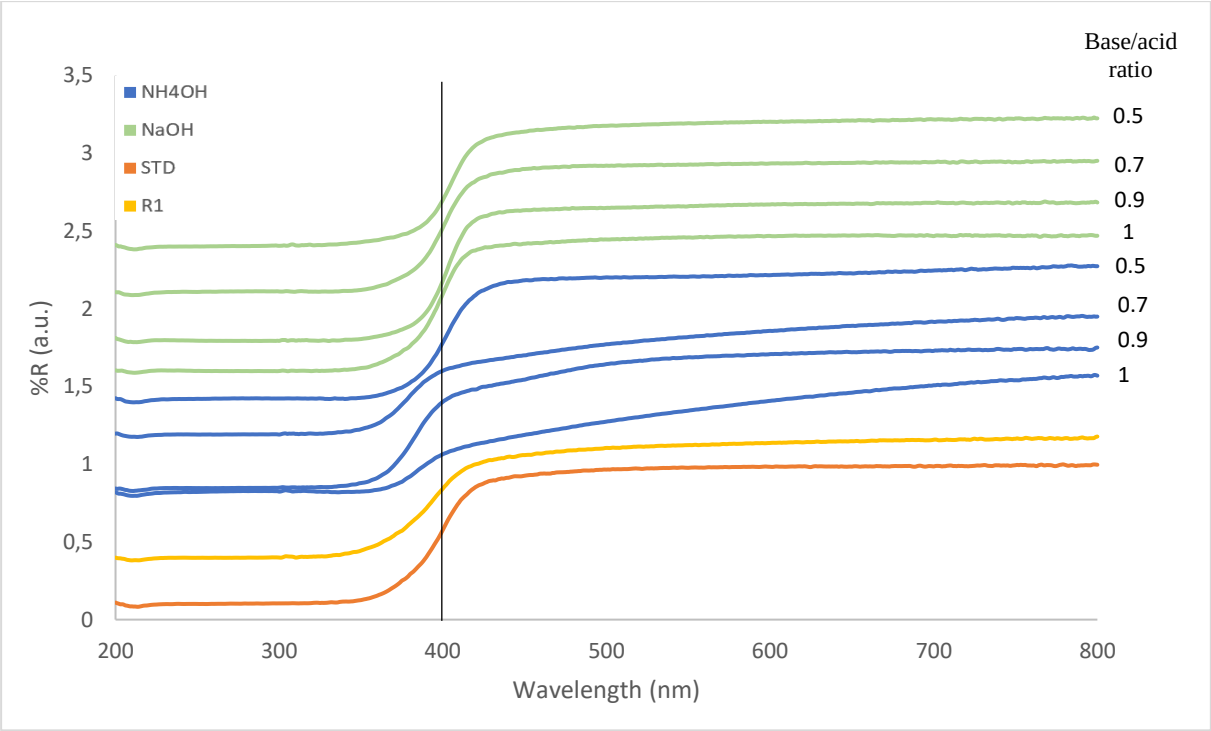

***Graph 4.1-E**. DRS spectra of TiO_2-m obtained via the STD (orange curve), its modification R1 (yellow curve) and the neutralization syntheses. The curves in blue represent the syntheses with NH_4OH, while the ones in green are for the syntheses with NaOH. The base/acid ratio of each sample is expressed directly on the graph.*

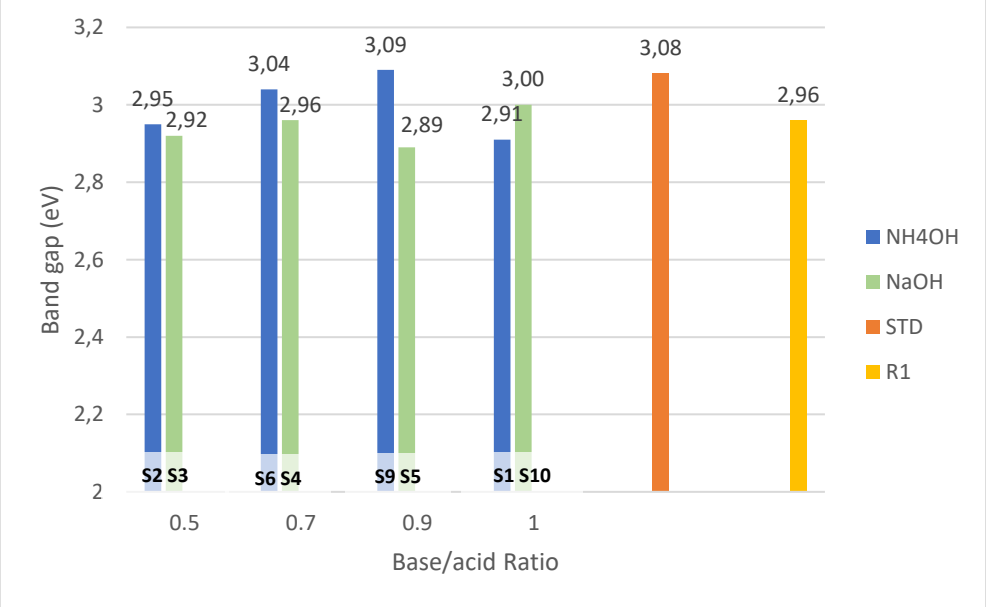

***Graph 4.1-F**. Comparison of band gap for the samples obtained through the neutralization syntheses, the STD sample (orange bar) and the modification of the STD one (yellow bar). The bars in blue represent the syntheses with NH_4OH, while the ones in green are for the syntheses with NaOH. The name of the samples is reported at the bottom of each bar.*

4.1.1. Further investigations on N-doped TiO_2

The possibility to synthetize a N-doped TiO_2 is highly interesting since it may have better properties with respect to the regular titania, as many studies have already reported[81–84]. Some research analysed the properties of N-doped titania through different characterization techniques. In general, it is reported that the presence of nitrogen in the titania crystalline structure is affecting the colour of the powder, turning it into yellow[78,80]. Therefore, the absorption of light in the visible range has been widely studied since it increases if nitrogen is present in the crystalline structure of titania[78,80,85]; while bare TiO_2 absorbs predominantly in the UV range of the spectrum.

As previously showed in this project, the samples synthesised with NH_4OH and a base/acid ratio greater than 0.5 (0.7, 0.9 and 1), all present a pale-yellow colour and a lowering in reflectance around 650 nm (**Graph 4.1-E**), thus confirming the absorption in the visible light range of the spectrum.

In general, the XPS analysis will allow to know the actual composition of the titania powders and so the effective presence of nitrogen in the samples, but this instrument was not available during the course of this project. Anyway, other characterization techniques can be used as support data for the detection of nitrogen in the titania samples.

Jia et al. performed an EDS-SEM analysis with N-mapping showing, the effective incorporation of nitrogen in the titania crystalline structure[85]. The same analysis is carried out on the samples S6 and S1 (NH_4OH with base/acid ratio 0.7 and 1, respectively), but nitrogen is not detected, probably due to its presence in low amounts.

An increased photo-activity is generally associated with N-doped titania-based catalyst with respect to bare titania, as reported in literature[81,83,85]. This effect is noticed for the sample S6, but not for the S1 one (see *Paragraph 4.3.2*, **Graph 4.3.2-A**), so it is possible that other properties of the titania powders influence the photo-activity of the titania catalysts, as the surface area which is greater for the sample S6.

Wang et al. noticed a Raman positive shift of 6.5 cm^{-1} for a TiO_2 sample containing oxygen vacancies with respect to a reference sample[86]. An O-vacancy may be created when the doping with N is obtained. Indeed, Cheng et al. observed a Raman shift of a N-doped TiO_2 sample with respect to a reference sample of bare titania[87]. Therefore, the sample S6 and S1 are analysed with the Raman spectroscopy. The STD sample and the commercial titania P-25 were also

tested and used as the reference samples. A positive shift of 3 cm^{-1} for the main peak of anatase is observed for the sample S6 with respect to the STD sample; moreover, a positive peak shift of 5.5 cm^{-1} is noticed with respect to the reference P-25 sample. This indicates the presence of oxygen vacancies which could have formed as a result of the N-doping. Conversely, the S1 sample only shows a 2.5 cm^{-1} positive shift with respect to the commercial P-25, that is the same value obtained for the STD sample. This difference in the shift values of the two yellow samples (S6 and S1) can explain the greater activity of the sample S6 over the S1 one, since a higher amount of oxygen vacancies is present in the sample S6.

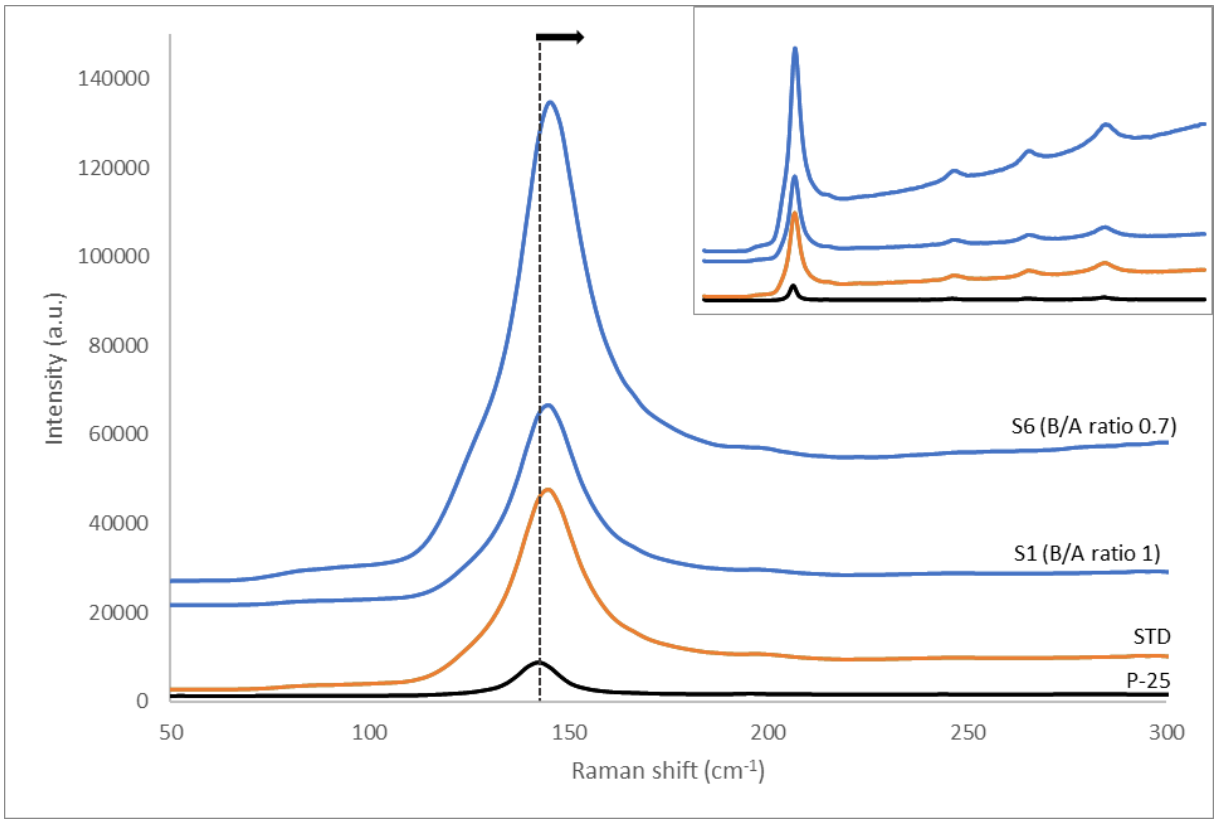

***Graph 4.1.1-A**. Raman spectra for the samples prepared with NH_4OH and the base/acid ratio 0.7 and 1. The STD sample and the commercial P-25 are inserted for reference.*

To sum up, the presence of nitrogen in the yellow-coloured TiO_2 samples has been supported by the UV-VIS spectra and by an increased photo-activity, while the Raman spectra only showed the presence of oxygen vacancies. A XPS analysis would definitively confirm the effective synthesis of N-doped titania powders and it will be carried out as soon as the instrument is available.

4.1.2. Modifications of the operative conditions on the synthesis of S6

As previously mentioned, the synthesis S6 was modified in two ways, obtaining the samples S6-B and S6-C. The aim is to investigate whether different operative conditions affect the kinetic of the reaction and if, eventually, there is an effect on the titania nanoparticles formation and properties. The order of addition of the components and microemulsions was previously studied and used in this project as defined in Paragraph 3.1, but different set ups are also considered. So, the synthesis S6-B analyses the effect on the modified order of addition of the two microemulsions, one with the acid and the other with the base (**Figure 4.1.2-A**). On the other hand, the synthesis S6-C is designed to limit the action of the acid by being directly neutralized to avoid the alteration of the micelles containing the base (**Figure 4.1.2-B**). Also in this case, there is an outcome on the kinetic of the reaction.

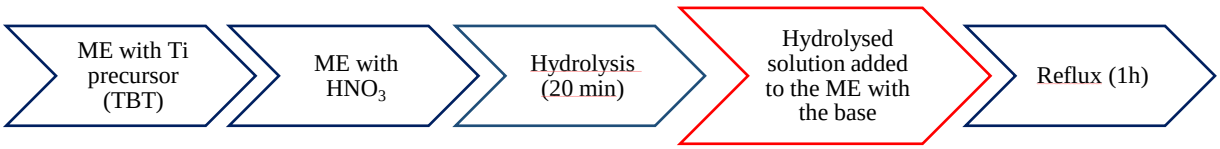

Figure 4.1.2-A. *Operative scheme for the synthesis S6-B which is a modification of the synthesis S6.*

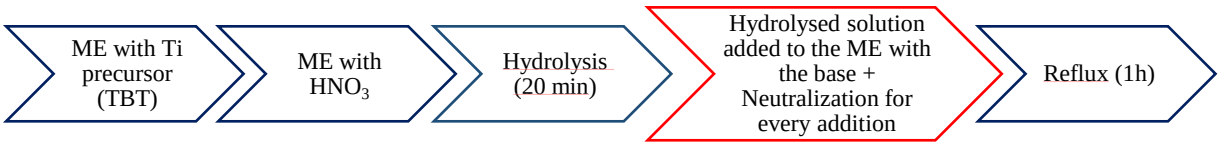

Figure 4.1.2-B*. Operative scheme for the synthesis S6-C which is a modification of the synthesis S6.*

The properties of the powders for the samples S6-B and S6-C, obtained after calcination, are studied and the data from the characterization analyses are presented in **Table 4.1.2-A**.

Sample	**Bulk Density (g/ml)**	**S_{BET} (m^2/g)**	**Band Gap (eV)**	**TiO_2 crystalline phase**	**d_{XRD} Anatase (nm)**	**d_{XRD} Rutile (nm)**
S6	0.58	197	3.04	Anatase	8	/
S6-B	0.79	90	3.05	Anatase	6	/
S6-C	0.82	100	3.02	Anatase	7	/

Table 4.1.2-A. *Summary of the main characterization data obtained from the titania samples synthesised with the modifications on the synthesis S6. The S_{BET} is measured on the samples after calcination. The d_{XRD} values express the dimensions of crystallites.*

The XRD spectra (**Graph 4.1.2-A**) are equal to the one of the S6 sample and the anatase phase is present as the only polymorph in both samples. Rutile is not detected, so also in this case the synthesis is selective for just one crystalline phase. The data for the dimensions of crystallites are presented in the **Graph 4.1.2-B**. In general, the crystallites are slightly smaller than the original S6 sample, but all the values are still comparable.

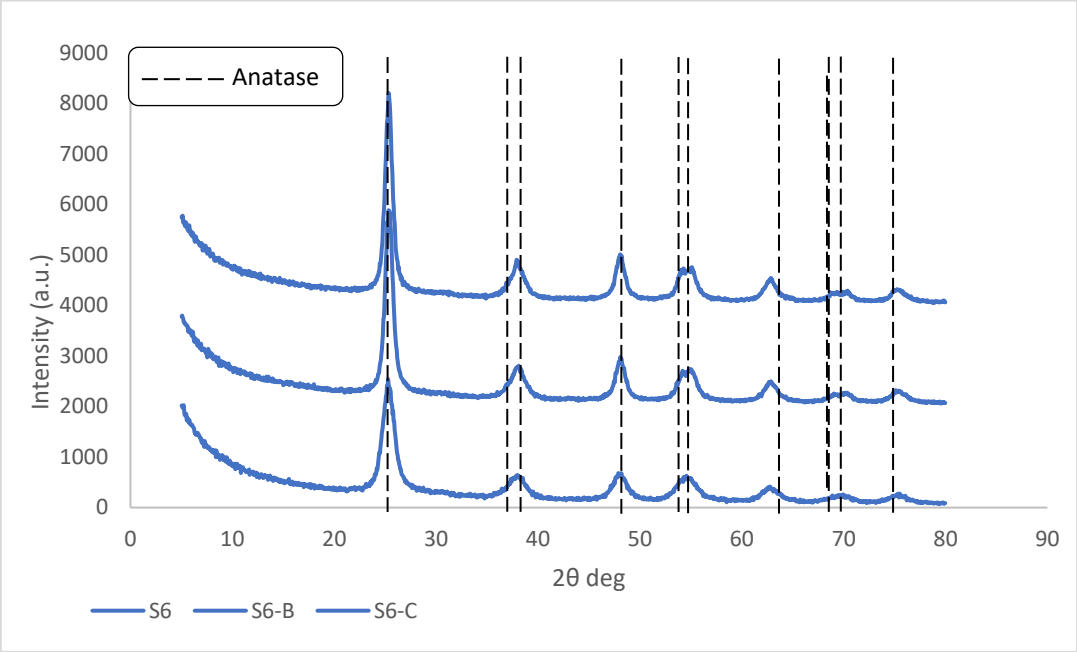

***Graph 4.1.2-A**. Comparison of XRD spectra obtained after the operative modifications on the synthesis S6, which is put as reference in the graph.*

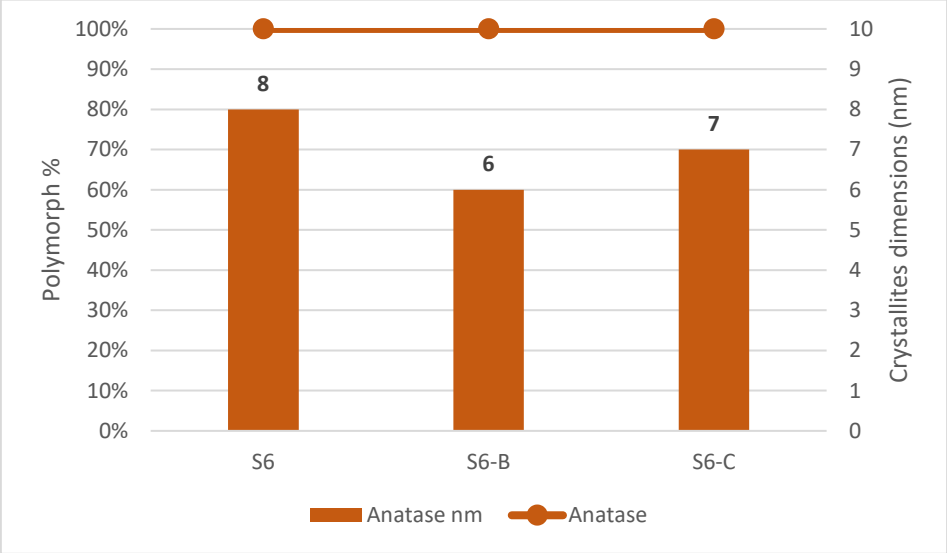

***Graph 4.1.2-B**. Comparison for the dimensions of crystallites in the samples obtained after the operative modifications on the synthesis S6, which is put as reference in the graph. The data are calculated from the XRD spectra in the Graph 4.1.1-A. The straight line is for the polymorph percentage, while the bars are for the dimensions of crystallites.*

In **Graph 4.1.2-C**, both the data of bulk density and specific surface area are presented. It is possible to confirm the trend already noticed in the neutralization syntheses. Indeed, as the surface areas of both samples S6-B and S6-C lower, with respect to the sample S6, their bulk densities increase. Besides that, the bulk densities of the two powders are still considered to be comparable with the sample S6, even though slightly higher. Given the fact that the stirring time of the hydrolysis is always the same in the synthesis S6 and its modifications, it may be supposed that the order of addition of the microemulsion has a relevant effect on the stability of the system producing titania with a higher bulk density. This can also be an explanation in the case of the synthesis S6-C because the use of a basic solution to neutralize every addiction of the acidic microemulsion may alter consistently the system and the micelles.
Conversely, the specific surface area is not comparable with the one obtained from the original S6 synthesis, but the values are similar to each other. These values are even lower that the S_{BET} of the STD sample (135 m^2/g).

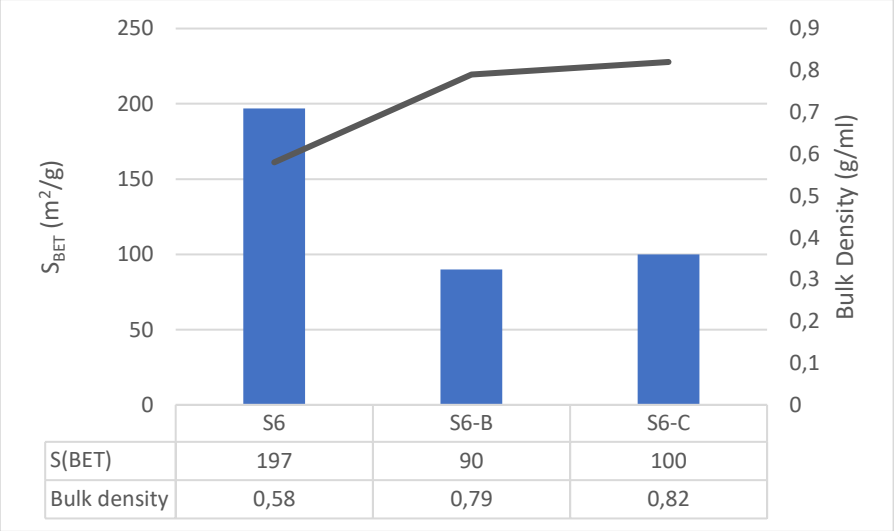

***Graph 4.1.2-C**. Comparison of bulk density and specific surface area for the samples obtained from the modifications of the synthesis S6. The STD sample is put as reference. The bars show the value of S_{BET}, while the line is the bulk density.*

Considering the DRS analysis, the two samples S6-B and S6-C are both yellow, so the spectra presented in **Graph 4.1.2-D** were expected, as previously seen for the other samples that showed the same colour. Indeed, the reflectance starts to lower in the visible range of light and then it drops around 400 nm. The band gap values are comparable, also with the original sample S6, as shown in **Graph 4.1.2-E**, and overall higher than the STD sample. For these reasons, it could be interesting to test these two powders in the photo-reforming of glycerol, even though

the bulk density and the surface area are not optimal values for the wanted catalyst. In fact, the analysis of the reaction products and parameters could be an indicator of whether a low bulk density and high surface area have a considerable effect on the reaction progression and outcome.

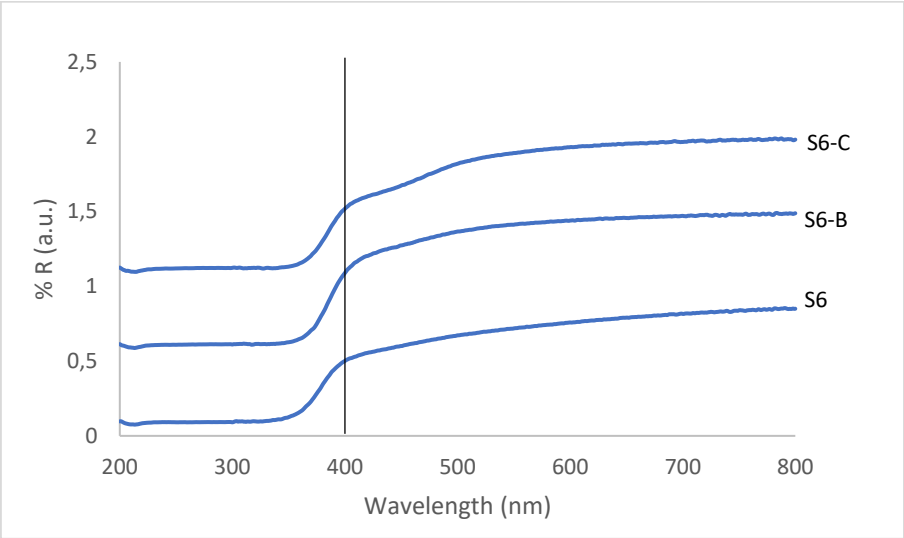

***Graph 4.1.2-D**. DRS spectra of the TiO_2 samples obtained after the operative modifications on the synthesis S6, which is put as reference in the graph.*

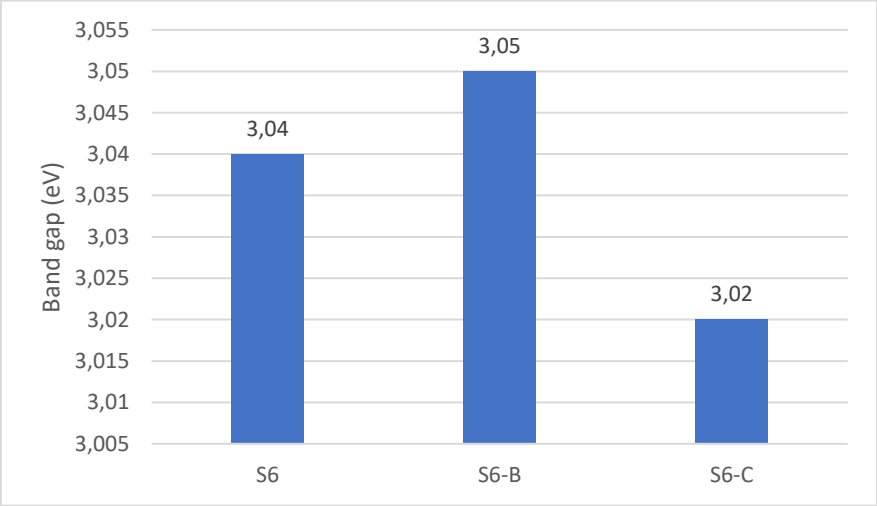

***Graph 4.1.2-E**. Bang gap values of the samples obtained after the operative modifications on the synthesis S6, which is put as reference in the graph, along with the STD sample. Data obtained from the elaboration of the spectra in Graph 4.1.1-D.*

4.1.3. Reproducibilityof the synthesis S6

Overall, within the scope of the project, the sample S6 (NH_4OH with base/acid ratio 0.7) shows the most promising characteristics to be used as a photocatalyst, namely a high surface area and a low bulk density. Moreover, it is composed only of the anatase polymorph with quite small dimensions of the crystallites in the order of the nanoscale. Therefore, the synthesis S6 is replicated to verify its reproducibility and the samples are analysed as the others before to confirm the consistency of the data.

Sample	Bulk Density (g/ml)	S_{BET} (m^2/g)	Band Gap (eV)	TiO_2 crystalline phase	d_{XRD} Anatase (nm)	d_{XRD} Rutile (nm)
S6	0.58	197	3.04	Anatase	8	/
S6 (3)	0.74	138	3.04	Anatase	9	/
S6 (4)	0.72	120	3.09	Anatase	10	/

***Table 4.1.3-A**. Summary of the main characterization data for the reproducibility of the synthesis S6. The S_{BET} is measured on the samples after calcination. The d_{XRD} values express the dimensions of crystallites.*

The XRD spectra concerning the reproducibility of the synthesis S6 are showed in the **Graph 4.1.3-A**. The two replicas show the exact same results since only the anatase phase is present in the powder, as in the original sample S6. Rutile is not detected in any of the samples. Also, the dimensions of the crystallites (**Graph 4.1.3-B**) are comparable with the initial sample S6, and overall, they all are below 10 nm.

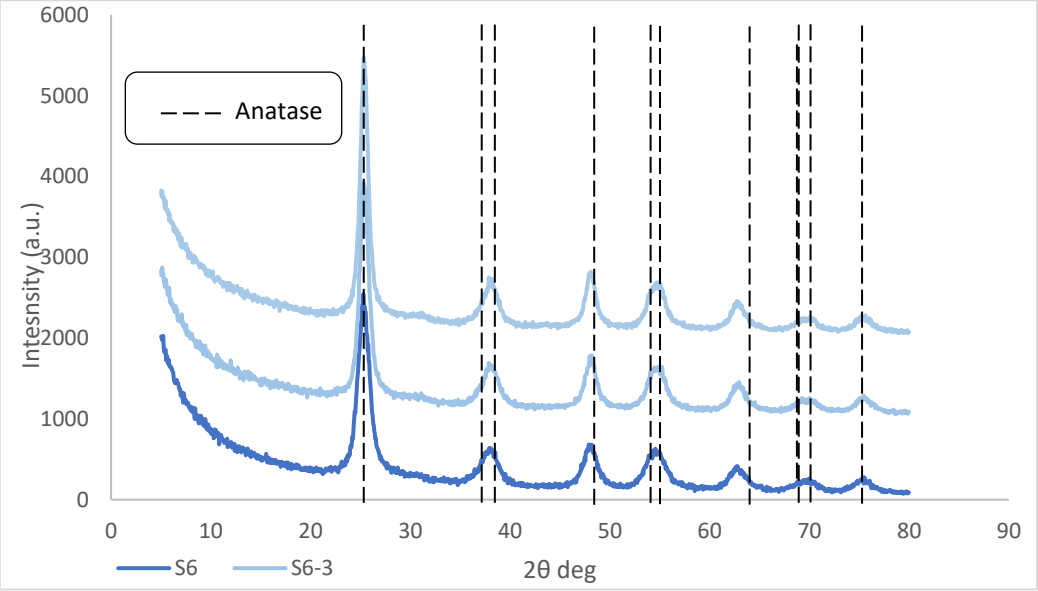

***Graph 4.1.3-A**. Comparison of XRD spectra for the reproducibility (light blue) of the synthesis S6 (blue).*

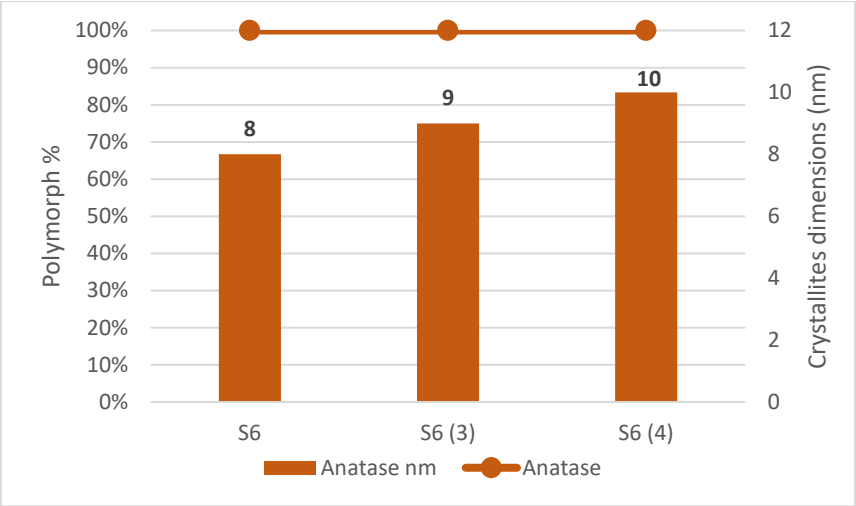

***Graph 4.1.3-B**. Comparison for the dimensions of crystallites in the samples for the reproducibility of the synthesis S6. The data are calculated from the XRD spectra in the Graph 4.1.2-A. The straight line is for the polymorph percentage, while the bars are for the dimensions of crystallites.*

The two replicas give a value of bulk density comparable within each other, but slightly higher with respect to the initial synthesis S6. The data are presented in the **Graph 4.1.3-C**. For what concerns the surface area, the two reproductions of the S6 synthesis give two high values for the surface area, which are lower when compared to the synthesis S6 performed at the beginning, but they are similar to the STD sample (135 m^2/g).

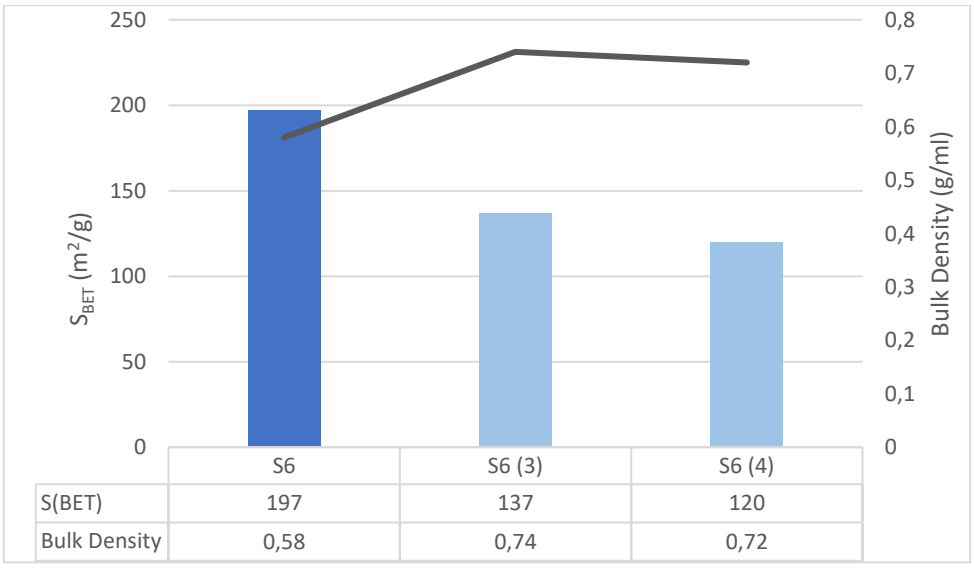

***Graph 4.1.3-C**. Comparison of bulk density and specific surface area for the reproducibility of the synthesis S6. The STD sample is put as reference. The bars show the value of S_{BET}, while the line is the bulk density.*

In **Graph 4.1.3-D**, the DRS spectra obtained by the replicas are presented. The two reproductions of the synthesis S6 give two samples with the same type of spectra depicted previously. As also these powders are yellow, the reflectance starts to lower already in the range of visible light. The drop in reflectance is still quite and it occurs around 400 nm. **Graph 4.1.3-E** presents the data of band gap energy values, which are all similar to each other, also with the S6 sample.

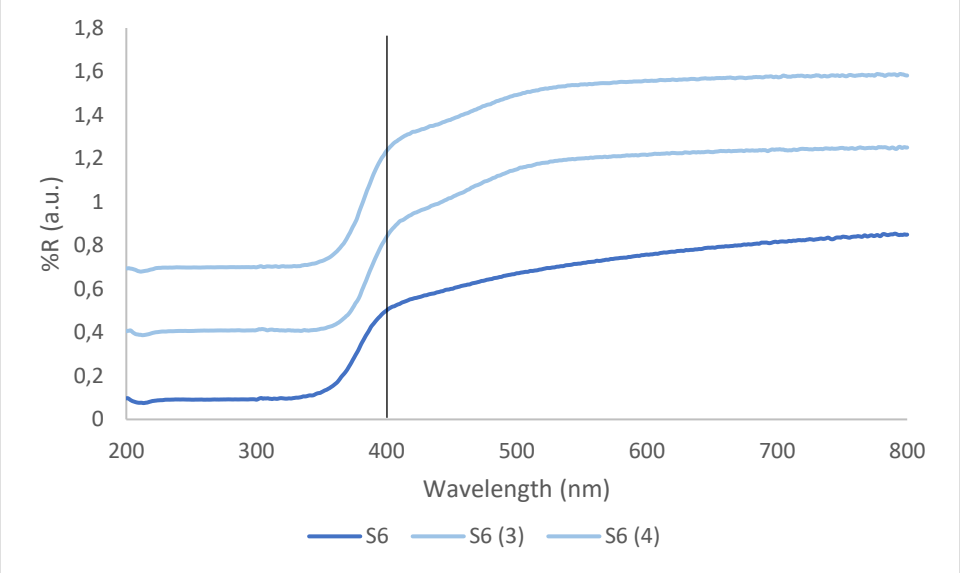

***Graph 4.1.3-D**. DRS spectra of titania samples for the reproducibility (light blue) of the synthesis S6.*

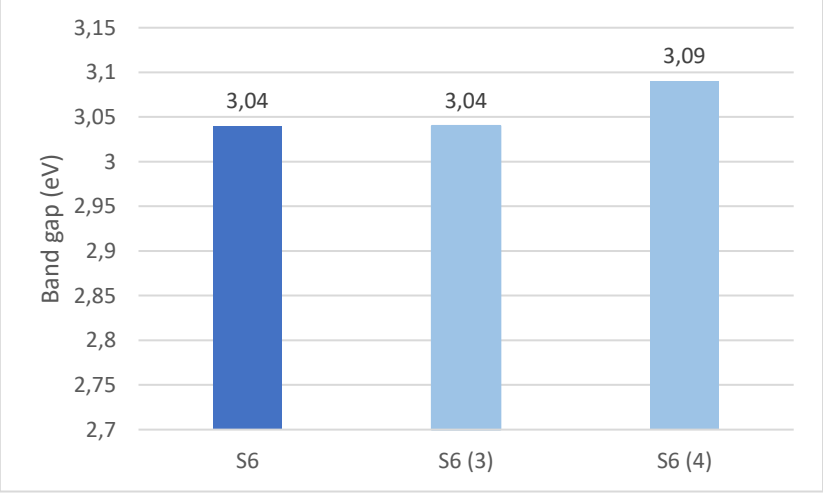

***Graph 4.1.3-E**. Band gap values for the reproducibility of the synthesis S6. The STD sample is put as reference. The data are obtained from the elaboration of the spectra in graph 4.1.2-D.*

4.2. Synthesis of the rutile polymorph

Rutile is another polymorph of titania that can be obtained selectively by modifying some parameters during the synthesis, as the stirring time and the type of acid used.

In this work, the hydrolysis time is firstly modified to be longer so that rutile will form, since it is the thermodynamic product. According to literature[70], the optimal stirring time to do that is 4 days (sample R-4gg). After that, the change of the acid is analysed. The STD synthesis is based on the use of nitric acid and it can be substituted with hydrochloric acid. The literature proposes a synthesis using the same starting reagents as the STD synthesis and hydrochloric acid with a concentration 10M[28,88]. In this project, the concentration of HCl tested is 5M since this allows the system to reach a higher value of water-to-surfactant ratio (Rw) that is equal to the one used in the STD synthesis (Rw=21). The data resulting from the characterization of these two samples are presented in **Table 4.2-A**, along with the values for the STD sample, which is put as a reference. Moreover, the operative conditions for the syntheses are reported since they are quite different.

Sample	Synthesis	Bulk density (g/ml)	S_{BET} (m^2/g)	Band gap(eV)	TiO_2 crystalline phase	d_{XRD} Anatase (nm)	d_{XRD} Rutile (nm)
STD	HYD 1h, R 5h; HNO_3	1.2	135	3.08	A=95%; R=5%	9.8	8.5
R-4gg	HYD 4d; HNO_3	0.59	50	2.99	Rutile	/	15.1
S-HCl	HYD 24h, R 5h; HCl	0.69	30	2.95	R=94%; A=6%	25	13

***Table 4.2-A**. Summary of the main characterization data obtained from the attempts to synthetize the rutile polymorph. HYD = hydrolysis time, R = reflux time.*

- XRD analysis

The two samples (R-4gg and S-HCl) are prepared with operative conditions quite different, but they are both composed of rutile. Actually, the sample obtained with HCl has a low percentage of anatase (6%) that is visible from the XRD spectra in **Graph 4.2-A**. Conversely, anatase is not detected in the sample prepared with a longer stirring time (R-4gg).

The dimensions of the crystallites for both samples are presented in **Graph 4.2-B**. The value for the sample R-4gg (15 nm) is consistent with the results reported in literature for the same

synthesis[28,70], and also the sample S-HCl is obtained with crystallites in the same range of size (13 nm). Rutile is usually the most stable form of titania when its dimensions are bigger than 35 nm, since it tends to grow fast as soon as it forms; while anatase is the most stable form for values below 14 nm[29]. Therefore, both syntheses are able to develop rutile nanoparticles, even comparable with the dimensions of crystallites for the anatase phase.

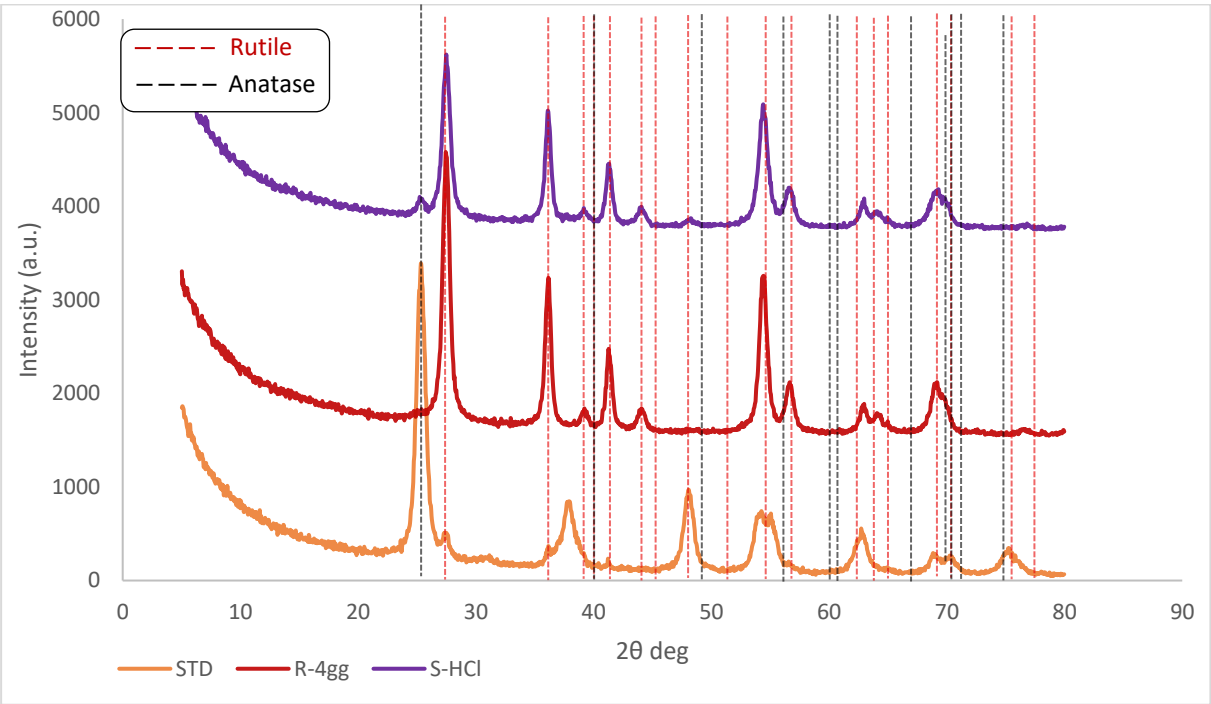

***Graph 4.2-A**. XRD spectra for the samples S-HCl, R-4gg and STD. The reference pattern for anatase and rutile are also inserted in the graph.*

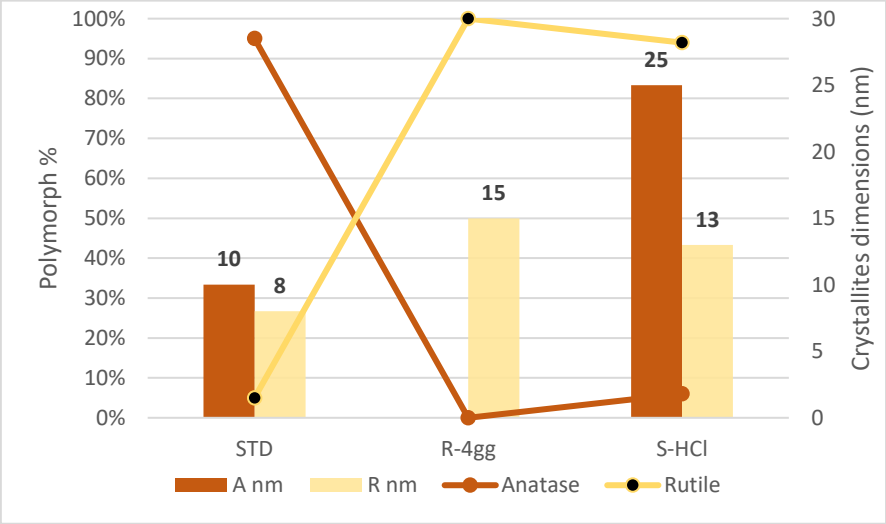

***Graph 4.2-B**. Comparison of the dimensions of crystallites for the sample S-HCl, R-4gg and STD. Also, the percentage of each crystalline phase is inserted in the graph. The data are obtained from the elaboration of the spectra in Graph 4.2-A. The straight line is for the polymorph percentage, while the bars are for the dimensions of crystallites. A=anatase, R=rutile.*

- Bulk Density and Specific Surface Area (S_{BET})

In **Graph 4.2-C**, the data for both bulk density and specific surface area are presented. The STD sample is always put as a reference. The bulk density of the two samples is similar and more than half when compared with the STD sample. The values are also comparable with the data obtained from the neutralization syntheses even though in this case the base is not used and the acid is still HNO_3. For this reason, the explanation for a lower bulk density is in the stirring time, which is far longer for the sample R-4gg, or in the heating step, that is not present in this synthesis. On the other hand, for the sample obtained with the use of hydrochloric acid, an explanation for this lower bulk density could also lie in the type of acid. Indeed, HCl has a strong influence on morphological and physical properties of the final titania, since Cl^- and NO_3^- anions have a different chemical complexation on the crystalline structure[20].

Concerning the specific surface area, both samples show a low value. The one for the sample R-4gg is equal to the study from which the procedure was taken[70]. Also, the sample S-HCl gives a value slightly lower than the one reported in literature[28], even though the concentration of the acid used in this project is lower and the operating procedure was partially modified.

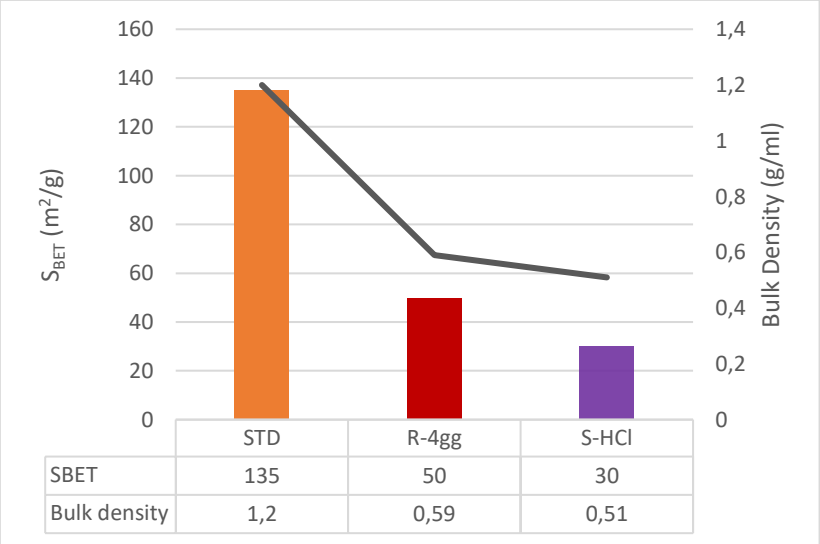

***Graph 4.2-C**. Comparison of bulk density and specific surface area for the sample R-4gg and S-HCl. The STD sample is put as a reference. The bars represent the S_{BET}, while the line is the bulk density.*

- DRS spectra and Band Gap calculation

The DRS spectra (**Graph 4.2-D**) for these two samples are analogous to the STD titania, thus the drop of reflectance is around 400 nm. Nitrogen is not expected to be presented inside the crystalline structure of these two samples since no base is used and the acid is switched from

HNO_3 to HCl. In fact, the two powders are white. The values of band gap (**Graph 4.2-E**) are comparable with each other and they are consistent with the data in literature for the rutile crystalline phase of titania, as the band gap should be ~ 3.03 eV[70].

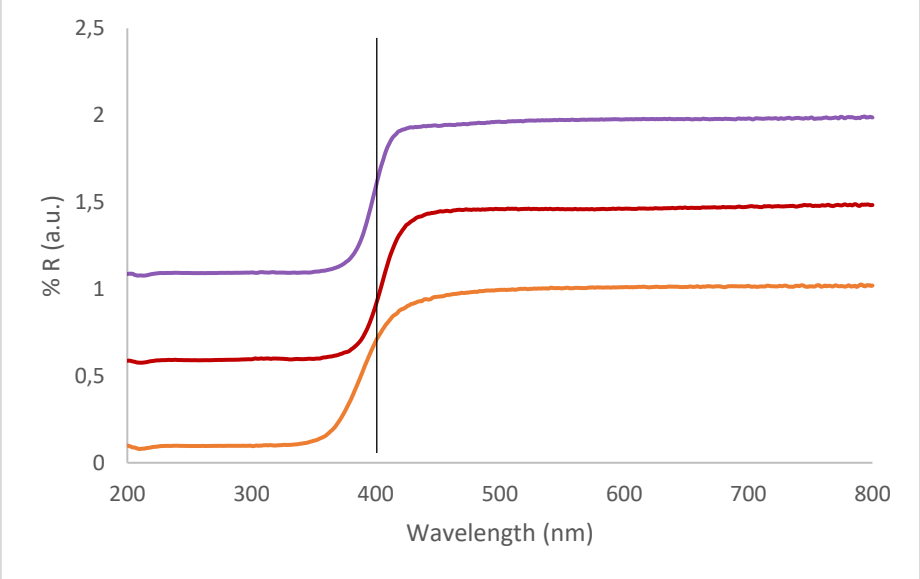

***Graph 4.2-D**. DRS spectra of the sample S-HCl (purple), R-4gg (red) and the STD sample (orange), which is put as a reference.*

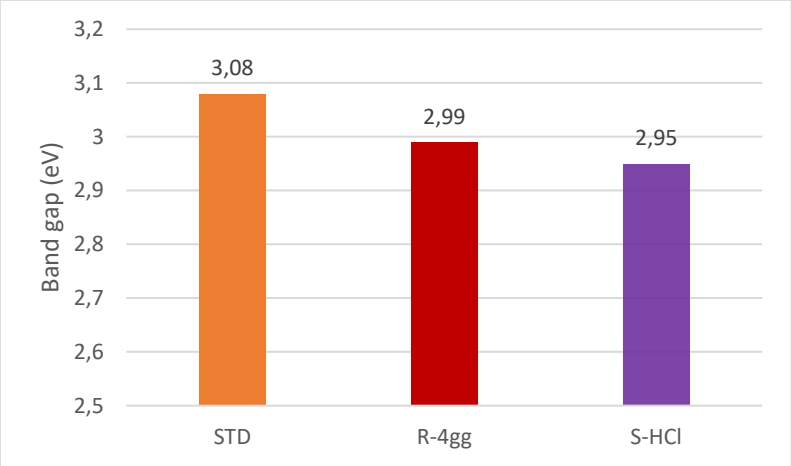

***Graph 4.2-E**. Comparison of band gap values for the samples S-HCl, R-4gg and STD. The data are obtained from the elaboration of the DRS spectra in Graph 4.2-D.*

4.2.1. Synthesis of rutile polymorph using HCl and the neutralization approach

As previously mentioned, a second way to obtain the rutile crystalline phase of titania is by changing the type of acid. Since the synthesis with HCl is not broadly studied, some further tests are done using the neutralization approach developed within this project with the aim of synthesizing the rutile form of titania. In this case (**Figure 4.2.1-A**), both ammonium hydroxide and sodium hydroxide are tried in the best base/acid ratio (0.7) already discovered when HNO_3 is used. While, for longer hydrolysis time only ammonium hydroxide is used (**Figure 4.2.1-B**), since sodium hydroxide did not show good properties in terms of surface area and bulk density in the previous synthesis.

***Figure 4.2.1-A**. Operative scheme for the synthesis of titania with the neutralization approach when HCl is used. The hydrolysis and reflux time are 1 hour; both NH_4OH and NaOH are tested.*

***Figure 4.2.1-B**. Operative scheme for the synthesis of titania with the neutralization approach when HCl is used. The hydrolysis is 16 or 24 hours and the reflux is 5 hours in both cases; NH_4OH is only used.*

The results from the characterization of these samples are presented in **Table 4.2.1-A** and the operative conditions of the syntheses are also reported for a better understanding. The STD sample is put as a reference, while the sample S-HCl is inserted for comparison since the operative modification are done on its synthesis. In particular, the aim is to verify that the neutralization approach in the ME synthesis using HCl can produced titania samples mainly composed of the rutile polymorph.

Sample	Synthesis	Bulk density (g/ml)	S_{BET} (m^2/g)	Band gap(eV)	TiO_2 crystalline phase	d_{XRD} Anatase (nm)	d_{XRD} Rutile (nm)
STD	HYD 1h, R 5h; HNO_3	1.2	135	3.08	A=95%; R=5%	9.8	8.5
S-HCl	HYD 24h, R 5h; HCl	0.69	30	2.95	R=94%; A=6%	25	13
S7-24h	HYD 24h, R 5h; HCl + NH_4OH	0.48	230	3.14	Anatase	9.4	/
S7-16h	HYD 16h, R 5h; HCl + NH_4OH	0.51	48	3.11	Anatase	11	/
S7R	HYD 1h, R 1h; HCl + NH_4OH	0.67	198	3.08	Anatase	5.9	/
S8R	HYD 1h, R 1h; HCl + NaOH	0.36	10	3.14	/	/	/

***Table 4.2.1-A**. Summary of the main characterization data obtained from the attempts to synthetize the rutile polymorph with the neutralization approach. HYD = hydrolysis time, R = reflux time.*

- XRD analysis

Firstly, it was not possible to perform this analysis on the sample synthesized with NaOH and 1 hour of hydrolysis. Indeed, due to the yield of the synthesis, there is not the proper amount of titania powder to be analysed with the XRD instrument; moreover, it is not worth doing the analysis because of the low yield of the synthesis. Furthermore, the Raman analysis carried out on the sample was not helpful as well. Eventually, the SEM analysis showed the strong presence of NaCl in the sample, making the detection of titania polymorphs difficult with the previous characterization techniques.

All the other samples are formed only by the anatase polymorph as it is confirmed by the XRD spectra (**Graph 4.2.1-A**). So, the neutralization approach applied to the syntheses with HCl is not selective for the rutile crystalline phase; conversely it is selective for the synthesis of pure anatase. Moreover, the hydrolysis time is studied, but in this case a longer stirring time does not result in the formation of rutile. Probably the time was not long enough for the thermodynamic product to form. The base may favour the formation of the anatase polymorph, as the sample obtain with just HCl is composed mainly of rutile (*Paragraph 4.2.*) and the stirring time is 24 hours.

The dimensions of crystallites (**Graph 4.2.1-B**) for the samples with the longer hydrolysis times, 24h and 16h, are comparable with the one for the STD sample. On the other side, the sample obtained after 1 hour of hydrolysis has smaller dimensions of crystallites, which are more consistent with the values obtained with the neutralization of the HNO_3 microemulsions as the stirring time is closer to these preparations.

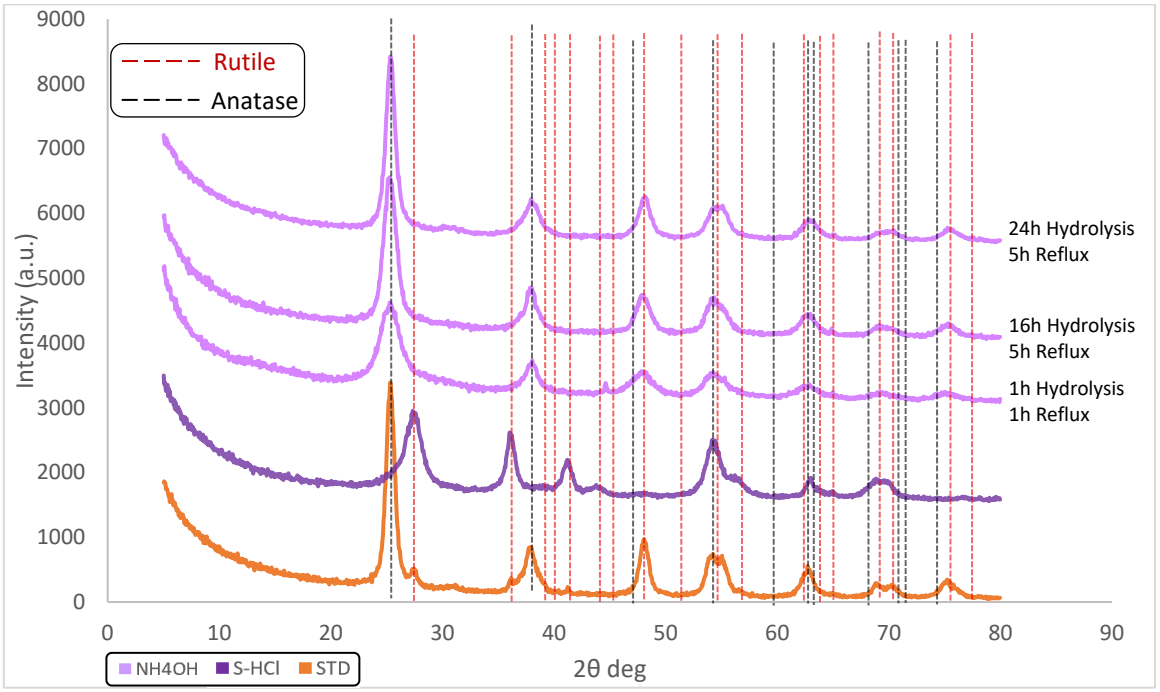

***Graph 4.2.1-A**. XRD spectra of the samples obtained after the neutralization approach when HCl is used. The samples S-HCl and STD are put as references.*

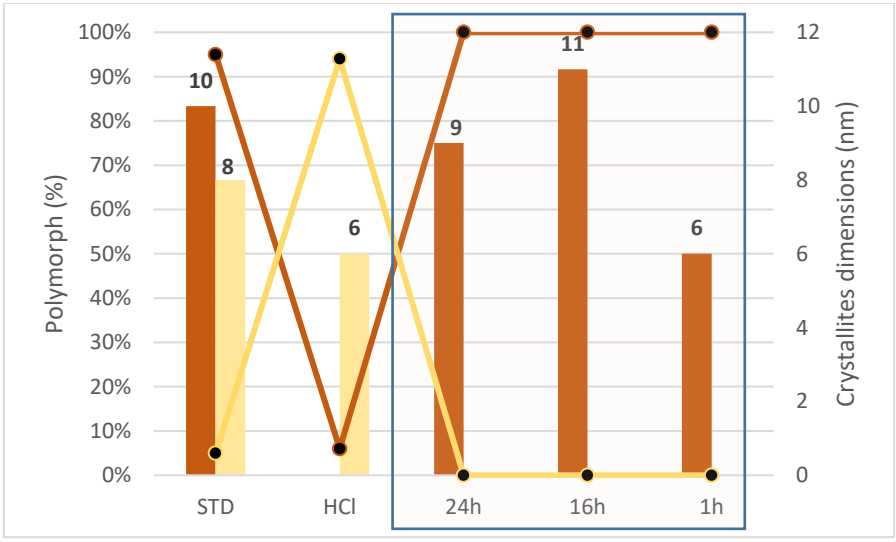

***Graph 4.2.1-B**. Dimensions of crystallites for the samples obtained after the neutralization approach when HCl is used. The samples S-HCl and STD are put as reference. The data come from the elaboration of the XRD spectra in Graph 4.2.1-A. The straight line is for the polymorph percentage, while the bars are for the dimensions of crystallites. A=anatase, R=rutile.*

- Bulk density

This set of syntheses (see Figure 4.2.1-A and 4.2.1-B) show values of bulk density lower than the syntheses with the neutralization of the HNO_3 microemulsion. The characterization data (**Graph 4.2.1-C**) are all below the bulk density of the sample prepared with HCl and no neutralization. In particular, when the hydrolysis is longer, more than 16 hours, the bulk density tends to be lower. The sample prepared with 1 hour of hydrolysis has a value of bulk density closer to the samples with the neutralization of the HNO_3 microemulsion. This is probably because the hydrolysis times are quite similar among each other, 1 hour and 20 minutes, respectively; moreover, the time for heating with reflux is the same.

The sample prepared with NaOH and 1 hour of hydrolysis seems to be quite interesting. The bulk density is considerably low with respect to the other samples and among all the syntheses, it is the only powder with a value closer to the bulk density of the commercial P-25 (0.1 g/ml). in this case, it is difficult to define an explanation, since it was not possible to obtain such value in the neutralization syntheses with HNO_3, so, probably the HCl plays an important role in determining the bulk density of the powder. Anyway, as previously seen in the XRD section, this sample displays a strong presence of the NaCl salt as an impurity and the value of bulk density might not be the real one.

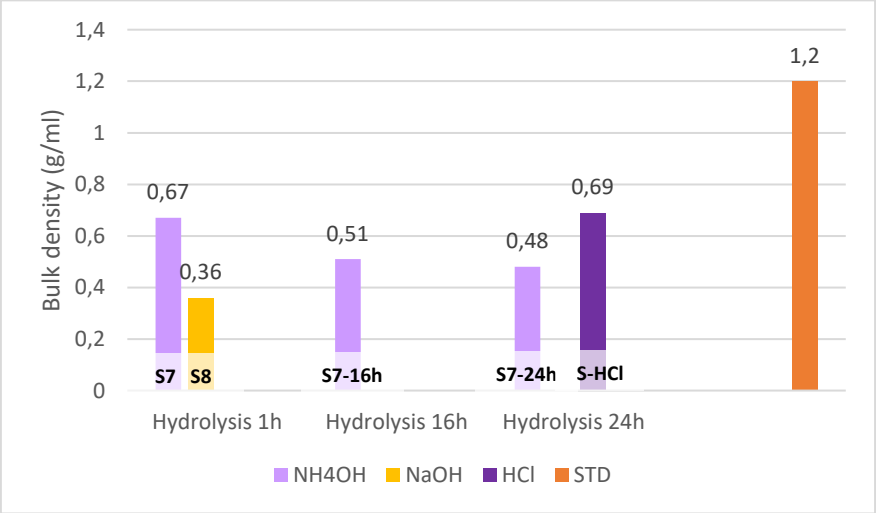

***Graph 4.2.1-C**. Comparison of bulk density for the samples obtained after the neutralization approach when HCl is used. The samples S-HCl and STD are put a reference.*

- Specific surface area (S_{BET})

The samples obtained *via* the ME synthesis with the neutralization of HCl show quite different surface areas depending on the hydrolysis time. All the values for the samples prepared with

NH_4OH are higher than the STD sample (135 m^2/g); the sample obtained with 24 hours of hydrolysis is even higher than the sample S6 (198 m^2/g) which is the best data in the set of syntheses with neutralization approach when HNO_3 is exploited. It seems like, when using a preparation method based on the neutralization approach, the type of acid is not important as high-surface area anatase will form. On the other side, the type of base has a crucial role since, when sodium hydroxide is used in the same conditions of ammonium hydroxide (considering the synthesis with 1 hour of hydrolysis), the surface area extremely drops to the lowest value obtained in all the syntheses performed in this project. This is in contrast with the data obtained before from the bulk density since usually as the surface area decreases, the bulk density increases. This trend was confirmed in the first set of syntheses with neutralization. Otherwise, in this case, the S_{BET} of the sample with NaOH is a very small value, but also the bulk density lowers considerably. Conversely, the other samples confirm the trend previously noticed in the first set of syntheses with neutralization.

Thus, the sample prepared with NaOH shows quite peculiar characteristics. It has a very low surface area and a little value of bulk density, which is one of the goals of this paper.

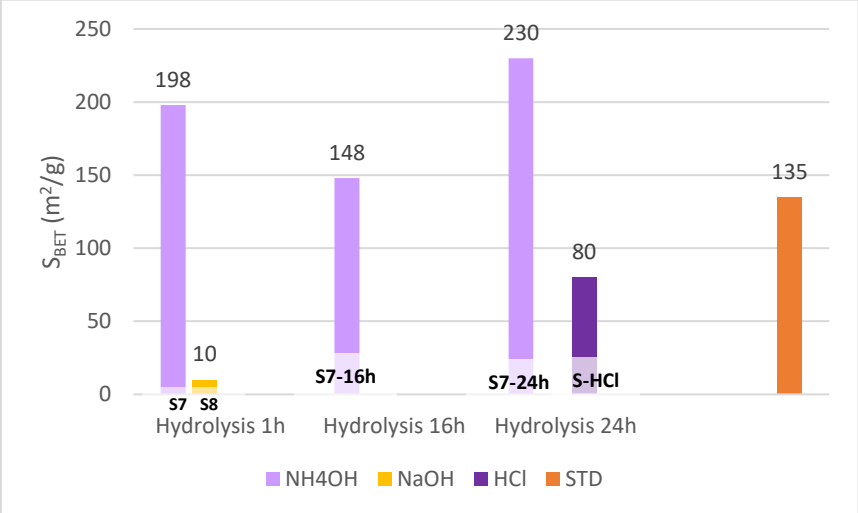

***Graph 4.2.1-D**. Comparison of specific surface area for the samples obtained after the neutralization approach when HCl is used. The samples S-HCl and STD are put as reference.*

- DRS spectra and Band Gap calculation

The DRS spectra of all the samples are similar (**Graph 4.2.1-E**). They show a drop in reflectance that starts around 400 nm. Their band gaps, presented in **Graph 4.2.1-F**, are in

general higher values with respect to the samples obtained in the neutralization of the HNO_3 microemulsion, even though they are composed of anatase.

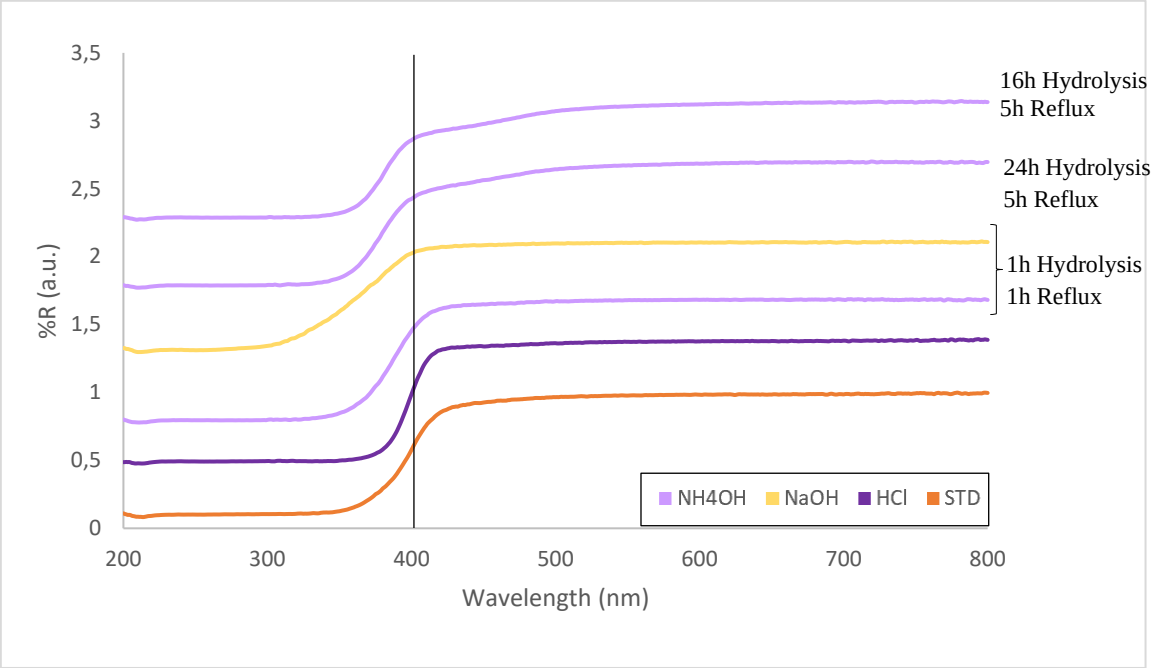

***Graph 4.2.1-E**. DRS spectra for the samples obtained after the neutralization approach when HCl is used. The samples, where NH_4OH is used, are pink, while the one prepared with NaOH is yellow. The samples S-HCl (purple) and STD (orange) are put as a reference.*

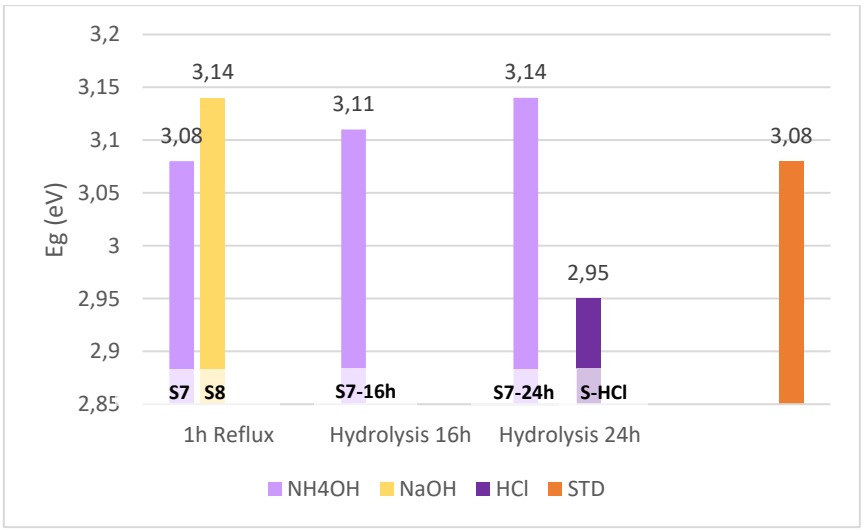

***Graph 4.2.1-F**. Band gap values for the samples obtained after the neutralization approach when HCl is used. The samples S-HCl and STD are put as a reference. The data are obtained after the elaboration of the spectra in Graph 4.2.1-E.*

4.3. Photocatalytic activity of TiO_2-m

After the synthesis and characterization of all the samples, the ones with the optimal properties are selected to test their photoactivity, since the final goal is to use the titania as a catalyst in the photo-reforming of glycerol. A first set of reactions is done by using the bare support, eventually comparing the hydrogen production rate and the liquid products obtained for each sample. Before the catalytic tests, an attempt to calculate the quantum efficiency of the titania catalysts is done (*Paragraph 4.3.1*); moreover, a study on the transmittance of the systems was carried out (*Paragraph 4.3.2*).

4.3.1. Quantum Efficiency calculation

In photocatalytic processes, the efficiency for the conversion of the light energy to chemical energy could be an interesting parameter to consider. In fact, it enables to understand which are the photo-catalytically active sites since the light is not reaching the surface of the catalyst due to shading. So, it is relevant to define the part of light effectively used by the catalyst. The efficiency can be calculated as the quantum efficiency, or quantum yield (QY), indicating the ratio of the products obtained and the photons absorbed (**equation 11**)[89]. The product considered is H_2 (in moles), while the number of photons absorbed is obtained from the intensity of the light at one wavelength (see *Paragraph 3.6.2*).

$$QY = \frac{amoun\ of\ product\ formed}{amount\ of\ photons\ absorbed} \quad (\mathbf{11})$$

Before calculating the quantum efficiency for the titania samples, some tests are performed to define the transmitted and scattered light for the system. Indeed, the light irradiated (I_0) from the solar simulator is not the same amount of light transmitted (I_T) at the bottom of the reactor since there may be adsorption (I_A) and scattering (I_S) of light that can occur in the system. So, the light irradiated is the sum of all these phenomena (**equation 12**) that must be taken into consideration when calculating the quantum efficiency.

$$I_0 = I_T + I_A + I_S \quad (\mathbf{12})$$

Moreover, it is necessary to find the proper instrument to use, the fibre optic spectrometer or the radiometer, so both are tested to understand if the possibility to use the radiometer is viable since it is a faster way to perform the analysis.

- Optic fibre spectrometer

The fibre optic spectrometer is exploited to verify the data obtained by the radiometer with the two probes (UV and Visible regions). The radiometer is faster to use since it gives a direct value of the measure; moreover, the fibre optic spectrometer has some structural limitations since it has an optimal angle of detection which is not easy to observe in these kinds of measurements due to the structure of the reactor. For these reasons, this instrument is used just for the first analyses.

In the following graphs, the transmitted and scattered light are measured when there is just the filter at 400nm with nothing in between (**Graph 4.3.1-A**), when the reactor is placed under the lamp (**Graph 4.3.1-B**) and when the reaction mixture, without the catalyst, is put inside the reactor (**Graph 4.3.1-C**). In the last case, the reaction mixture is composed of the solvent (water) and the substrate (glycerol) in the same amounts used during the photocatalytic reaction to simulate the system that is usually present. The light transmitted lowers, as the reactor is placed below the lamp and then again when the reaction mixture is added. At the same time, the scattering increases. The scattering is not measured in the first case as nothing is between the source of light and the probe of the spectrometer, so ideally there is not scattering.

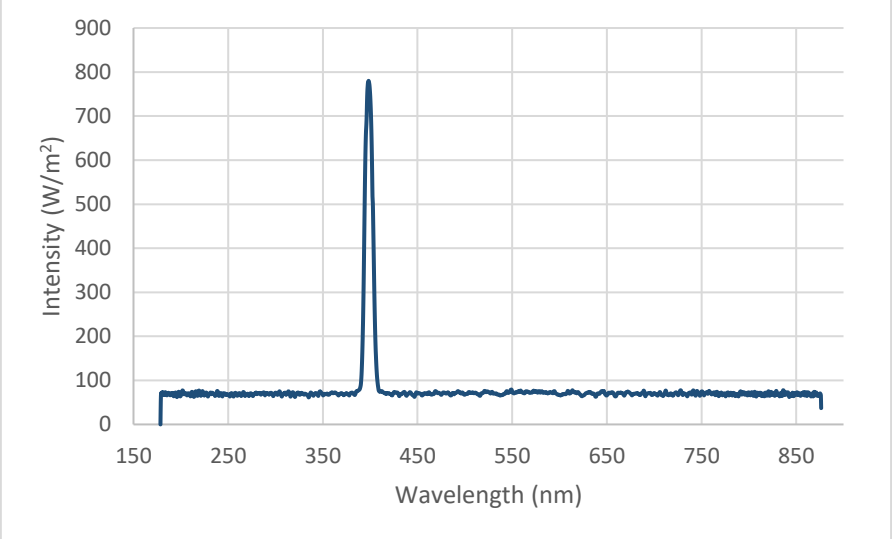

***Graph 4.3.1-A**. Transmitted light of the lamp with a 400nm filter. Analysis performed with a fibre spectrometer.*

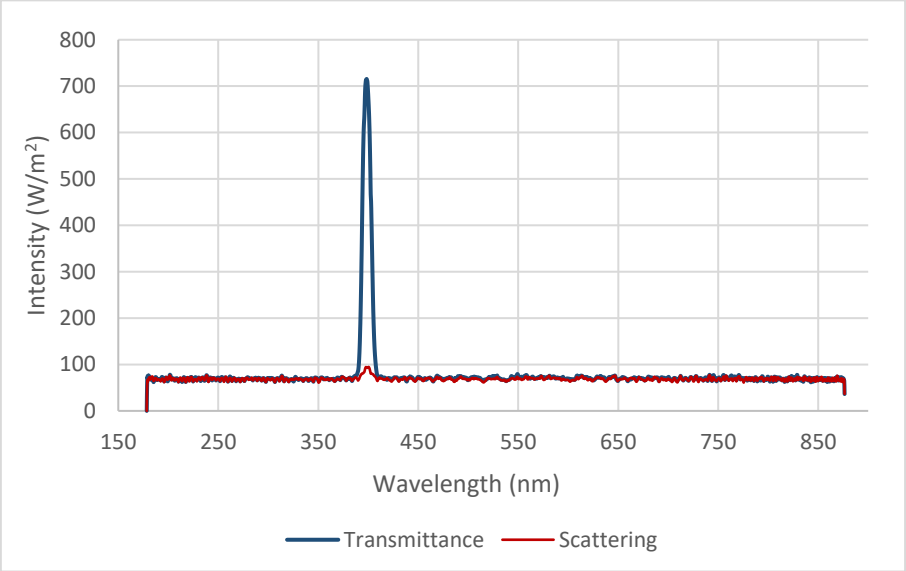

***Graph 4.3.1-B**. Transmitted and scattered light with a 400nm filter when the reactor is placed below the lamp. Analysis performed with a fibre spectrometer.*

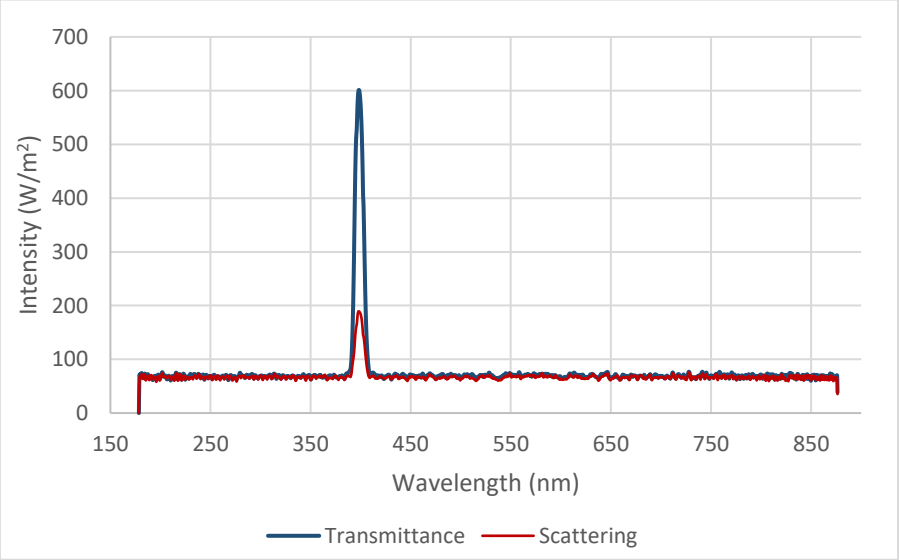

***Graph 4.3.1-C**. Transmitted and scattered light with a 400nm filter when the reactor with the reaction mixture is placed below the lamp. Analysis performed with a fibre spectrometer.*

- Radiometer with probes in the UV and Visible range of the spectrum

The radiometer is used in the same way as the fibre optic spectrometer, but instead of producing the whole spectrum, it just gives the value of the light intensity detected.

The **Graphs 4.3.1-D** collect the values of light intensity, both transmitted and scattered, in the UV and visible range in three conditions:

- Direct source of light,
- Reactor placed below the lamp,
- Reaction mixture added to the system (solvent and substrate).

The trend is the same showed with the optic fibre spectrometer, even though the measures are less precise. Indeed, the transmittance seems to increase when the reaction mixture is added to the reactor, in both cases. Anyway, the values for the light intensity are all quite low, so the difference between the intensity in the three cases can be considered as part of the instrument error. In general, it can be stated that the overall system (glass, solvent and substrate) has a low relevance in the scattering phenomena, as most of the light is directly transmitted to the bottom of the reactor.

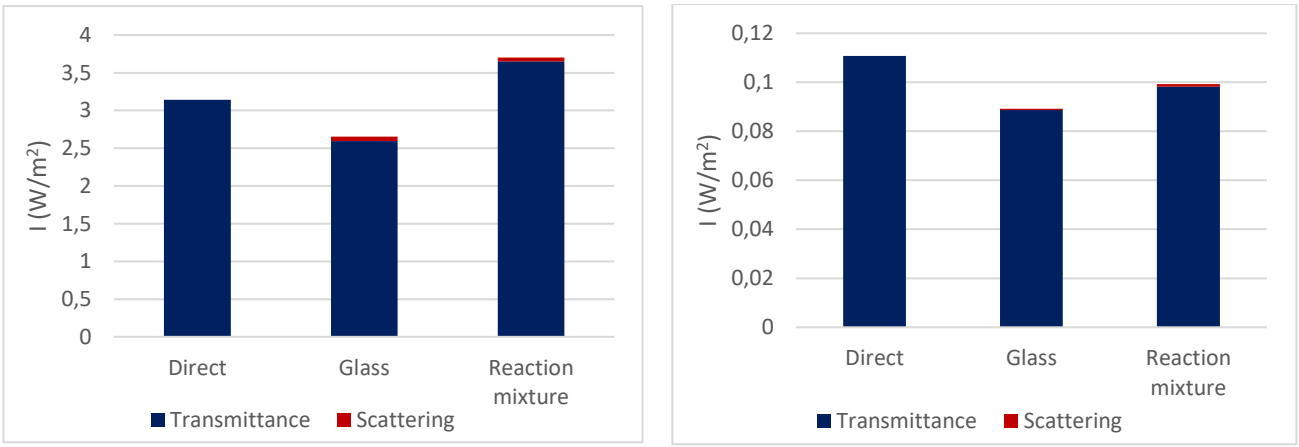

***Graph 4.3.1-D**. Transmitted and scattered light with a 400nm filter in three conditions. Analysis performed through a radiometer with a probe in the visible range (graph on the left) and one in the UV (graph on the right).*

After confirming that the radiometer can be used for these kinds of measurements, the following analyses with the titania powder are performed just with this instrument. Therefore, the commercial titania P-25 is tested at increasing concentrations: 0.2 g/L, 0.5 g/L and 0.8 g/L. As before, the data are collected in two graphs (**Graph 4.3.1-E**) separating the two ranges of the probes. In both graphs the trend is the same; the transmittance lowers as the concentration increases, while the scattering is quite similar for all the concentrations tested. Moreover, it can be noticed that the intensity of the light transmitted, when the filter is placed on the lamp of the solar simulator, is 1000 times lower than the light intensity if there is no filter (see values in *Paragraph 4.3.2*). This aspect represents a problem since the hydrogen production rate is too little when the filter is used in the photocatalytic reaction used to calculate the quantum yield.

The intensity of the light transmitted is not high enough and the bare titania used in the reaction is not sufficiently active to produce hydrogen. So, if platinum is added to the titania powder, obtaining a supported Pt/TiO_2 catalyst, it is possible that the activity is sufficiently high to produce enough hydrogen to be detected by the GC analysis instrument.

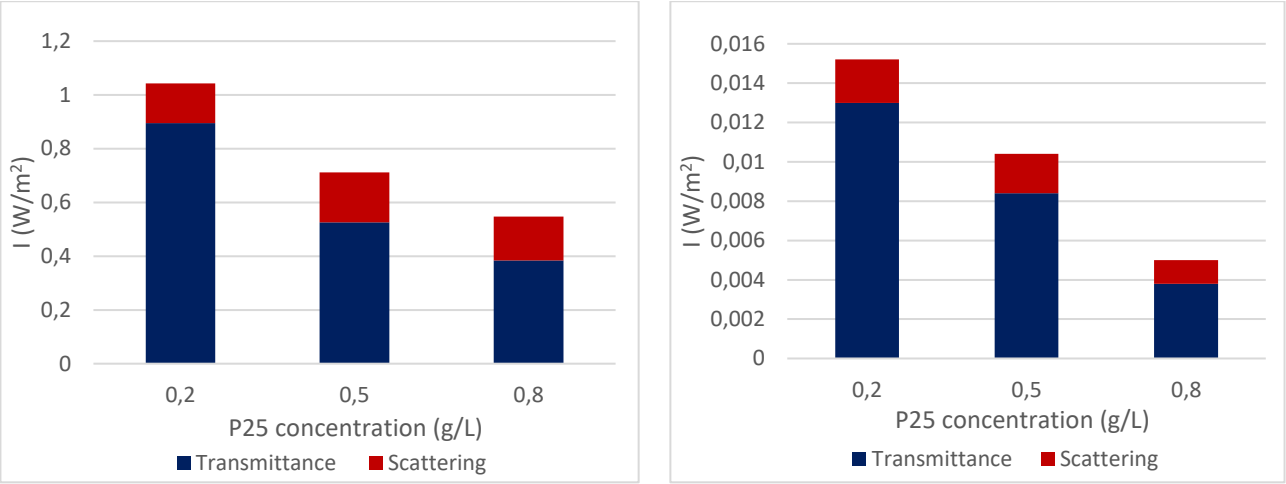

***Graph 4.3.1-E**. Transmitted and scattered light with a 400nm filter when the catalyst is inserted in the reaction mixture. Three different concentrations of the commercial titania P-25 are tested. Analysis performed through a radiometer with a probe in the visible range (graph on the left) and one in the UV (graph on the right).*

4.3.2. Photocatalytic reforming of glycerol

The photo-reforming of glycerol is a degradation reaction where the substrate is converted into other products and eventually oxidized to CO_2, together with the production of hydrogen. Therefore, a wide number of products can be obtained. A reaction mechanism was proposed by some previous studies and it involves the production of hydrogen as a gas and some liquid products, namely dihydroxyacetone, glyceraldehyde and glycolaldehyde. So, to better analyse the photocatalytic reaction, the liquid and gaseous products are discussed separately.

As previously stated, not all the samples obtained by the different preparation methods are tested in the photocatalytic reaction of glycerol, so the results are presented divided per type of synthesis to allow a clearer understanding of the data. For a better comprehension of the results, the **Table 4.3.2-A** presents a summary of the main characterization data for the titania powders tested in the photo-catalytic reaction.

The STD sample is inserted as a reference; moreover, the commercial titania P-25 is tested for comparison. The samples S1, S2, S4 and S6 are obtained with the neutralization approach and they show the best properties, especially the specific surface area. Additionally, the sample S4

is synthetized with NaOH in the ratio 0.7 and it shows quite good properties, so a comparison with the sample S6 (NH_4OH ratio 0.7) is done. Then, the samples S6-B and S6-C are tried out to compare their photo-activity with the original S6 sample. Moreover, the two samples obtained to confirm the reproducibility of the synthesis S6 are used in the photocatalytic reaction to verify they have the same activity.

Sample	**Synthesis**	**S_{BET} (m^2/g)**	**Bulk density (g/ml)**	**Band gap (eV)**	**Crystalline phase**	**d_{XRD} (nm)**
STD	HYD 1h, R 5h; HNO_3	135	1.2	3.08	A=95%; R=5%	A=9.8
P-25	Commercial TiO_2	49	0.1	3.15	A=80%; R=20%	A=21.7
S1	HYD 20 min, R 1h; HNO_3 + NH_4OH (1)	158	0.99	2.91	Anatase	9.5
S2	HYD 20 min, R 1h; HNO_3 + NH_4OH (0.5)	87	0.75	2.95	A=91%; R=9%	A=9.4
S4	HYD 20 min, R 1h; HNO_3 + NaOH (0.7)	144	0.76	2.96	A=66%; R=34%	A=6.6
S6	HYD 20 min, R 1h; HNO_3 + NH_4OH (0.7)	197	0.58	3.04	Anatase	7.9
S6-B	HYD 20 min, R 1h; HNO_3 + NH_4OH (0.7)	90	0.79	3.05	Anatase	5.6
S6-C	HYD 20 min, R 1h; HNO_3 + NH_4OH (0.7)	100	0.82	3.02	Anatase	7

***Table 4.3.2-A**. Summary of the characterization data for the samples successively tested in the photo-reforming of glycerol.*

- Gaseous products analysis

The activity of the catalyst is analysed as the H_2 production rate expressed in μmol $H_2/g_{catalyst}$*h to be consistent with the data present in literature and make a comparison. The best value for H_2 productivity in glycerol PR is around 600 μmol $H_2/g_{catalyst}$*h for bare titania formed by rutile polymorph[31] , while the commercial titania P-25 shows a slightly lower value of 450 μmol $H_2/g_{catalyst}$*h[70].

Firstly, the data for the neutralization syntheses (**Graph 4.3.2-A**) show a high value of H_2 production rate for the sample S6 (NH_4OH with ratio 0.7) which is more than twice the value for the STD sample. In addition to that, the sample S6 shows a higher H_2 production rate than the titania powders tested in other studies with the same conditions, even greater than the commercial P-25[31,70].The possibility to have a N-doped TiO_2 catalyst could explain this great activity of the sample S6. Also, the sample S1 (NH_4OH with ratio 1) is thought to contain nitrogen in the crystalline structure, but it does not show an activity as high as the sample S6. So, there is something else contributing which may be the surface area of the catalyst. Indeed, as more species can be absorbed on the surface of the titania, a higher number of organic substrates and intermediates will be dehydrogenated, releasing H_2.

The sample obtained with NaOH and the same base/acid ratio of the sample S6 (0.7) is also tested in the glycerol PR reaction, but it does not display a good value of H_2 productivity, not even comparable with the one of the STD sample.

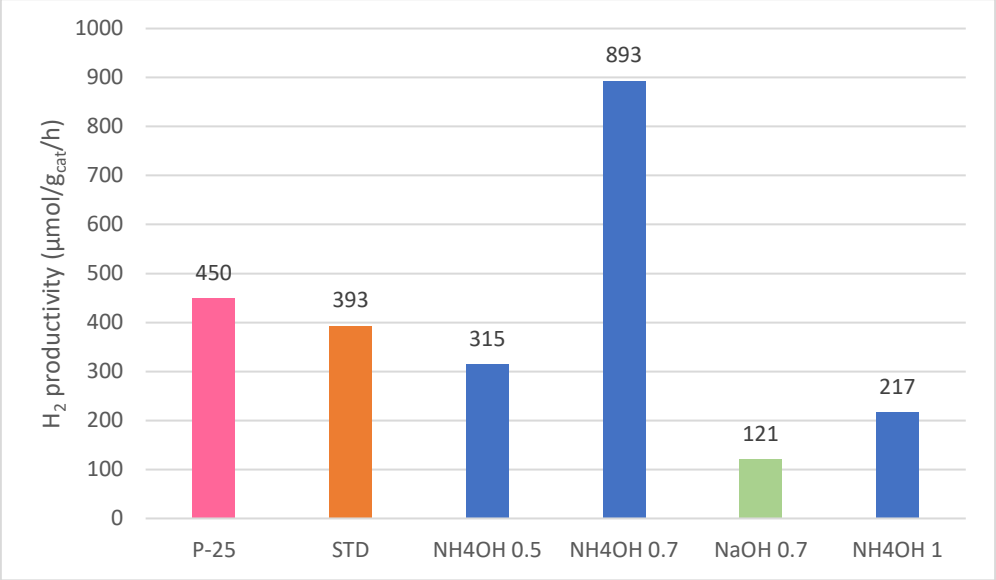

***Graph 4.3.2-A**. Comparison of the H_2 production rate for the neutralization samples (when HNO_3 is used). The STD sample is put as reference.*

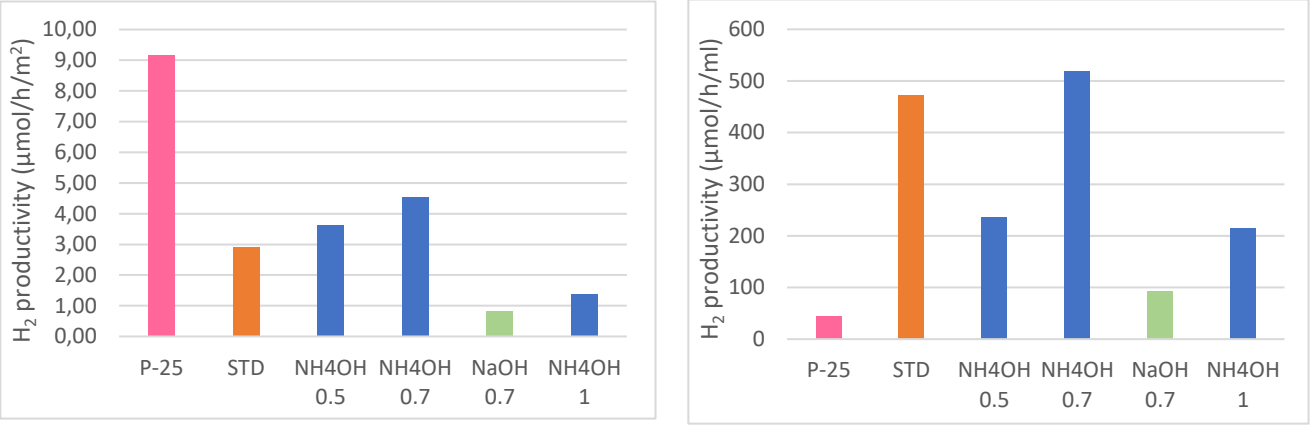

***Graph 4.3.2-B**. H_2 productivity for the samples obtained with the neutralization synthesis when HNO_3 is used. The graphs are a normalisation on the S_{BET} (left) and on the bulk density (right). Data elaborated from the graph 4.3.3-A.*

In the case of the sample obtained by the modifications of the synthesis S6, the H_2 productivity is lower than the one of the original sample S6, and also of the STD sample (**Graph 4.3.2-C**). The bulk density of these two samples (S6-B and S6-C) is slightly higher than the one of the S6 sample, but it is still lower than the STD one. Despite that, the hydrogen production rate for the sample S6-B and S6-C is significantly lower than the STD one. What changes substantially is the surface area of the two modified S6 samples which is half the original S6 sample. So, the specific surface area has a great impact on the reaction and on the H_2 productivity. These considerations are confirmed by the normalization of the H_2 productivity on the surface area while the one on the bulk density (**Graph 4.3.2-D**) would require more investigation of the absorption radiation. The surface area and the density are not the only parameters influencing the photo-catalytic activity, which is also determined by the morphology, the active site and the band gap. Regarding this parameter, it has to be noted that even if the samples are all yellow, which suggests a lower band gap and the presence of nitrogen as dopant, this seems to have a less significant effect with respect to the surface area. In fact, it has to be remembered that it was not possible to determine whether N is efficiently inserted in the crystalline structure, so the presence of a N-doped titania is just an assumption.

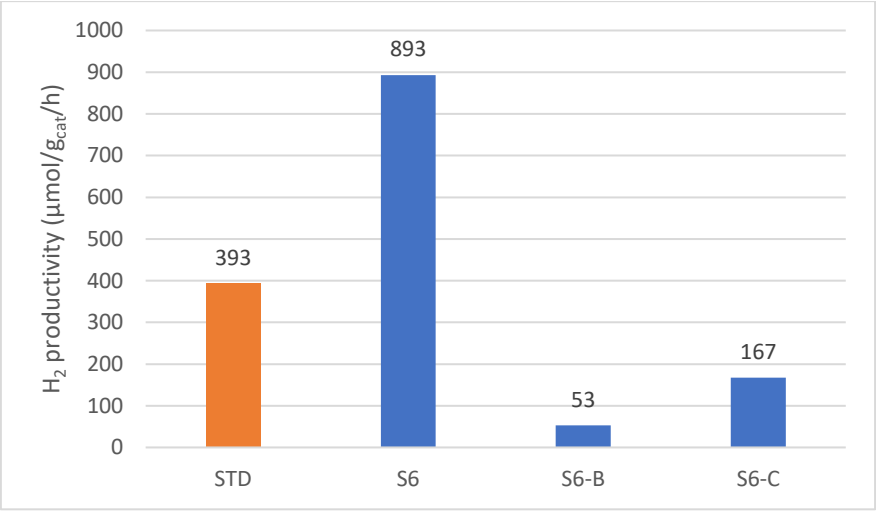

***Graph 4.3.2-C**. Comparison of the H_2 production rate for the samples obtained after the modifications of the synthesis S6. The STD sample is put as reference.*

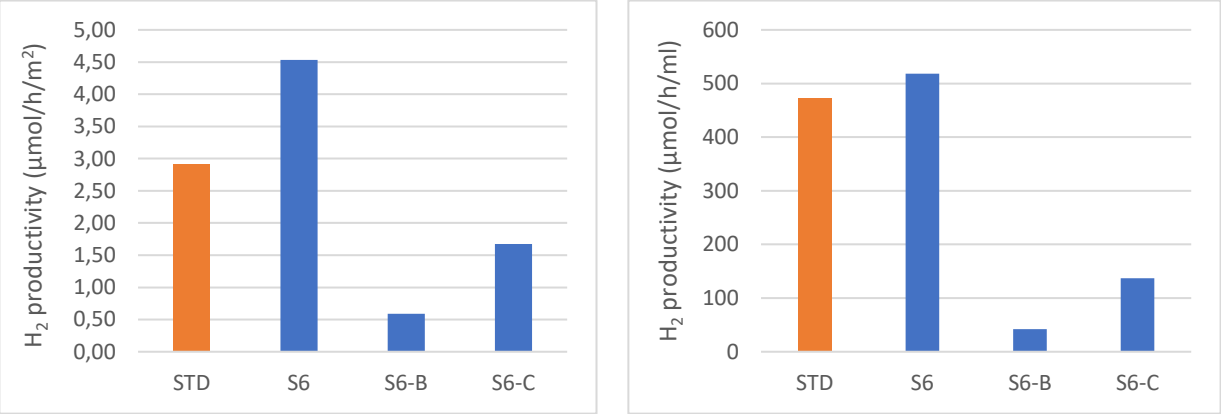

***Graph 4.3.2-D**. H_2 productivity for the samples obtained after the modifications of the synthesis S6. The graphs are a normalisation on the S_{BET} (left) and on the bulk density (right). Data elaborated from the graph 4.3.3-C.*

Concerning the reproducibility of the synthesis S6, the H_2 production rate of the first replica is almost equal to the original synthesis, even though the surface area is lower and the bulk density is slightly higher than the original sample S6. Indeed, when normalized on these values (**Graph 4.3.2-E**), the first replica displays the greater H_2 productivity for both parameters. When the second replica of the sample S6 is tested in the PR reaction, a definitely lower value of H_2 productivity is obtained, which is difficult to explain. Indeed, the properties of the sample S6(3) and S6(4) are comparable and a similar activity was expected.

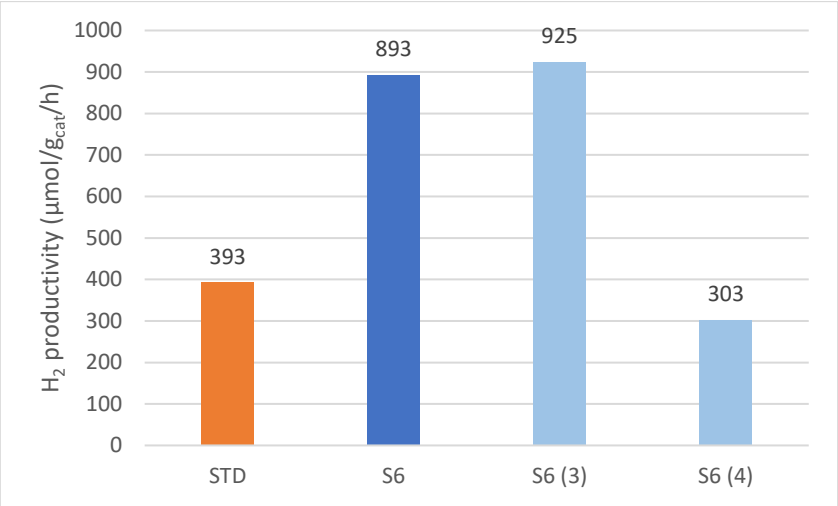

***Graph 4.3.2-E**. Comparison of the H_2 production rate for the reproducibility (light blue) of the synthesis S6. The STD sample is put as reference.*

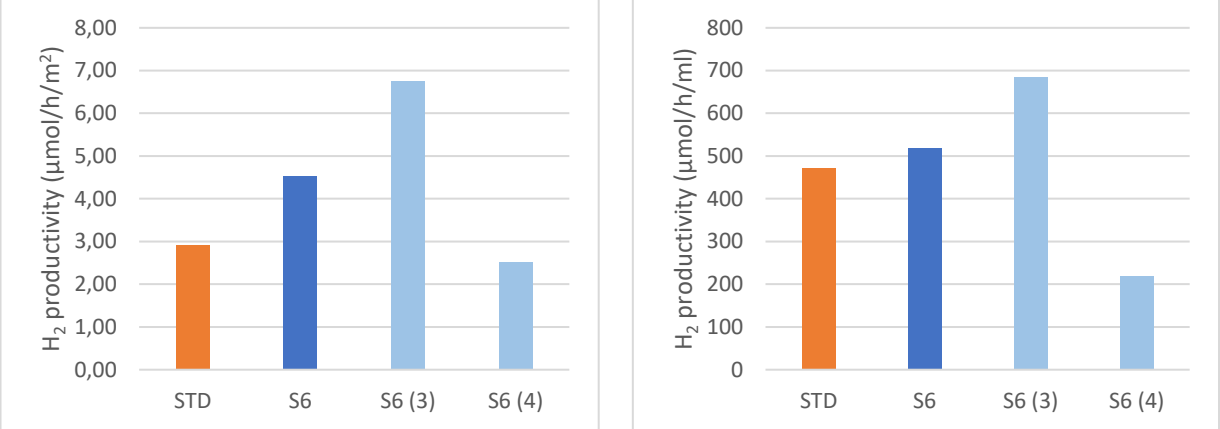

***Graph 4.3.2-F**. Normalization of the H_2 productivity on the S_{BET} (graph on the left) and on the bulk density (graph on the right). The samples analysed are the ones for the reproducibility of the synthesis S6.*

- Liquid Products analysis

From the HPLC chromatograms it is possible to verify the type of liquid products formed during the reaction and quantify them. Some possible products for the reforming of glycerol are dihydroxyacetone (DHA), glyceraldehyde and glycolaldehyde. Dihydroxyacetone is not detected for any titania sample used, while glyceraldehyde and glycolaldehyde are found in some of the samples. The STD titania is not able to transform glycerol into other products since the conversion is 0 (**Graph 4.3.2-G**), but from the GC analysis it is known that H_2 is produced. So, the reaction that takes place is the water splitting:

$$2\ H_2O \rightarrow 2\ H_2 + O_2$$

The same goes with the sample S2 (NH_4OH ratio 0.5), but in this case, the properties of the sample are not optimal and thus such behaviour can be expected. However, both with the sample STD and S2, the conversions are zero because of a problem in the HPLC instrument.

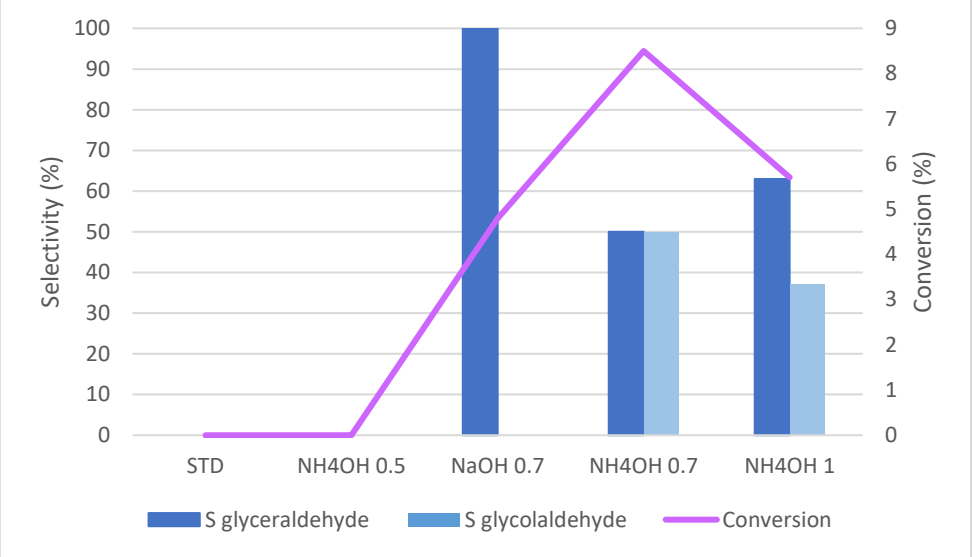

***Graph 4.3.2-G**. Selectivity and conversion for the titania samples synthetised with the neutralization approach (when HNO_3 is used). The selectivity is on the two main products: glyceraldehyde and glycolaldehyde.*

Otherwise, the titania samples obtained with NH_4OH in higher base/acid ratios (0.7 and 1) allow to form both glyceraldehyde and glycolaldehyde. The best conversion is given by the sample S6 (ratio 0.7) which confirms the idea that this is the best catalyst synthesized within the project. Indeed, it has the highest specific surface area and lowest bulk density, even though not comparable with the commercial P-25, it is composed of pure anatase with particles in the nano-dimensions; moreover, it may contain N in its crystalline structure due to the yellow colour of the powder.

A comparison with the sample obtained with NaOH in the ratio 0.7 is performed. This catalyst enables to produce only glyceraldehyde as a liquid product, in contrast with the results of Maslova et al. where the presence of rutile is reported to have a superior selectivity for glycolaldehyde[70]. In addition to that, this titania sample is formed by a mixture of anatase and rutile (see *Paragraph 4.1*, XRD analysis), which should have a greater activity than the pure anatase of the sample S6, as reported in literature[75,76]. This can be explained by the promotion of a photoinduced electron from the anatase conduction band to rutile, promoting charge separation and thus increasing the overall photo-activity of TiO_2[76].

Moreover, the conversion of this titania sample is lower with respect to the samples prepared with NH_4OH, especially the S6 one. Probably in this case the better properties of the TiO_2 S6 played a fundamental role, such as in the production of H_2 previously discussed.

For what concerns the samples S6-B and S6-C, modifications of the synthesis S6, the conversion is comparable with the sample S6, 8.2 and 9.4 respectively, but glycerol is not converted to any valuable liquid product as the conversion is zero.
On the other side, the reproducibility of the sample S6 (NH_4OH ratio 0.7) gave slightly different results, that are presented in **Graph 4.3.2-H**. The conversion for the first replica is lower, moreover only glyceraldehyde is produced. The second replica does not show any liquid product, so glycerol is not converted during the reaction. Furthermore, also in this case the conversion is negative.

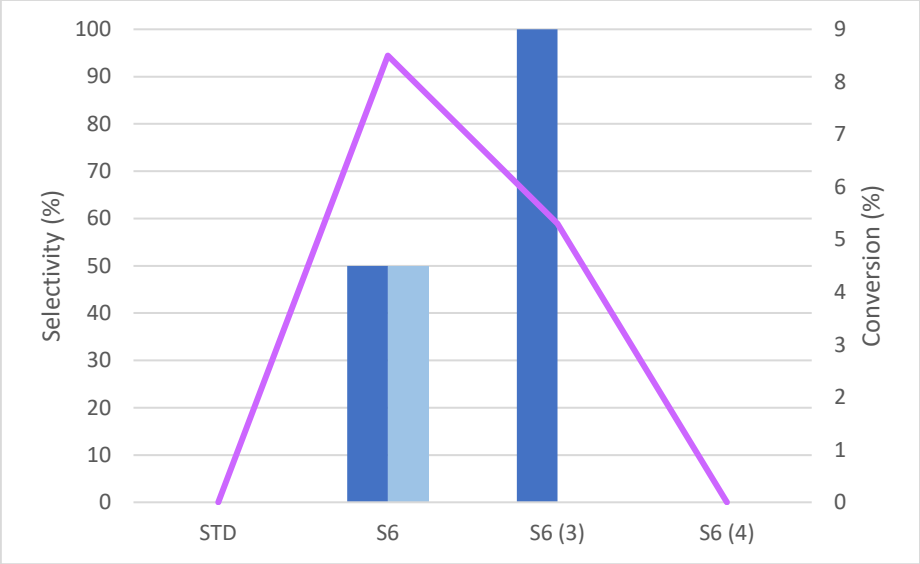

***Graph 4.3.2-H**. Selectivity and conversion for the titania samples in the reproducibility of the synthesis S6. The selectivity is on the two main products: glyceraldehyde and glycolaldehyde.*

The samples tested in this project (**Table 4.3.2-A**) allow to obtain mainly glyceraldehyde and in some cases glycolaldehyde. So, the reaction of glycerol reforming is thought to proceed with an indirect mechanism where glyceraldehyde is formed as one of the primary products, as already mentioned (see *Paragraph 1.5*). According to this mechanism, glyceraldehyde and glycolaldehyde form as the first decomposition products in glycerol PR. Indeed, CO_2 is not detected in the GC analysis meaning that the oxidation of glycerol is not completed, probably due to the low activity of the bare TiO_2 catalysts used.

5. CONCLUSIONS

This project is focused on the development of TiO_2 synthesised through the microemulsion approach, which allows to tune the morphological and optical properties of the final powder. Subsequently, synthetised titania is used in the photo-catalytic conversion of glycerol which is a by-product of the biodiesel production. Photo reforming (PR) reactions could play an important role in sustainable development since they exploit solar light to decompose organic substrates. In addition to that, from the glycerol PR reaction, H_2 is produced, which is a renewable-based energy vector.

Nanoparticles of titanium dioxide were successfully synthesised using the microemulsion (ME) technique. Moreover, the standard ME synthesis was modified introducing a neutralization step. Neutralization is achieved by the addition of a ME containing a base (NH_4OH or NaOH) with different base/acid ratios (0.5-1).

The neutralization approach allowed to obtain powders only composed of the anatase polymorph of titania with small dimensions of the particles (< 10nm) if NH_4OH is used with a base/acid ratio higher than 0.7. When NH_4OH was used with a lower base/acid ratio (0.5) or if NaOH was employed in the synthesis, also the rutile crystalline phase formed. In particular, one of the samples synthetised (S6) showed great morphological properties, namely a high surface area (198 m^2/g), a low bulk density (0.58 g/ml) and slightly stronger absorption in visible light range. Moreover, this sample (S6) presented a yellow colour which could be an indicator for the presence of nitrogen in the crystalline structure of titania (N-doped titania), as it is supported by the absorption of visible light in the UV-VIS spectra. In addition to that, a Raman positive shift demonstrated the presence of oxygen vacancies, which could have formed because of the N-doping. Unfortunately, it was not possible to definitively have the confirmation of the N presence through the XPS analysis, but it will be carried out when the instrument is available,

Because of the final characteristics of the powder, the synthesis S6 was tested for the reproducibility, resulting in two comparable samples. Nevertheless, the original S6 sample had slightly better properties, namely a higher surface area and a lower bulk density.

In the PR of glycerol, the sample S6 showed a H_2 productivity greater than any of the other samples obtained with the neutralization ME synthesis, and even than the STD one and the P-25. In addition to that, glyceraldehyde was obtained as a liquid product when the sample S6 is

tested, meaning that the decomposition of glycerol was significant, while for the other titania samples only the water splitting reaction was observed. In addition, also when the sample obtained through neutralization with a bigger base/acid ratio (1) was tested in the same photoreaction, glyceraldehyde formed along with glycolaldehyde, while at a lower base/acid ratio (0.5) no liquid products were present. Dihydroxyacetone was not detected for any of the titania samples. So, the course of the photo-reforming reaction proceeded only in the first steps of glycerol decomposition and while no CO_2 was observed after the reaction time (6 hours).

Rutile was also synthesised, exploiting two different approaches. In the first case (synthesis R-4gg), a longer hydrolysis time (4 days), no reflux and the use of HNO_3 allowed to form small nanoparticles of rutile (15 nm), while usually rutile is more stable at bigger dimensions. In the second case (synthesis S-HCl), a hydrolysis of 24 hours, reflux of 5 hours and the use of HCl resulted in the synthesis of titania mainly composed of rutile with a low percentage of anatase. The crystallites dimensions were similar to the previous case (13 nm). When the neutralization approach was used in this synthesis with HCl, only anatase formed with no trace of rutile. The effect of the base seemed to be more impacting than the type of acid used, even though better properties in the titania powders were obtained when HNO_3 was used rather than HCl. The PR testing of the samples containing rutile is not present in this work because of issues in the testing set-up, but it could be useful to see the differences in photo-activity for the two polymorphs of the synthesised titania.

Eventually, an attempt to calculate the quantum efficiency of the titania catalyst was done. Unfortunately, H_2 was not detectable when working at a single wavelength (365 nm or 400 nm) if bare titania is used, so it was not possible to calculate the quantum efficiency. Anyway, preliminary measures before the photoreaction showed an increase in the scattered light when the commercial titania P-25 was inserted in the system, along with a lowering in the transmitted light to the bottom of the reactor.

Future developments of the project may comprehend the synthesis of a supported Pt/TiO_2 catalyst both to be tested in the glycerol PR reaction and for the calculation of the quantum efficiency, since a higher photo-activity is expected with this type of catalysts.

BIBLIOGRAPHY

1. Malik, M. A., Wani, M. Y. & Hashim, M. A. Microemulsion method: A novel route to synthesize organic and inorganic nanomaterials: 1st Nano Update. *Arab. J. Chem.* **5**, 397–417 (2012).
2. Tartaro, G., Mateos, H., Schirone, D., Angelico, R. & Palazzo, G. Microemulsion Microstructure(s): A Tutorial Review. *Nanomaterials* **10**, 1657 (2020).
3. Moulik, S. & Paul, B. Uses and applications of microemulsions. *Curr. Sci.* **80**, (2001).
4. Laurén, S. What is critical micelle concentration? https://www.biolinscientific.com/blog/what-is-critical-micelle-concentration.
5. Paschalidou, P. & Theocharis, C. R. Comparison of Surface Characteristics of Mesoporous Titania Prepared in Matrix-Free Solutions and Using Triton X Reverse Micelles. *Mater. Sci. Appl.* **11**, 715–732 (2020).
6. M, S. Z. S., W, H. & Mr, M. A Review of The Lesser-Studied Microemulsion-Based Synthesis Methodologies Used for Preparing Nanoparticle Systems of The Noble Metals, Os, Re, Ir and Rh. *Mater. Basel Switz.* **12**, (2019).
7. Kale, S. N. & Deore, S. L. Emulsion Micro Emulsion and Nano Emulsion: A Review. *Syst. Rev. Pharm.* **8**, 39–47 (2016).
8. Pileni, M.-P. The role of soft colloidal templates in controlling the size and shape of inorganic nanocrystals. *Nat. Mater.* **2**, 145–150 (2003).
9. Sanchez-Dominguez, M., Pemartin, K. & Boutonnet, M. Preparation of inorganic nanoparticles in oil-in-water microemulsions: A soft and versatile approach. *Curr. Opin. Colloid Interface Sci.* **17**, 297–305 (2012).
10. Karunaratne, D. N., Pamunuwa, G. & Ranatunga, U. Introductory Chapter: Microemulsions. *Prop. Uses Microemulsions* (2017) doi:10.5772/intechopen.68823.

11. Callender, S. P., Mathews, J. A., Kobernyk, K. & Wettig, S. D. Microemulsion utility in pharmaceuticals: Implications for multi-drug delivery. *Int. J. Pharm.* **526**, 425–442 (2017).

12. Boutonnet, M., Lögdberg, S. & Elm Svensson, E. Recent developments in the application of nanoparticles prepared from w/o microemulsions in heterogeneous catalysis. *Curr. Opin. Colloid Interface Sci.* **13**, 270–286 (2008).

13. Xiong, L. & Manthiram, A. Nanostructured Pt–M/C (M=Fe and Co) catalysts prepared by a microemulsion method for oxygen reduction in proton exchange membrane fuel cells. *Electrochimica Acta* **50**, 2323–2329 (2005).

14. Xiong, L. & Manthiram, A. Catalytic activity of Pt?Ru alloys synthesized by a microemulsion method in direct methanol fuel cells. *Solid State Ion.* **176**, 385–392 (2005).

15. Agrell, J., Germani, G., Järås, S. G. & Boutonnet, M. Production of hydrogen by partial oxidation of methanol over ZnO-supported palladium catalysts prepared by microemulsion technique. *Appl. Catal. Gen.* **242**, 233–245 (2003).

16. Agrell, J., Hasselbo, K., Jansson, K., Järås, S. G. & Boutonnet, M. Production of hydrogen by partial oxidation of methanol over Cu/ZnO catalysts prepared by microemulsion technique. *Appl. Catal. Gen.* **211**, 239–250 (2001).

17. Xu, S., Zhao, R. & Wang, X. Highly coking resistant and stable Ni/Al2O3 catalysts prepared by W/O microemulsion for partial oxidation of methane. *Fuel Process. Technol.* **86**, 123–133 (2004).

18. Yeung, C. M. Y., Meunier, F., Burch, R., Thompsett, D. & Tsang, S. C. Comparison of New Microemulsion Prepared “Pt-in-Ceria” Catalyst with Conventional “Pt-on-Ceria” Catalyst for Water−Gas Shift Reaction. *J. Phys. Chem. B* **110**, 8540–8543 (2006).

19. Richard, B., Lemyre, J.-L. & Ritcey, A. M. Nanoparticle Size Control in Microemulsion Synthesis. *Langmuir* **33**, 4748–4757 (2017).

20. Matijevic, E. The Role of Chemical Complexing in the Formation and Stability of Colloidal Dispersions. *J. Colloid Interface Sci.* **58**, 16 (1977).

21. Sharon, M. Titania based nanocomposites as a photocatalyst: A review. *AIMS Mater. Sci.* **3**, 19.

22. Mital, G. S. & Manoj, T. A review of TiO2 nanoparticles. 19 (2011).

23. Zhang, Y. Titanate and titania nanostructured materials for environmental and energy applications: a review. *RSC Adv.* 32 (2015).

24. Chen, X. & Burda, C. Photoelectron Spectroscopic Investigation of Nitrogen-Doped Titania Nanoparticles. *J. Phys. Chem. B* **108**, 15446–15449 (2004).

25. Macwan, D. P., Balasubramanian, C., Dave, P. N. & Chaturvedi, S. Thermal plasma synthesis of nanotitania and its characterization. *J. Saudi Chem. Soc.* **18**, 234–244 (2014).

26. Satoh, N., Nakashima, T. & Yamamoto, K. Metastability of anatase: size dependent and irreversible anatase-rutile phase transition in atomic-level precise titania. *Sci. Rep.* 7 (2013).

27. Fasolini, A., Lombardi, E., Tabanelli, T. & Basile, F. Microemulsion Derived Titania Nanospheres: An Improved Pt Supported Catalyst for Glycerol Aqueous Phase Reforming. *Nanomaterials* **11**, 1175 (2021).

28. Yan, M., Chen, F., Zhang, J. & Anpo, M. Preparation of Controllable Crystalline Titania and Study on the Photocatalytic Properties. *J. Phys. Chem. B* **109**, 8673–8678 (2005).

29. Andersson, M., Kiselev, A., Österlund, L. & Palmqvist, A. E. C. Microemulsion-Mediated Room-Temperature Synthesis of High-Surface-Area Rutile and Its Photocatalytic Performance. *J. Phys. Chem. C* **111**, 6789–6797 (2007).

30. Erica Lombardi. Catalytic aqueous phase conversion of polyoils to hydrogen and chemicals. (2017).

31. Maslova, V. *et al.* Highly-dispersed ultrafine Pt nanoparticles on microemulsion-mediated TiO2 for production of hydrogen and valuable chemicals via oxidative photo-dehydrogenation of glycerol. *J. Environ. Chem. Eng.* **9**, 105070 (2021).

32. Wetchakun, N., Incessungvorn, B., Wetchakun, K. & Phanichphant, S. Influence of calcination temperature on anatase to rutile phase transformation in TiO2 nanoparticles synthesized by the modified sol–gel method. *Mater. Lett.* **82**, 195–198 (2012).

33. Dubey, R. S. Temperature-dependent phase transformation of TiO2 nanoparticles synthesized by sol-gel method. *Mater. Lett.* **215**, 312–317 (2018).

34. Hu, Y., Tsai, H.-L. & Huang, C.-L. Phase transformation of precipitated TiO2 nanoparticles. *Mater. Sci. Eng. A* **344**, 209–214 (2003).

35. Khitab, A. *et al.* Synthesis and Applications of Nano Titania Particles: A Review. *Rev. Adv. Mater. Sci.* **53**, 90–105 (2018).

36. Al Jitan, S., Palmisano, G. & Garlisi, C. Synthesis and Surface Modification of TiO2-Based Photocatalysts for the Conversion of CO2. *Catalysts* **10**, 227 (2020).

37. Ali, I., Suhail, M., Alothman, Z. A. & Alwarthan, A. Recent advances in syntheses, properties and applications of TiO $_2$ nanostructures. *RSC Adv.* **8**, 30125–30147 (2018).

38. Parangi, T. & Mishra, M. K. Titania Nanoparticles as Modified Photocatalysts: A Review on Design and Development. *Comments Inorg. Chem.* **39**, 90–126 (2019).

39. Henry, R. J. Biofuels from Crop Plants. in *Encyclopedia of Applied Plant Sciences* 177–179 (Elsevier, 2017). doi:10.1016/B978-0-12-394807-6.00169-6.

40. Tursi A. A review on biomass: importance, chemistry, classification and conversion. *Biofuel Res. J.* **22**, 962–979 (2019).

41. Mike Lancaster. *Green Chemistry: An Introductory Text*. (RSC Publishing, 2010).

42. Ciriminna, R., Pina, C. D., Rossi, M. & Pagliaro, M. Understanding the glycerol market: Understanding the glycerol market. *Eur. J. Lipid Sci. Technol.* **116**, 1432–1439 (2014).

43. Tan, H. W., Abdul Aziz, A. R. & Aroua, M. K. Glycerol production and its applications as a raw material: A review. *Renew. Sustain. Energy Rev.* **27**, 118–127 (2013).

44. Sahar *et al.* Biodiesel production from waste cooking oil: An efficient technique to convert waste into biodiesel. *Sustain. Cities Soc.* **41**, 220–226 (2018).

45. Faried, M. *et al.* Biodiesel production from microalgae: Processes, technologies and recent advancements. *Renew. Sustain. Energy Rev.* **79**, 893–913 (2017).

46. Ananthi, V. *et al.* A realistic scenario on microalgae based biodiesel production: Third generation biofuel. *Fuel* **284**, 118965 (2021).

47. Yang, F., Hanna, M. A. & Sun, R. Value-added uses for crude glycerol--a byproduct of biodiesel production. *Biotechnol. Biofuels* **5**, 13 (2012).

48. Chapter 1. Glycerol: Properties and Production. in *Green Chemistry Series* 1–17 (Royal Society of Chemistry, 2008). doi:10.1039/9781847558305-00001.

49. Gebremariam, S. N. & Marchetti, J. M. Economics of biodiesel production: Review. *Energy Convers. Manag.* **168**, 74–84 (2018).

50. IPCC, 2021: A summary for Policymakers. (2021).

51. European Commision. A hydrogen strategy for a carbon-neutral Europe. (2020).

52. Energy and the Green Deal. *European Commission - European Commission* https://ec.europa.eu/info/strategy/priorities-2019-2024/european-green-deal/energy-and-green-deal_en (2021).

53. European Commission. Directorate General for Energy., Guidehouse., & Tractebel Impact. *Hydrogen generation in Europe: overview of costs and key benefits.* (Publications Office, 2021).

54. The Future of Hydrogen – Analysis. *IEA* https://www.iea.org/reports/the-future-of-hydrogen.

55. Dawood, F., Anda, M. & Shafiullah, G. M. Hydrogen production for energy: An overview. *Int. J. Hydrog. Energy* **45**, 3847–3869 (2020).

56. Mehmeti, A., Angelis-Dimakis, A., Arampatzis, G., McPhail, S. & Ulgiati, S. Life Cycle Assessment and Water Footprint of Hydrogen Production Methods: From Conventional to Emerging Technologies. *Environments* **5**, 24 (2018).

57. Roussanaly Simon, Anantharaman Rahul, & Fu Chao. Low-Carbon Footprint Hydrogen Production from Natural Gas: A Techno-Economic Analysis of Carbon Capture and Storage from Steam-Methane Reforming. *Chem. Eng. Trans.* **81**, 1015–1020 (2020).

58. Cormos, C.-C., Petrescu, L. & Cormos, A.-M. Assessment of Hydrogen Production Systems based on Natural Gas Conversion with Carbon Capture and Storage. in *Computer Aided Chemical Engineering* vol. 33 1081–1086 (Elsevier, 2014).

59. Damen, K., Troost, M. van, Faaij, A. & Turkenburg, W. A comparison of electricity and hydrogen production systems with CO2 capture and storage. Part A: Review and selection of promising conversion and capture technologies. *Prog. Energy Combust. Sci.* **32**, 215–246 (2006).

60. Nikolaidis, P. & Poullikkas, A. A comparative overview of hydrogen production processes. *Renew. Sustain. Energy Rev.* **67**, 597–611 (2017).

61. Kayfeci, M., Keçebaş, A. & Bayat, M. Hydrogen production. in *Solar Hydrogen Production* 45–83 (Elsevier, 2019). doi:10.1016/B978-0-12-814853-2.00003-5.

62. Christoforidis, K. C. & Fornasiero, P. Photocatalytic Hydrogen Production: A Rift into the Future Energy Supply. *ChemCatChem* **9**, 1523–1544 (2017).

63. Rodriguez, C. A., Modestino, M. A., Psaltis, D. & Moser, C. Design and cost considerations for practical solar-hydrogen generators. *Energy Env. Sci* **7**, 3828–3835 (2014).

64. Rossetti, I. Hydrogen Production by Photoreforming of Renewable Substrates. *ISRN Chem. Eng.* **2012**, 1–21 (2012).

65. Nwosu, U. *et al.* Selective biomass photoreforming for valuable chemicals and fuels: A critical review. *Renew. Sustain. Energy Rev.* **148**, 111266 (2021).

66. Bowker, M. *et al.* The Photocatalytic Window: Photo-Reforming of Organics and Water Splitting for Sustainable Hydrogen Production. *Catal. Lett.* **145**, 214–219 (2015).

67. Panagiotopoulou, P., Karamerou, E. E. & Kondarides, D. I. Kinetics and mechanism of glycerol photo-oxidation and photo-reforming reactions in aqueous TiO2 and Pt/TiO2 suspensions. *Catal. Today* **209**, 91–98 (2013).

68. Christoforidis, K. C. & Fornasiero, P. TiO2 polymorphs for hydrogen photoproduction. in *Current Developments in Photocatalysis and Photocatalytic Materials* 127–140 (Elsevier, 2020). doi:10.1016/B978-0-12-819000-5.00009-6.

69. Sanwald, K. E., Berto, T. F., Eisenreich, W., Gutiérrez, O. Y. & Lercher, J. A. Catalytic routes and oxidation mechanisms in photoreforming of polyols. *J. Catal.* **344**, 806–816 (2016).

70. Maslova, V., Fasolini, A., Offidani, M., Albonetti, S. & Basile, F. Solar-driven valorization of glycerol towards production of chemicals and hydrogen. *Catal. Today* S0920586121001176 (2021) doi:10.1016/j.cattod.2021.03.008.

71. López, R. & Gómez, R. Band-gap energy estimation from diffuse reflectance measurements on sol–gel and commercial TiO2: a comparative study. *J. Sol-Gel Sci. Technol.* **61**, 1–7 (2012).

72. Wypych, A. *et al.* Dielectric Properties and Characterisation of Titanium Dioxide Obtained by Different Chemistry Methods. *J. Nanomater.* **2014**, 1–9 (2014).

73. Pio Gramazio. Sintesi per microemulsione di materiali fotocatalitici basati su nanoparticelle di ossido di titanio. (2020).

74. Allen, N. S., Mahdjoub, N., Vishnyakov, V., Kelly, P. J. & Kriek, R. J. The effect of crystalline phase (anatase, brookite and rutile) and size on the photocatalytic activity of calcined polymorphic titanium dioxide (TiO 2). *Polym. Degrad. Stab.* **150**, 31–36 (2018).

75. Su, R. *et al.* How the Anatase-to-Rutile Ratio Influences the Photoreactivity of TiO_2. *J. Phys. Chem. C* **115**, 24287–24292 (2011).

76. Jing, L., Li, S., Song, S., Xue, L. & Fu, H. Investigation on the electron transfer between anatase and rutile in nano-sized TiO2 by means of surface photovoltage technique and its effects on the photocatalytic activity. *Sol. Energy Mater. Sol. Cells* **92**, 1030–1036 (2008).

77. Kim, D. S., Han, S. J. & Kwak, S.-Y. Synthesis and photocatalytic activity of mesoporous TiO2 with the surface area, crystallite size, and pore size. *J. Colloid Interface Sci.* **316**, 85–91 (2007).

78. Petala, A. *et al.* Synthesis and characterization of N-doped TiO2 photocatalysts with tunable response to solar radiation. *Appl. Surf. Sci.* **305**, 281–291 (2014).

79. Tokudome, H. & Miyauchi, M. N-doped TiO_2 Nanotube with Visible Light Activity. *Chem. Lett.* **33**, 1108–1109 (2004).

80. Mrowetz, M., Balcerski, W., Colussi, A. J. & Hoffmann, M. R. Oxidative Power of Nitrogen-Doped TiO2 Photocatalysts under Visible Illumination. 5.

81. Suwannaruang, T., Kidkhunthod, P., Chanlek, N., Soontaranon, S. & Wantala, K. High anatase purity of nitrogen-doped TiO2 nanorice particles for the photocatalytic treatment activity of pharmaceutical wastewater. *Appl. Surf. Sci.* **478**, 1–14 (2019).

82. Asahi, R. Visible-Light Photocatalysis in Nitrogen-Doped Titanium Oxides. *Science* **293**, 269–271 (2001).

83. Gombac, V. *et al.* TiO2 nanopowders doped with boron and nitrogen for photocatalytic applications. *Chem. Phys.* **339**, 111–123 (2007).

84. Liu, Y., Chen, X., Li, J. & Burda, C. Photocatalytic degradation of azo dyes by nitrogen-doped TiO2 nanocatalysts. *Chemosphere* **61**, 11–18 (2005).

85. Jia, T. *et al.* Sonochemical Synthesis, Characterization, and Photocatalytic Activity of N-Doped TiO_2 Nanocrystals with Mesoporous Structure. *Int. J. Photoenergy* **2014**, 1–7 (2014).

86. Wang, J., Zhang, P., Li, X., Zhu, J. & Li, H. Synchronical pollutant degradation and H2 production on a Ti3+-doped TiO2 visible photocatalyst with dominant (001) facets. *Appl. Catal. B Environ.* **134–135**, 198–204 (2013).

87. Cheng, X., Yu, X., Xing, Z. & Yang, L. Synthesis and characterization of N-doped TiO2 and its enhanced visible-light photocatalytic activity. *Arab. J. Chem.* **9**, S1706–S1711 (2016).

88. Andersson, M. Preparation of Nanosize Anatase and Rutile TiO2 by Hydrothermal Treatment of Microemulsions and Their Activity for Photocatalytic Wet Oxidation of Phenol. 6.

89. Melchionna, M. & Fornasiero, P. Updates on the Roadmap for Photocatalysis. *ACS Catal.* **10**, 5493–5501 (2020).

ACKNOWLEDGEMENTS

First of all, I would like to thank professor Basile and professor Albonetti for giving me the opportunity to work in a catalysis laboratory and for having welcomed me in their research group. I also want to thank Andrea for all the help and worthy advice on the project and all the people in the catalysis lab for always helping me out. Moreover, I would like to thank Pio, with whom I worked closely in these past months, who helped me expanding my theorical and practical knowledge, and taught me the art of getting by in a chemical laboratory.

Thanks to all my university friends for brightening our study and lab days, making life quite easier during these years. Our lunch breaks will be very missed.
Also, I want to thank my best friends for always being there for me, even though we don't see each other as we would.

A special thanks goes to Martina, my partner in crime during all these years, with whom I shared almost everything, from a room to many lockdowns, down to my food and my brush. Thank you for teaching me a lot, I will miss everything we did together. I am sure all the years would have been much more boring without you.

I am extremely thankful to my parents for always supporting me with every decision I made and for allowing me to live these amazing years in Bologna. Moreover, I want to thank all my family, for sharing with me a lot of anxious moments and for always backing me up.

Lastly, I am deeply thankful to Lorenzo for everything he does for me. I cannot express how grateful I am to have you in my life.